

Microscope Images indicate that Water Clusters are the cause of Phyllotaxis

(Weblink to : [Overview of the Water Cluster Hypothesis](#))

- by **Dipl. Ing. (FH) Harry K. Hahn** -
Ettlingen / Germany

20. April 2020 - Update from 9. July 2020

Note: This study is not allowed for commercial use !

Abstract :

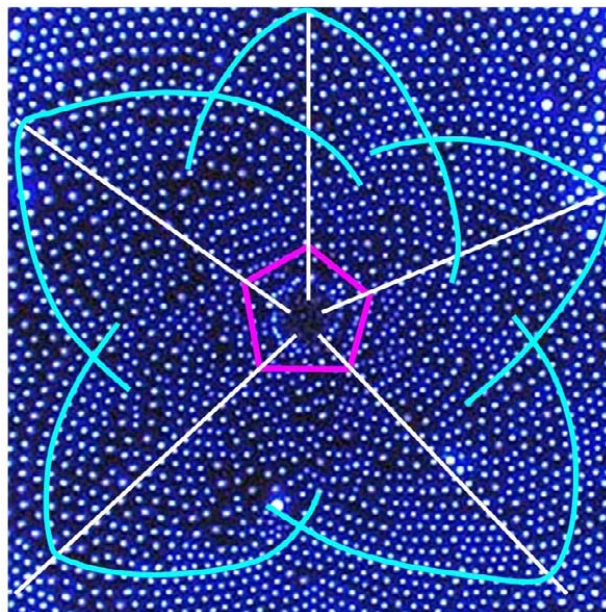
With my study I want to advance a hypothesis that Phyllotaxis is caused by a lattice of Ice-Crystals or large Water Clusters which are stabilized (coated) by certain proteins, e.g. special Ice-binding- or Water-Cluster-binding-proteins. The microscopic image of the remains of an evaporated water droplet shows a phyllotactic pattern that formed during the evaporation of the water droplet on a silicon wafer. This image is a proof that Water itself must be the main contributor which causes Phyllotaxis ! The physical process Evaporation, and electric charge and coulomb forces caused by evaporation also seem to play a role in the pattern formation and in the precise orientation and positioning of the water clusters in the pattern.

Important for the formation of a phyllotactic Fibonacci pattern seems to be a large central Water Cluster, that may have icosahedral Mackay-geometry, consisting of large icosahedral Sub-Clusters formed by the stable icosahedral water clusters $(H_2O)_{100}$ or $(H_2O)_{280}$. Typical cluster numbers of Mackay-Clusters are 13 and 55 which are Fibonacci Numbers ! Additional proof comes from SEM-Images of the Sunflower Capitulum. These images indicate that new primordia are caused by rhombic crystals, which seem to be either ice-crystals or large water cluster crystals that formed with the help of ice-binding proteins or similar. Proof for a physical cause of Phyllotaxis is also provided by a study about variations in the Fibonacci-spiral patterns of twigs of the three "Pinus Mugo" which shows that the Fibonacci-pattern variation depends on altitude and temperature- / radiation- conditions. With the results of this study I developed an infinite Fibonacci-Number-Sequences-Table that contains all existing Fibonacci-Sequences and all natural numbers. Finally I present a mathematical discovery regarding constant Phi. All natural numbers and their square roots, as well as constant Pi (π), can be expressed by only using constant Phi (1.618...) and the base unit 1.

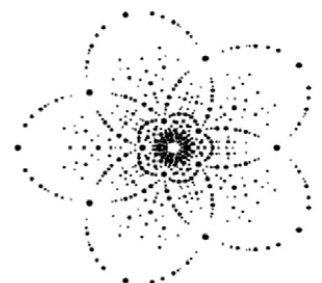
Part III of the book "**Symmetry in Plants**" emphasizes the thesis that the resolution of an important part of the mystery of Phyllotaxis can be found in the basic laws of nature responsible for the homologies of structure, and that a global and synthetic view on nature can give important keys for the understanding of Phyllotaxis.



Myosotis
A flowering plant



Microscope Image of a water-cluster lattice visible in the residue of a small water droplet that evaporated on a silicon wafer in an Electron Beam Lithography System. This image was made by Devin K. Brown from the IEN at Georgia Tech /USA
"The blue sunflower" - by courtesy of NSF



simulated Laue pattern
for X-ray diffraction from
an **icosahedral quasicrystal**
(→ see this [Study](#) - page 36)

CONTENTS :		Page
1	Primordia in the generative zone of the Sunflower capitulum show crystalline structures	4
1.1	Crystals with rhombic (bi-pyramidal) shape seem to form the base of new generated primordia	5
1.2	The rhombic crystals that form the base of primordia may grow on Ice-binding proteins :	5
2	Water / Ice-Crystals grown on Ice-binding Proteins are the probable cause of Phyllotactic Patterns	6
	Study 1 : Ice-Binding Proteins in Plants	6
	Study 2 : Polypentagonal Ice-like Water Networks emerge in an activity-improved Ice-binding Protein	6
3	Crystalline Structures seem to form the base of the Apical Meristem	7
4	The rhombic Sunflower Primordia may be caused by Ice-Crystals or by Water-Cluster-Crystals	8
5	The Microscope Image of an evaporated Water Droplet shows that Water is causing Phyllotaxis !	9
5.1	A Phyllotactic Pattern : A Water-Cluster-Lattice that is influenced by a large central Water Cluster	10
5.2	<u>The evaporated Water Droplet</u> : A description & analysis of the cause of the Phyllotactic Pattern	11
6	Fibonacci Numbers are defined by a large central Water-Cluster with MacKay-Cluster Geometry	13
6.1	Model of the Evaporated Water Drop	13
6.2	Model of the phyllotactic pattern source in the Sunflower meristem	13
7	Fibonacci Spiral Patterns seem to be the result of a circular crystal-like lattice of Water Clusters	14
7.1	PS-Clusters with a precise geometry which form during the evaporation of Water	14
8	The asymptotic ratio of successive Fibonacci numbers leads to the Golden Ratio constant φ (or Φ)	15
9	Icosahedral- and Dodecahedral Forms can be found in Crystals and they appear in many Organisms	16
10	Water Clusters	17
11	Water-Clusters seem to cause the formation of PS-Particle-Clusters with icosahedral Geometry	18
	Study 3 : Magic number colloidal clusters as minimum free energy structures	18
12	A physical mechanism (physical trigger) must be the fundamental cause of Phyllotaxis !	19
	Study 4 : Auxin influx carriers stabilize phyllotactic patterning	19
	Study 5 : A plausible model of phyllotaxis	19
13	Proof for a fundamental physical cause of Phyllotaxis that depends on Temperature / Radiation	20
	Study 6 : Changes in phyllotactic pattern structure in <i>Pinus mugo</i> due to changes in altitude	20
13.1	Different Temperatures at different altitudes caused changes in phyllotactic-pattern-variation	21
13.2	Radiation is different at different altitudes	21
13.3	Phyllotactic-pattern-variability seems to vary with the sunspot-cycle	21
13.4	Two more quantitative studies to phyllotactic-pattern-variations in Pine-Cones & Sunflowers	22
	Study 7 : Aberrant phyllotactic patterns in cones of some conifers : a quantitative study	22
	Study 8 : Novel Fibonacci and non-Fibonacci structure in the Sunflower	22
14	Electromagnetic-Radiation from specific wave-length-ranges can change Phyllotactic Patterns	23
15	Phyllotactic-pattern (bud induction) caused by far-red & infrared light : 750 nm to \approx 2000 nm	24
	Study 9 : Red Light Affects Flowering under long days in a Short-day Strawberry Cultivar	24
16	From Fibonacci-Sequences shown by <i>Pinus mugo</i> at 2500m an infinite Fibonacci-Table was developed	25
17	A general rule exists which connects numbers of different Fibonacci-Sequences by the golden ratio φ	26
17.1	Interesting properties of the Fibonacci-F1 Sequence (and other Fibonacci-Sequences) :	26
17.2	Constant φ (Φ) defines all Fibonacci-Sequences and the square roots of all natural numbers	27
17.3	To the discovery of an important algebraic equation regarding Constant φ (Phi)	27
17.4	The algebraic calculation of the square roots of all natural numbers only with constant φ and 1	28
17.5	Constant Pi (π) can be expressed by only using constant φ and 1 !	30
17.6	Referring to my discovery regarding constant φ (Phi), I want to define 12 Conjectures	31
18	References	32
<u>Appendix :</u>	A.) : MOVIES of : Standing-Wave-Patterns and Acoustic-Resonance in Water	34
	B.) : IMAGES of : <i>Coscinodiscus</i> Diatoms that show phyllotactic patterns (Phyllotaxis)	35
	C.) : Infinite Fibonacci-Number Sequence-Table : Sequences No. 1 to 33 shown (F1 – F33)	36
	D.) : Fibonacci-Sequence-Tables F1; F2 ; F6 ; F8	37

Introduction :

I am confident that my study will help to uncover and solve the mystery of Phyllotaxis. And I hope it will help to find new genetical approaches and measures, to increase the crop yield of cereal plants and other useful plants, e.g. by effectively increasing the number of seeds in seed heads (infructescence), in order to safely feed the growing world population.

In botany the term "Phyllotaxis" describes the arrangement of leaves on spiral paths on the stem of a plant. Phyllotactic spirals form a distinctive class of patterns in nature. But the true cause of these phyllotactic (Fibonacci) spiral patterns, which appear in most plants, still isn't found yet ! The current belief is that phyllotactic spiral patterns which can be explained and described by Fibonacci Number Sequences, is controlled by plant hormones like Auxin.

But this can't be correct as a number of studies indicate ! And microscopic images indicate fundamental physical and inorganic causes of Phyllotaxis. Water evaporation, coulomb forces caused by evaporation, and in particular Water's property to form large Water Clusters seem to play a major role → see weblink: "[Overview of Water Cluster Hypothesis](#)" A number of studies indicate that temperature and radiation (IR/black-body radiation) also seem to be crucial influential factors for phyllotactic pattern formation, probably because of their impact on the Water-Cluster-formation process.

The presented Microscope-Image of the remains of a small water droplet which evaporated on a silicon surface shows a phyllotactic pattern. This is a first proof that Water itself must be the main cause (contributor) of Phyllotaxis ! A central large Water Cluster seems to be responsible for the phyllotactic pattern formation and for the First (Fibonacci) Spiral Number of the phyllotactic pattern. And the geometry of the water cluster network which is surrounding this central Water Cluster seems to be responsible for the Second (Fibonacci) Spiral Number of the (Fibonacci) spiral pattern.

Therefore I want to ask scientists with access to a Microscope Laboratory and Nanotechnology-Experts to produce similar images of evaporating water droplets which show such phyllotactic patterns, to confirm the hypothesis !

To achieve usable microscope images and to analyse the dynamic process of the pattern formation, ideally a „live“-observation (examination) of the evaporating water droplet through the microscope should be done, either under atmospheric condition or under a vacuum in a transparent vacuum chamber. In that way the water droplet can be observed during evaporation and the dynamic behaviour of the water clusters can be observed and filmed precisely ! **Because it's not clear yet what role a Silicon support of the drop, electron flow, electric charge & possible defects in the silicon play, it may be necessary to place the drop on different Silicon-wafers during observation, and apply defined currents to achieve a phyllotactic pattern as shown in Chapter 5**

Another possible proof for a physical cause of Phyllotaxis comes from new generated primordia in the generative zone of the Sunflower Capitulum, that seem to be caused by rhombic crystals which may be either Ice-Crystals or large Water-Cluster-Crystals. These crystals probably formed with the help of Ice-binding- or Water-Cluster-binding proteins. **H₂O - evaporation in the generative zone seems to play an important role in the formation of these rhombic crystal-structures !!**

It would also be a good idea to produce more SEM-images of these rhombic shaped sunflower primordia, and to do diffraction analyses of these rhombic shaped crystals to find out their true crystal structure !

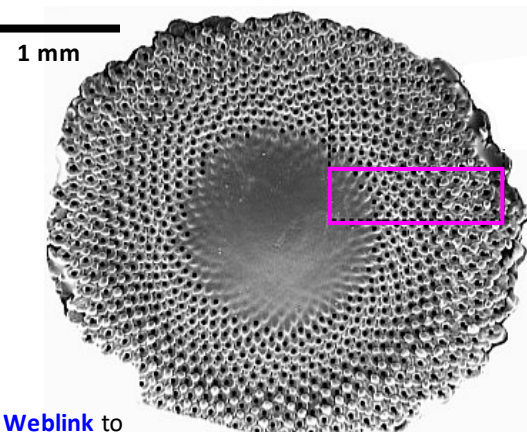
More proof for a fundamental physical origin of Phyllotaxis comes from **study 6** about variations in the phyllotactic patterns of "Pinus mugo" trees which are clearly linked to the different altitudes where this tree grows, and from **study 9** which shows that **far-red & infrared radiation with wave-lengths > 750 nm seems to trigger** floret bud-induction and **phyllotactic-pattern formation** in short-day-Strawberries & other plants

As a consequence of all these proof, biological processes linked to Phyllotaxis, for example the generation of Auxin-gradients, can only be secondary effects resulting from the primary behavior of Water !

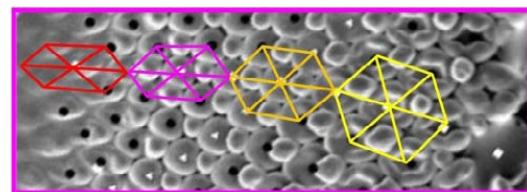
Or in other words, plants adapted to the property of Water to form phyllotactic patterns, and they used it as a reference for growth-processes and as reference for their own structure, in symbiosis with the pattern-forming property of Water!

Finally I present a mathematical discovery regarding constant **Phi** which defines the numbers of the Fibonacci-Sequences and the geometry of the Platonic Solids (e.g. Icosahedron and Dodecahedron). All natural numbers and their square roots, and the transcendental constant **Pi**, can be expressed mathematically by only using constant **Phi** and **base unit 1** This fact indicates the importance of constant **Phi** for the structure of matter and for the physical world (for Nature) !

1 Primordia in the generative zone of the Sunflower capitulum show crystalline structures



Weblink to the image & Phyllotaxis Study



"When we look at a **Sunflower Capitulum** then we see a finished product where the phylogenetic- and ontogenetic mechanisms responsible for its existence may not be apparent" Citation from: "**Symmetry in Plants**"

Detailed SEM-images of the disc-region of the sunflower capitulum show that the new appearing floret primordia in the generative zone have features (outlines) which are comparable with features of crystals. Precisely linear edges are visible and a rhombical structure seems to form the base of each new primordia which appears in the generative zone. Therefore I advance the hypothesis that Phyllotaxis is based on the formation of water cluster crystals within a complex crystal-lattice, during water evaporation, that is in symbiosis with tissue-structures of the generative zone of the capitulum

Note : The following scanning electron microscopy (SEM)-images which I used for my analysis are from this study :
 → [“Transductions_for_the_Expression_of_Structural_Pattern_Analysis_in_Sunflower”](#) by Luis F. Hernandez & Paul B. Green

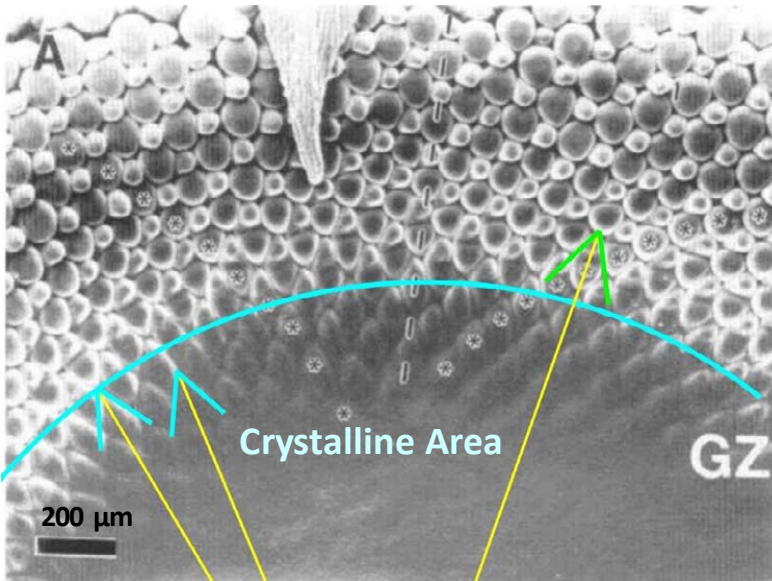


Fig. 1 : Fibonacci-array of floret primordia in the Sunflower -capitulum. The generative zone is marked as „Crystalline area“

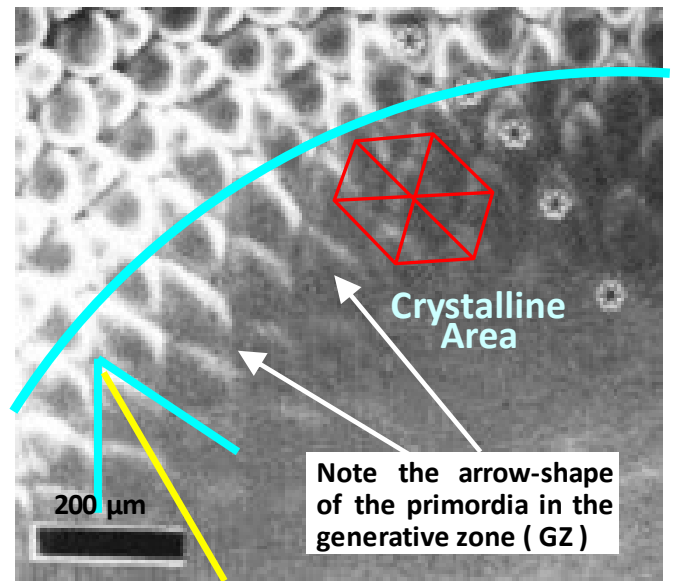


Fig. 2 : Inside of this „Crystalline Area“ the new appearing primordia have a sharp arrow-shape !

Detail SEM-images of the generative zone show crystal-like outlines of the new primordia :

On the image on the right I have drawn-in some lines in blue color to indicate edges and outlines of the new appeared primordia which show crystal-like structures that seem to be hidden under the epidermal layer. The sharp arrow-shaped tips of the new primordia point towards the circumference of the capitulum. The angle of the arrow-shaped tips is in the range of 50-60°. The enlarged detail below shows some of the precise linear edges in more detail. In this image it is also visible that the rhombical crystal-like structures under the epidermal layer break in two pieces in the further growth process (arrow).

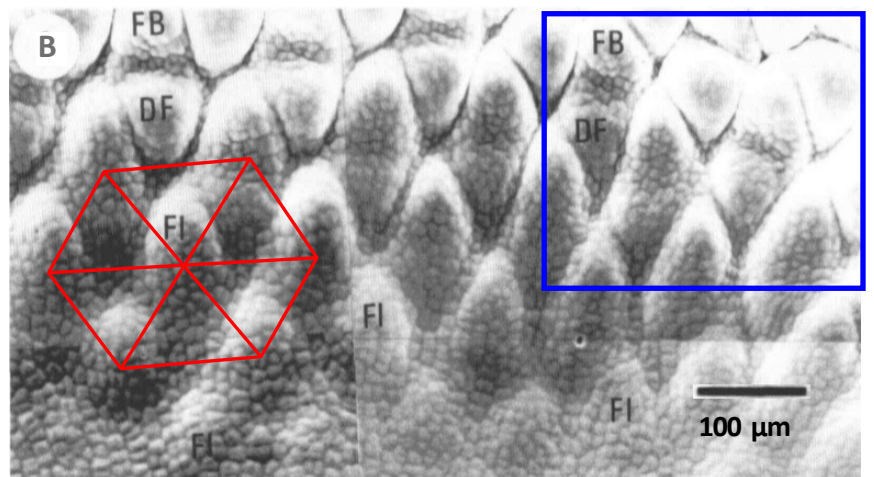
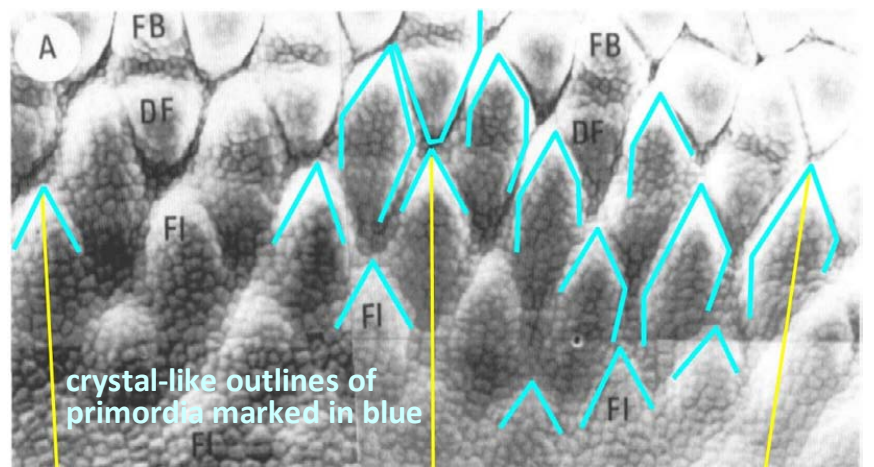


Fig. 3-A/B : A.) Detail image of the generative zone with some of the crystal-like outlines (primordia) marked in blue B.) unmarked image
Black Bar = 100 µm (bottom right) ; FI = floret primordia

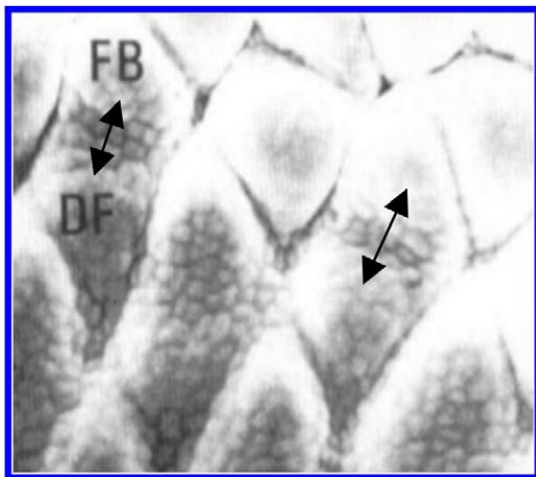


Fig. 4 : Detail of Fig. 3-B showing some of the precisely straight crystal-like outlines which are hidden under the epidermal layer

A close examination of the new generated primordia which appear from the featureless tissue of the capitulum shows that **rhombic (or bi-pyramidal) "crystal-like structures" form the base of each new generated floret primordium**. If we assume that these sharp geometrical structures are real crystals, then we look at precise rhombical (bi-pyramidal) crystals which initiate (trigger) the existence of each new primordium. However these rhombic crystals seem to have only a short lifetime. Shortly after their appearance these „rhombic crystals“ break in half, in the further growth-process of the primordia, and the two halves of the original crystal then form the bases of a disc-floret (DF) and a floret bract (FB).

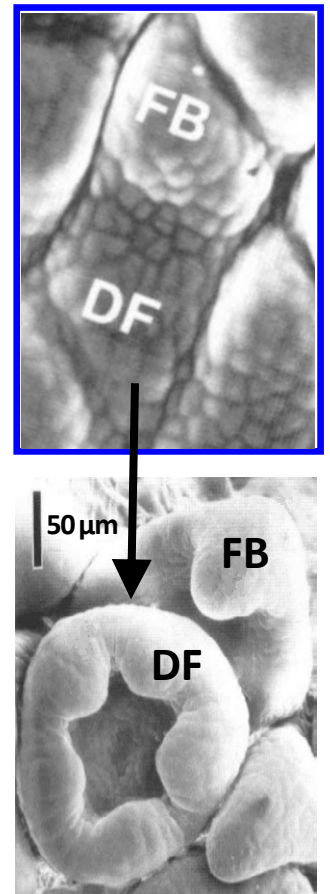
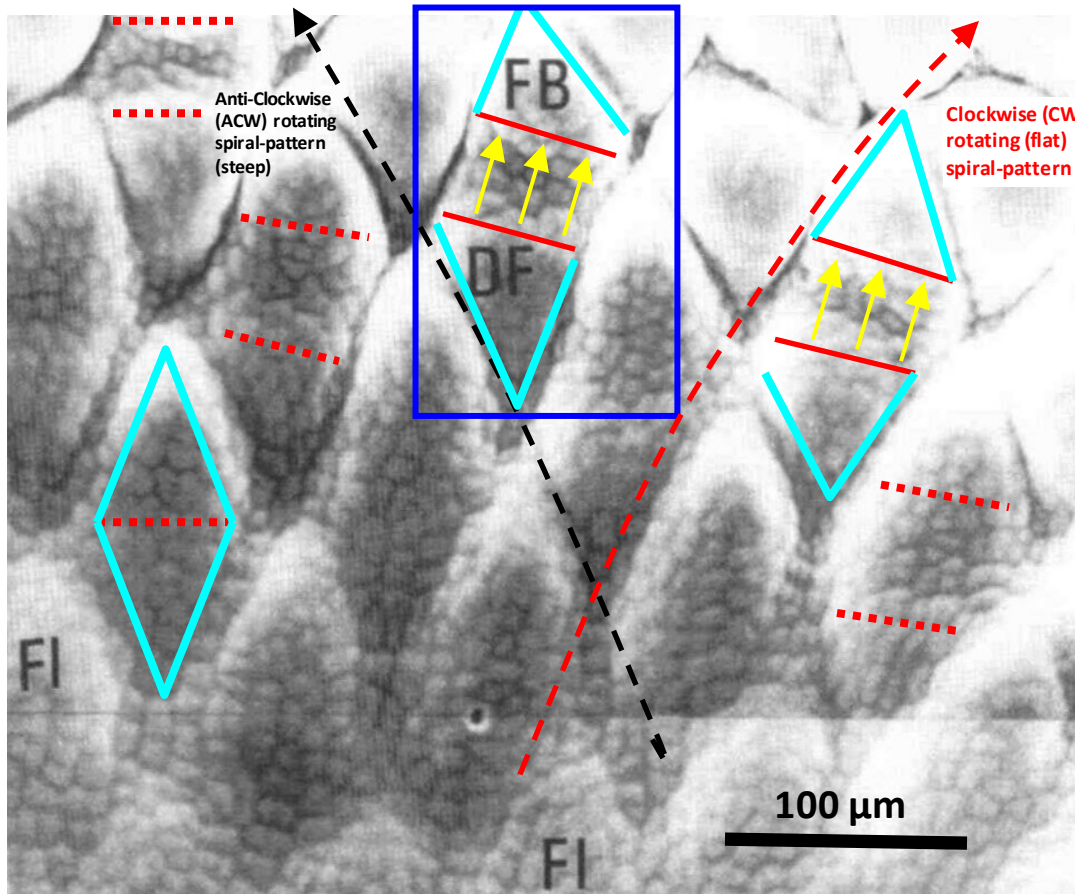


Fig. 5-A : Section of the generative zone (GZ) or „crystalline area“ showing in detail new generated primordia. Blue lines indicate rhombical-shaped „crystals“ which form the base-structure of the new primordia. Some of them are „broken“ in two pieces (red lines)

Fig. 6: A rhombic primordia broken-apart develops into a bract (FB) and a flower (DF)

1.2 The rhombic crystals that form the base of primordia may grow on Ice-binding proteins :

If we compare the shape and size of the rhombic-shaped primordia, visible in the SEM-images, with ice-crystals grown on Ice-binding Proteins, then we can see a close similarity ! The image below shows a rhombic (bi-pyramidal) Ice-crystal grown in an A-20 Ice-binding-Protein solution. The shape and size of this ice-crystal is very similar to the size and shape of the rhombic primordia visible in the SEM-image (see Fig. 5-B)

The rhombic crystals underneath the epidermal layer seem to have an inclined orientation (→section A-A) The red lines in Fig. 5-A indicate break-lines of the rhombic crystals, as they break in two pieces during the growth process. Some break-lines in Fig. 5-A have a slight inclination towards the right side. This trend may have decided over the rotary direction (red arrow) of the flat CW-spiral pattern

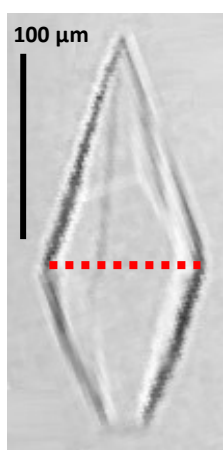


Fig. 8: A rhombic ice-crystal grown in a A20 Ice-binding-Protein solution

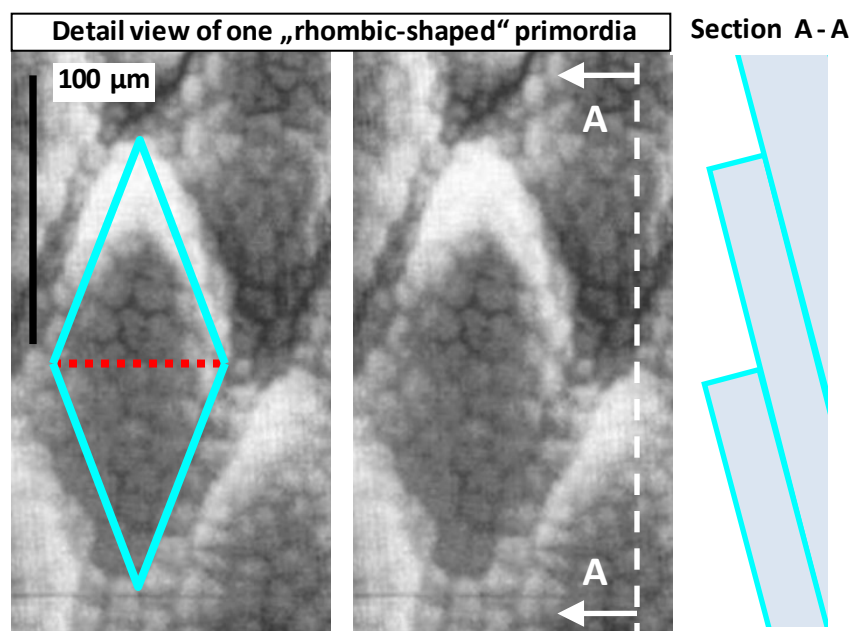


Fig. 5B: This detail view of Fig 5-A shows one new generated primordia. The rhombic shape is indicated by the blue outline. The schematic section A-A on the right shows the assumed inclination of the crystals.

2 Water/Ice-Crystals grown on Ice-binding Proteins are the probable cause of Phyllotactic Patterns

Primordia in plants seem to be caused (initiated) by rhombic crystals, probably made of water-Ice or water-clusters.

These rhombic (bi-pyramidal) crystals probably start growing on special Ice-binding proteins in the plant cells, and they seem to be responsible for phyllotactic pattern formation during water evaporation, with the help of a polypentagonal water network, or a lattice of water clusters (for example $(H_2O)_{12}$ or $(H_2O)_{100}$) that extends through the meristem

Study 1 : “Ice-Binding Proteins in Plants“

- by Melissa Bredow & Virginia K. Walker, Queen’s University, CA - [weblink to study : Ice-Binding Proteins in Plants](#)

Abstract : Sub-zero temperatures put plants at risk of damage associated with the formation of ice crystals in the apoplast. Some freeze-tolerant plants mitigate this risk by expressing **Ice-binding Proteins (IBPs)**, that adsorb to ice crystals and modify their growth. **IBPs** are found across several biological kingdoms, with their ice-binding activity and function uniquely suited to the lifestyle they have evolved to protect, be it in fishes, insects or plants. While IBPs from freeze-avoidant species significantly depress the freezing point, plant IBPs typically have a reduced ability to lower the freezing temperature. Nevertheless, they have a superior ability to inhibit the recrystallization of formed ice.

Study 2 : “Polypentagonal Ice-like Water Networks emerge in an activity-improved Ice-binding Protein“

- by Daichi Fukamia, Sheikh Mahatabuddina, Tatsuya Araia and others - [weblink : → Weblink to study](#)

Abstract : Polypentagonal water networks were recently observed in a protein capable of binding to ice crystals, or **Ice-binding Protein (IBP)**. To examine such water networks and clarify their role in icebinding, we determined X-ray crystal structures of a 65-residue defective isoform of a Zoarcidae-derived IBP (wild type, WT) and five single mutants (A20L, A20G,...). **Inclusion of a symmetrical water cluster in the polypentagonal network** showed a perfect complementarity to the waters constructing the (2021) pyramidal ice plane. The order of ice-binding strength was $A20L < A20G < WT < A20V...$

Ice-binding Proteins (IBPs) (or Antifreeze-proteins), and their function in plants and animals :

Different species have developed Ice-binding Proteins to reduce the risk of cell-damage associated with the formation of ice-crystals in the apoplast. Ice-binding proteins can control and modify the growth of ice crystals within the cell structure

Extracts from the Studies 1 and 2 :

Ice-Binding Proteins (IBPs) found in cold-hardy animals (e.g. fishes, insects and microbes) and in freeze-tolerant plants are unique macromolecules that are capable of binding to one or more ice-planes and creating a convex ice front on the plane between the bound IBPs through a Gibbs–Thomson effect. The ice-binding ability of an IBP also depresses the freezing point of water. Some freeze-tolerant plants have ice-binding proteins (IBPs) that adsorb to ice crystals and modify their growth. IBPs serve to control the growth of ice crystals and reduce freezing damage. Plant IBP’s also have a superior ability to inhibit the recrystallization of formed ice.

A poly-pentagonal water network consisting of Pentamers (H_2O)₅ and probably other H₂O-clusters, for example $(H_2O)_{20}$, $(H_2O)_{100}$ etc. connects the Ice-crystal to the IBP.

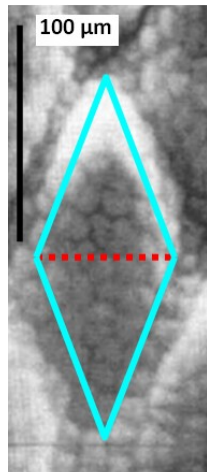


Fig. 1 : Rhomboidal shape of a primordia Shape & size as A20

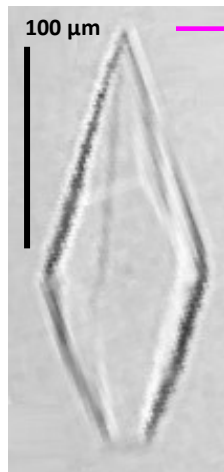


Fig. 2 : A20 (wild type) Ice crystal grown in a A20 - Protein Solution

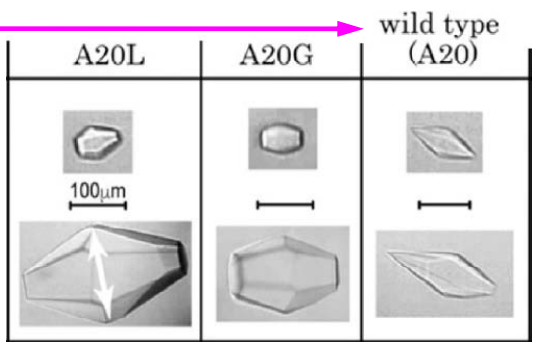


Fig. 3 : Modification and growth of single ice crystals into bi-pyramids (within 5 min.) in solutions with the Ice-binding-Proteins A20L, A20G & WT (wild-type)

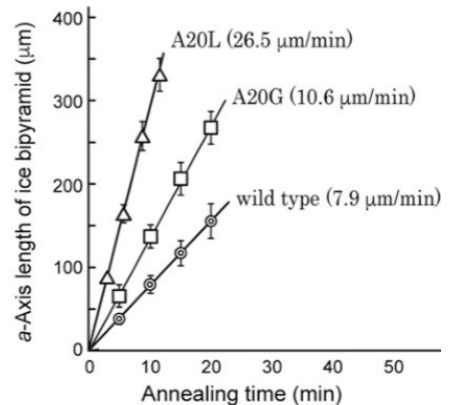


Fig. 4 : Comparison of ice-growth ability of the Ice-binding Proteins WT (wild-type), A20L, A20G

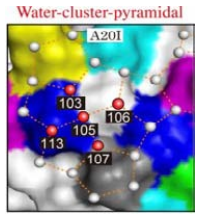


Fig. 5c : water-cluster with a space-match to pyramid crystal planes

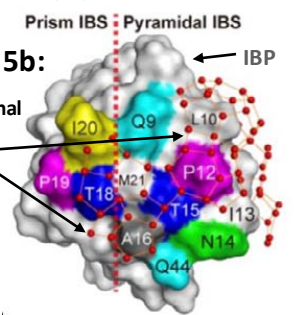
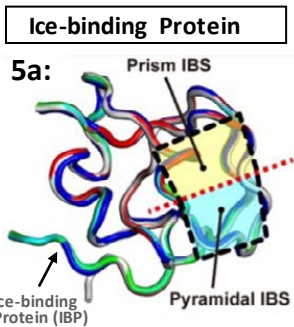


Fig. 5a : Overlay of the backbone structures of the WT-, A20L- & A20G-Ice-binding-proteins (IBPs) The two squares separated by a broken line indicate the location of two Ice-binding sites (IBS) One is the first prism plane (prism IBS yellow) and another the pyramidal plane (pyramidal IBS cyan)
Fig. 5b : Structure of the A20I-IBP with ≈50 semi-clathrate waters (water-clusters→ red) which form the polypentagonal network where the pyramidal water cluster (bipyramid-crystal) is connecting to.

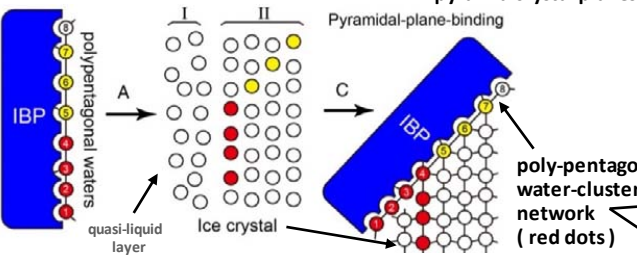


Fig. 5d : Function of the poly-pentagonal waters (water-clusters) The water clusters first merge with a disorderd quasi-liquid layer (I) which is connected to the ice-crystal-lattice (II). The water-clusters then connect to the pyramidal Ice-Crystal (bi-pyramid)

3 Crystalline Structures seem to form the base of the Apical Meristem

Primordia seem to be initiated by crystal-like structures which are located under the epidermal layer. During water evaporation from the meristem these crystal-structures, indicated by linear features in deeper layers of the meristem, initiate the process of primordia formation and development. Then as a secondary effect hormones like Auxin appear.

Below the epidermal layer linear features are visible that may be formed by a Water-Cluster Crystal

The following images show central sections through the apical meristem of *Arabidopsis*. The first image shows the meristem with no new initiated primordia. The second image shows a newly initiated primordium in the peripheral zone of the meristem. Both images show linear “crystal-like” structures under the outer epidermal layer. These linear “crystal-like” structures are indicated by cell material of the inner epidermal layers. The crystalline structures itself seem to be transparent and they seem to extend through the complete apical meristem, an apparent “open-cell structure”. These crystal-like structures seem to be formed by a large “water-cluster crystal” that may have a gel-like (clotted) consistency. The images are from **Study 4** (see also **Chapter 12**) : “Auxin influx carriers stabilize phyllotactic patterning” see : [study 4](#)

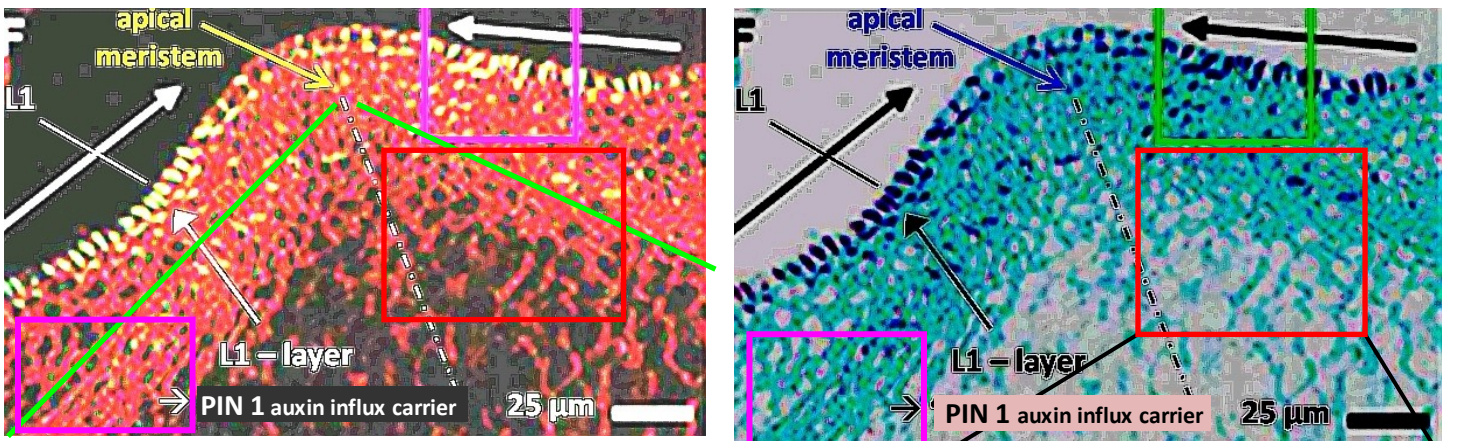


Image processing :
The original images were enhanced in color, contrast and brightness. In order to bring out the details a bit clearer the original images were inverted in colors (blue images) Linear features are indicated by lines aside these features

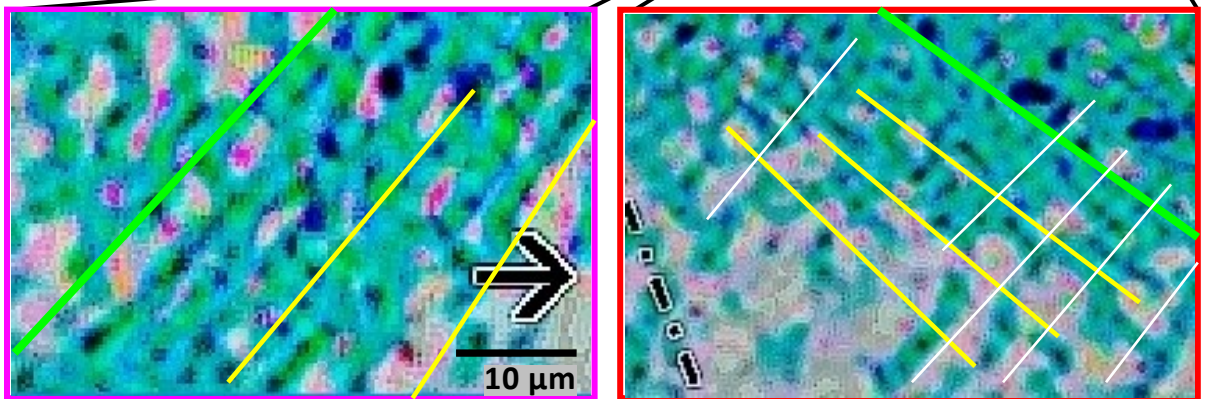


Fig 1: Details of the Central section through the apical meristem showing clear linear features ; black Bar = 25 μm

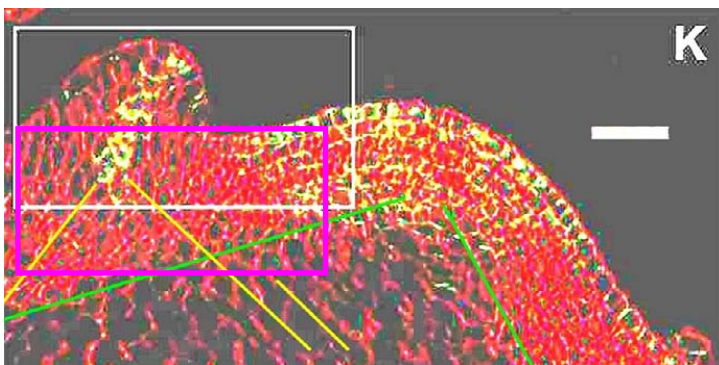
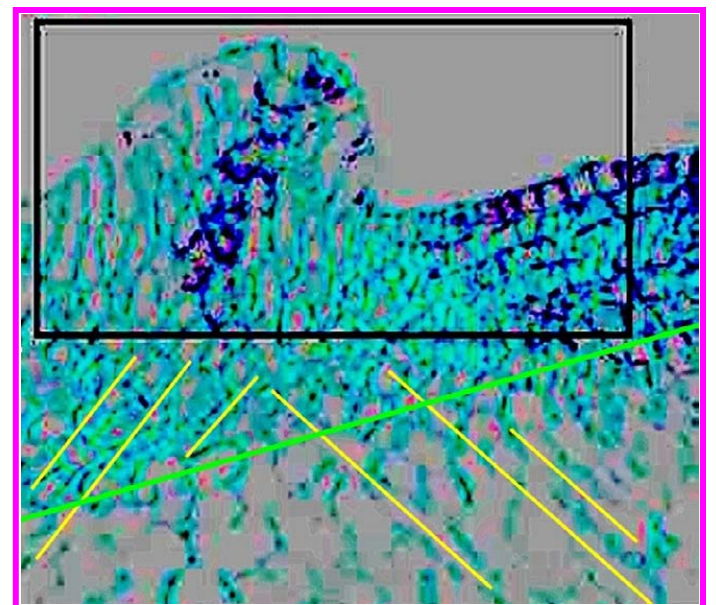
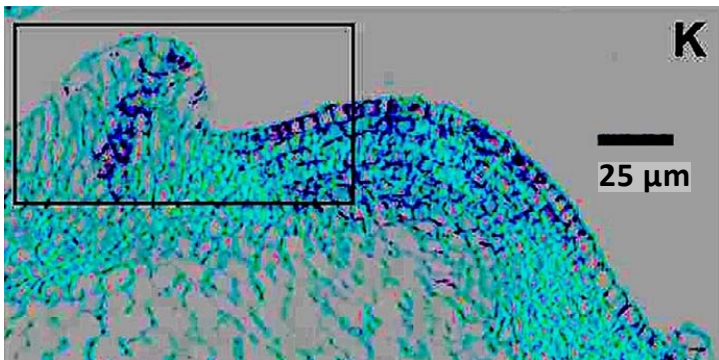
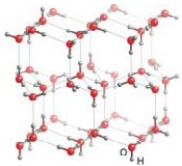


Fig 2: A newly initiated primordium in the peripheral zone of the meristem (see black box) . This primordium seems to grow on top of a secondary pyramidal crystal-structure (yellow) extending from a primary crystal structure (green)



4 The rhombic Sunflower Primordia may be caused by Ice-Crystals or by Water-Cluster-Crystals

There are two principle scenarios possible : In the **First scenario** the rhombic or bi-pyramidal structures are indeed formed by water-ice crystals grown on Ice-binding proteins. This is the most obvious scenario. But it can't explain how primordia would be initiated far above the freezing point. In the **Second scenario** a rhombic water-cluster lattice formed with support of similar proteins, initiates the growth of primordia. This is possible up to a temperature of $\approx +25^{\circ}\text{C}$



First Scenario : The rhombic crystals are indeed made of Water-Ice. This means the rhombic or bi-pyramidal crystal would have a **hexagonal crystalline structure** internally, denoted as **ice Ih**. The three-dimensional crystal structure of H_2O -ice is composed of bases of H_2O ice molecules located on lattice points within a two-dimensional hexagonal space lattice (\rightarrow left image). The bi-pyramidal crystal is then formed by hexagonal ice-plates which grow on top of each other, fixed in place by ice-binding-proteins.

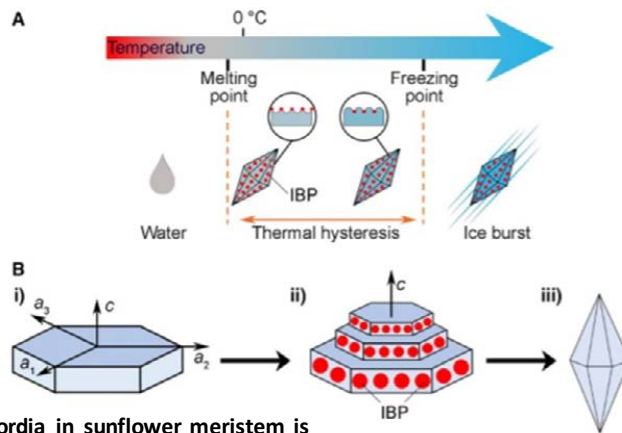
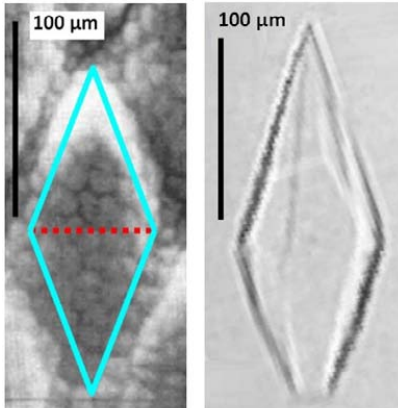


Fig. 1. Activities of IBPs. (A) TH. The adsorption of IBPs to the ice surface induces the lowering of the water freezing point and the raising of the ice melting point. At temperatures below the freezing point, it is possible to observe the growth of ice crystals in an explosive manner (ice burst). (B) Ice shaping. The morphology of ice crystals is strictly related to the ability of an IBP to bind one or more specific ice crystal planes. The hexagonal ice unit (i) is defined with a and c axes. The basal plane of the ice crystal is coloured blue, while the prismatic planes are light blue. IBPs bound to prismatic planes inhibit ice growth along the a -axes (ii), generating hexagonal bipyramid ice crystals (iii). IBPs stabilize small ice crystals and inhibit their growth into larger ones. IBPs are indicated as red spheres.

Fig. 2 : The rhombic shape and size of primordia in sunflower meristem is similar to bi-pyramid water-ice-crystals grown in Ice-binding protein solutions.

Ice-binding proteins are secreted into the environments around the host cells or are anchored on their cell membranes. Ice-binding proteins (IBPs) that perform a variety of biological roles have been isolated and characterized from different organisms, including fishes, insects, plants, bacteria, fungi, yeasts & algae. IBPs control growth & shape of ice crystals to cope with subzero temperatures in psychrophilic and freeze-tolerant organisms. IBPs in polar fishes block further growth of internalized ice and inhibit ice recrystallization of accumulated internal crystals. Algae use IBPs to structure ice. \rightarrow see : [Study to ice-binding proteins](#) by Tyler D. R. Vance and others, and \rightarrow [Study to IBPs_2](#)

Second Scenario : The rhombic crystal-like structures which form the primordia are caused by a „Water-Cluster-(Crystal)-lattice“.

Here we must consider the most stable water-clusters as base units for a large „Water-Cluster-Crystal“ with a multi-level structure as indicated in the images below. The small Pentamer $(\text{H}_2\text{O})_5$ and the pancake-shaped $(\text{H}_2\text{O})_{25}$ water-clusters, which are both **stable even in the vacuum and up to $\approx 25^{\circ}\text{C}$** , are the base elements of the much larger Icosahedral Water-Clusters $(\text{H}_2\text{O})_{100}$ and $(\text{H}_2\text{O})_{280}$. These stable **Icosahedral-Water Clusters** seem to be able to form thousand-times larger „Icosahedral Super-Clusters“, which then may form a „Rhombic-Super-Water-Cluster Crystal“ as shown below. The image on the bottom right shows a **6 µm** cluster of polystyrene particles which probably was formed by $(\text{H}_2\text{O})_{100}$ or $(\text{H}_2\text{O})_{280}$ Clusters \rightarrow see **Chapter 11 and 7** : “Magic number colloidal clusters”

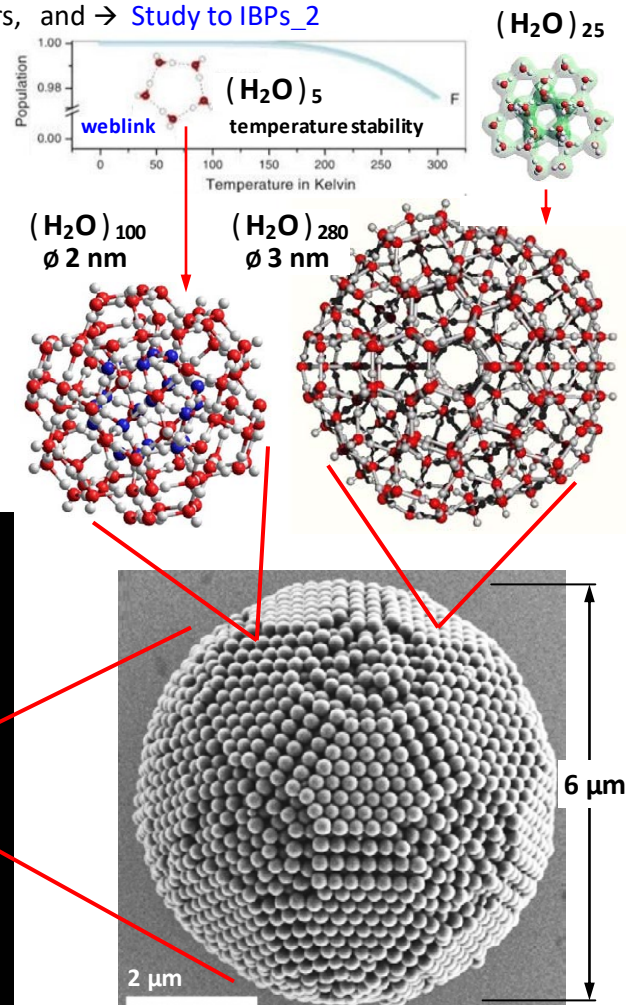
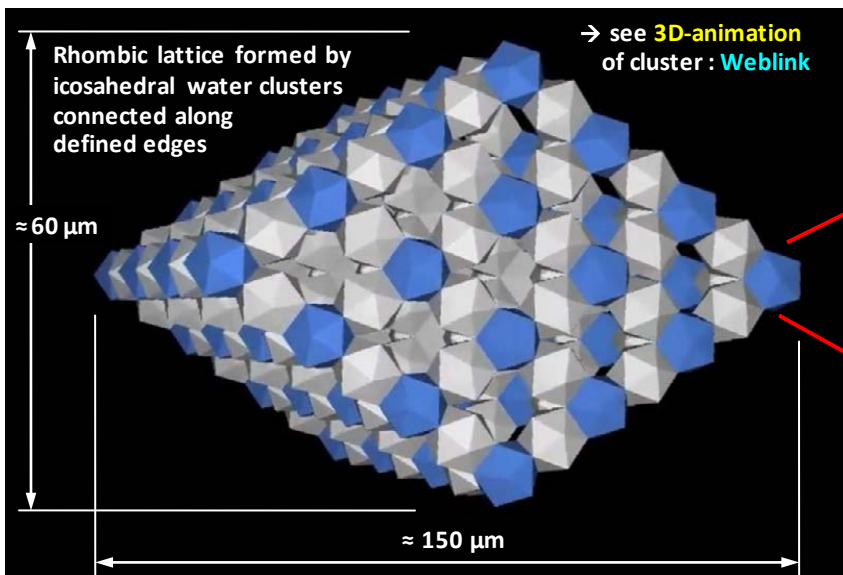


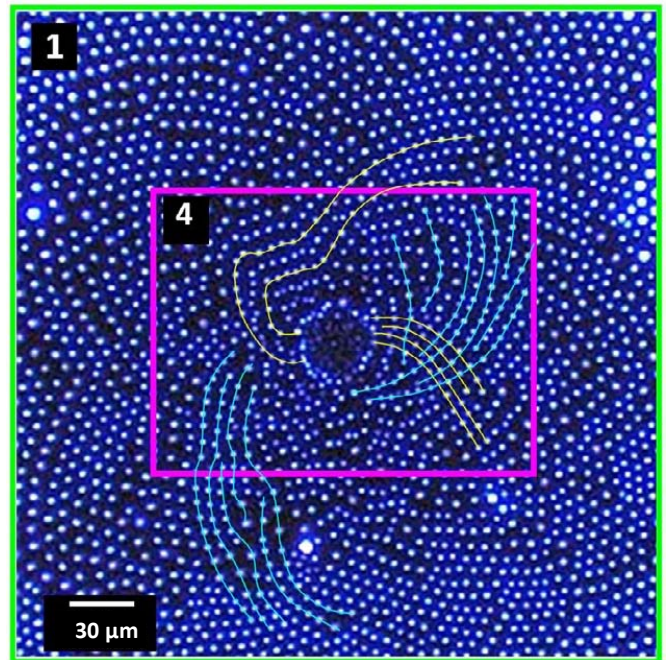
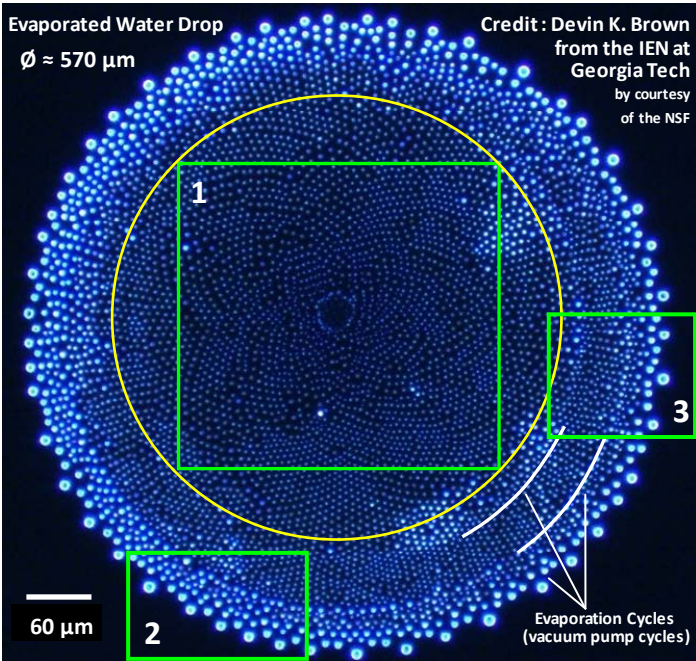
Fig. 3 : An icosahedral Cluster made of spherical Polystyrene particles ($\text{Ø}240\text{nm}$), formed during the evaporation of a Water / PS-particle suspension at $\sim 5^{\circ}\text{C}$ (\rightarrow Chapter 7 & 11)



5 The Microscope Image of an evaporated Water Droplet shows that Water is causing Phyllotaxis !

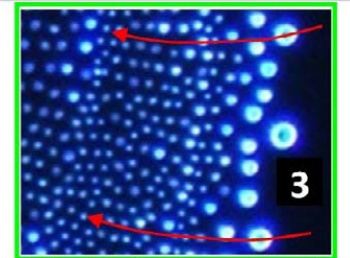
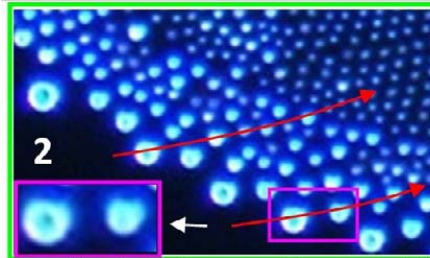
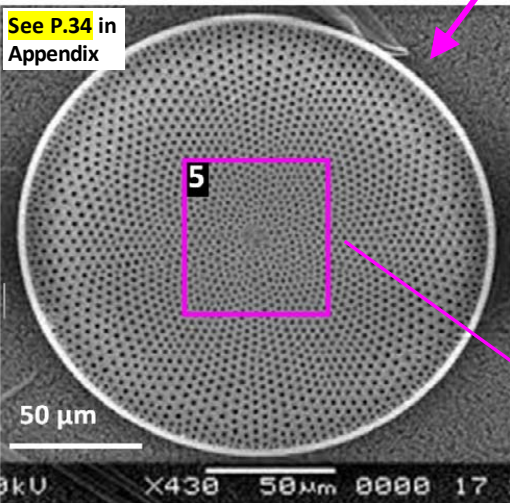
A Microscope Image of the residue of a small water drop, that evaporated on a silicon wafer, indicates that phyllotactic patterns seem to be caused by Water itself ! Electric charge and coulomb forces probably also play an important role !

Devin Brown an Engineer published this Image of an evaporated water drop in the web. (see : [news article 1](#); [article 2](#)) The little white dots, which are the remains of the evaporated water drop, are essentially water clusters with a \emptyset of approx. **3 μm** . These water clusters are arranged in a crystal-like lattice which obviously presents a phyllotactic pattern **Following Image-details are interesting** : 1.) The pattern seems to be strongly influenced by a large Central Cluster 2.) The residue of the large Central Water Cluster indicates a „**Super Water Cluster Crystal**“ as the center of the pattern.

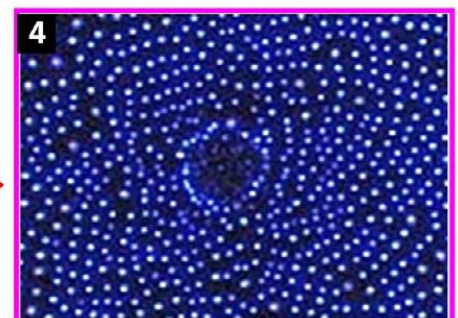
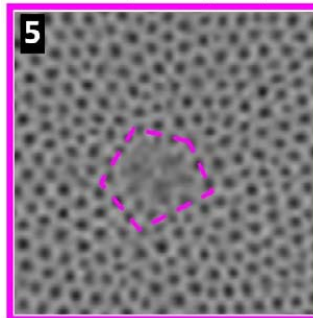


The Image shows the remains of an evaporated **Water Drop** Phyllotactic pattern with a ≈ 90 clockwise & ≈ 92 anti-clockwise parastichy-pair (spiral-pattern) visible. **Compare with Diatom !**

Detail 1: Central area of the evaporated Water Drop. The large Central Cluster seems to be responsible for the structure of the central area of the phyllotactic pattern



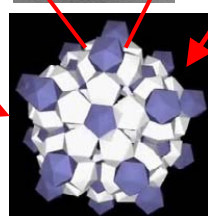
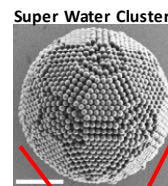
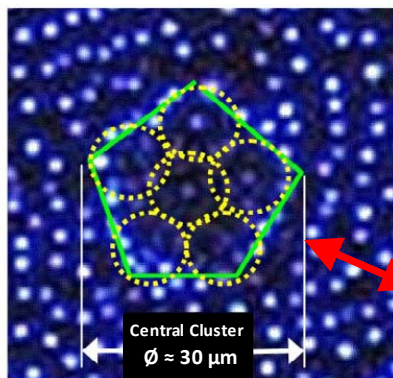
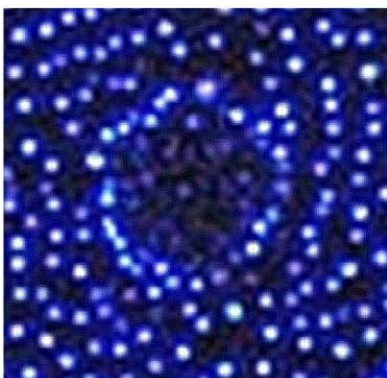
Detail 2 & 3 : It seems the water followed defined spiral-arms towards the center, during evaporation, as the deformed small "drops" indicate



Diatom with a phyllotactic pattern 60 anti-clockwise and 61 clockwise parastichy-pair, spiral-pattern, visible in **Coscinodiscus radiatus** Diatoms are micro-algae with SiO_2 cellwalls

Detail 5: Center of Diatom

Detail 4: Central Area & Central Cluster



To the Central Cluster : The roughly pentagonal shaped outline visible in the center of the Image seems to show the remains of an evaporated „**Dodecahedral Super Water Cluster-Crystal**“ as indicated on the image shown on the lefthand side. This **Dodecahedral Super Water Cluster Crystal** probably consisted of ≥ 6 „**Icosahedral Super Water Clusters**“ made of thousands of $(\text{H}_2\text{O})_{100}$ or $(\text{H}_2\text{O})_{280}$ Water Cluster \rightarrow **Chapter 6**

Central Cluster of Detail 4 (unmarked) Structure of Central Cluster indicated

5.1 A Phyllotactic Pattern : A Water-Cluster-Lattice that is influenced by a large central Water Cluster

The Image of the evaporated water drop indicates that a phyllotactic pattern is strongly influenced by a large pulsating (and rotating) Water-Cluster-(Crystal) at the center of the pattern, as the wave-groups marked in Fig. 2 show. The rim-area of the water-drop evaporated first. Then in the final stage the water in the center evaporated, leaving behind an outline (2D-projection) of the original central „Super Water Cluster Crystal“ in the form of a residue pattern. Each of the original „Super Water Clusters“ ($\varnothing \approx 3\text{-}10\ \mu\text{m}$) is represented by a white dot (\rightarrow cluster residue) on the image. The cluster residues indicate that the original water clusters were connected, as Fig. 4 indicates, e.g. for electric charge exchange.

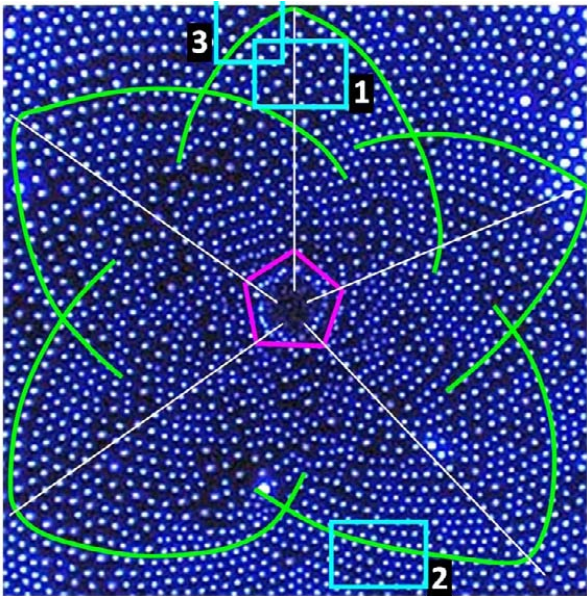


Fig 1 : Image of central area of an evaporated Water Drop. There is a clear connection visible between the pattern and the central cluster. The pattern is influenced by a pulsating Central Cluster.

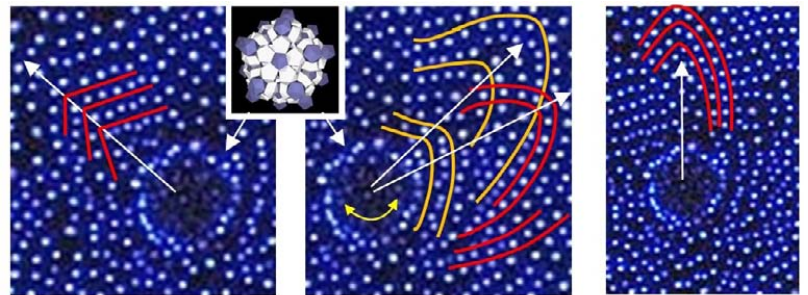


Fig 2 : Each corner of the pentagonal central cluster seems to be the starting point of one (or more) v-shaped wave-group (or shock-front)

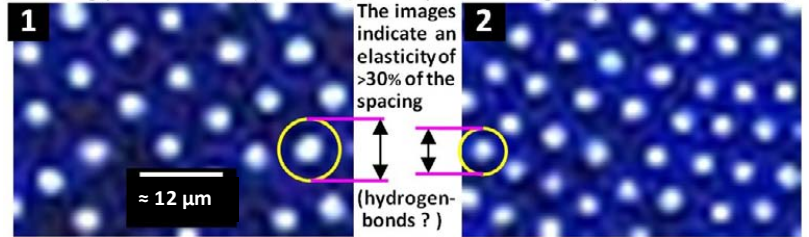
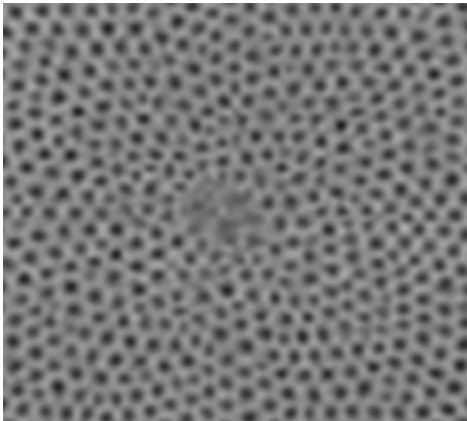


Fig 3 : Two same-size areas of the water-cluster-pattern that represents the evaporated water drop. The clusters in area 1 & 2 are equally spaced but density is different. Large „Super-Water-Clusters“ probably originally occupied the positions in the crystal-like lattice first



The phyllotactic pattern of this **Diatom** (micro-algae) is nearly identical to the pattern of the evaporated Water Drop.

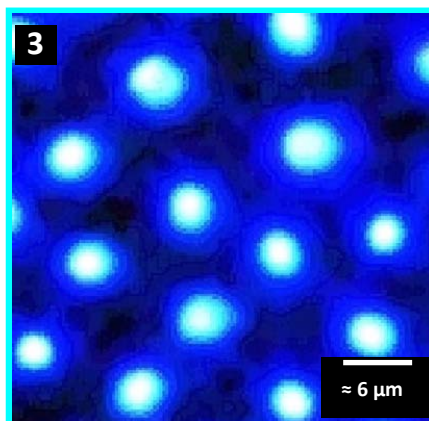
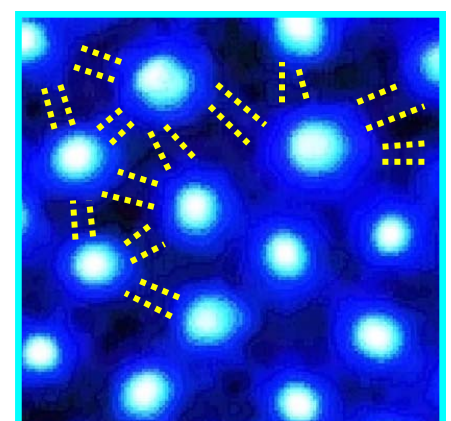


Fig 4 : The contrast- and brightness enhanced **Detail area 3** shows that the water-clusters ($\varnothing \approx 3 - 6\ \mu\text{m}$) which survived the evaporation process are still connected by a network of thin „water bridges“ as the yellow lines indicate.



The phyllotactic pattern formed by the evaporated water drop is similar to the pattern formed by the floret primordia on the sunflower capitulum. The difference is that the phyllotactic pattern of the sunflower shows more uniformity and it normally forms a Fibonacci-array (parastichy-pair) defined by two successive Fibonacci-Numbers from the **Fibonacci-Main Sequence F1**. These are usually



Fig 5 : Phyllotactic Pattern (Fibonacci-array) of the floret primordia in the Sunflower capitulum. This pattern is very similar but more uniform than Fig. 1

Fig 6: Sunflower capitulum with an unusual parastichy pair of **50**(blue)/**48** (red) - see Ch. 13.4

Fibonacci-Number pairs like **21, 34** or **34, 55**, out of the **F1-Fibonacci-Sequence**: 1, 1, 2, 3, 5, 8, 13, 21, 34, 55, ... or in rare cases out of other Fibonacci Sequences like F2, F7, F8 And in very rare cases also **Non-Fibonacci number-pairs as 48 & 50** are possible (see image). The mechanism that is responsible for Fibonacci-Number-pairs isn't clear yet! But the principle cause of Fibonacci-spiral-patterns seems to be a big **central „Super Water Cluster Crystal“** that defines at least one of the parastichy-numbers.

5.2 The evaporated Water Drop : A description & analysis of the cause of the Phyllotactic Pattern

This is a first try to describe how the [phyllotactic pattern](#) evolved in the evaporated water droplet shown in Chapter 5 :

To the origin of the Image : The image of the evaporated (dried) water droplet was made by **Devin K. Brown** a senior research engineer at the Georgia Tech Institute for Electronics and Nanotechnology. He discovered the droplet with the phyllotactic pattern when he was etching microscopic grooves in a silicon chip (wafer) with an electron beam. (see contrast enhanced image on the right) He used a special [Electron Beam Lithography System](#) for this task. Similar like a scanning electron microscope the Lithography System has a vacuum chamber for the electron beam, which holds the sample (in this case the chip/wafer). When Devin Brown was etching (grooving) the silicon chip (wafer) he noticed an accidental droplet of water with around half a millimeter diameter just outside his target area. Curious, he decided to make a photo of this water droplet with an optical microscope (an Olympus MX61 with an 10X eyepiece). **This image made by Devin Brown won the Grand Prize 2013 in the 2013 Electron, Ion and Photon Beam Technology and Nanofabrication micrograph contest.** → [Weblink](#)

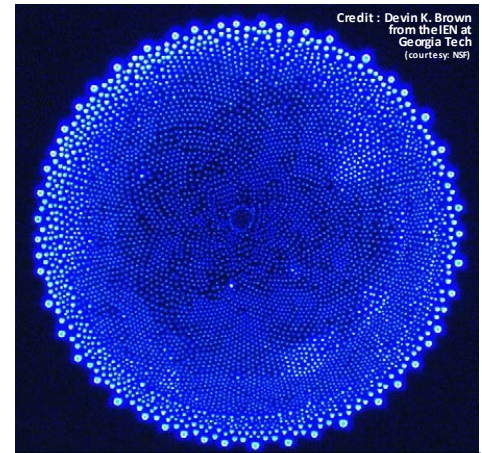
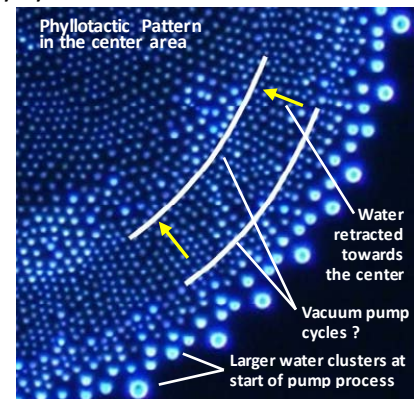


Fig. 1 : Evaporated (dried) water droplet on silicon wafer \varnothing 574 μ m

The possible source of water droplet : The droplet either was an accidental drop of water with other chemicals, that hit the sample, or it was caused by condensation in the vacuum chamber of the lithography system. Water can condensate on an object in a vacuum chamber if the temperature of this object is below the boiling (or sublimation) point at the current pressure inside the vacuum chamber. The chip had a relatively dark color. Therefore it was a good radiator and probably lost more heat than other surfaces in the chamber. The relatively cold surface of the chip may have supported condensation during the evacuation of the vacuum chamber.

How the pattern started to form : I made some own **microscopic experiments** which indicate that the visible circular pattern (lattice) of small water clusters already developed inside the water drop, on the surface of the silicon. It seems that electric charge on the surface of the silicon wafer, and probably a defect in the silicon wafer also played an important role for starting the pattern formation. In my experiments small micelle- or liposome-like clusters developed inside the water drop, settled down on the silicon support and started to form the circular pattern. The same was probably true in Devin Brown's case. Small amounts of membrane-forming molecules in the water were responsible for forming the micelle- or liposome-like clusters, → essentially water clusters enclosed in thin membranes. **The phyllotactic pattern that developed in the center area of the droplet** was strongly influenced by the large Central Cluster. The pattern formation seems to be the result of electric charge on the silicon surface & electric charge on the micelle- or liposome-like water clusters, causing coulomb forces between these water clusters. (Infos about charged water here [Interfacial water](#))



To the formation of the phyllotactic pattern and what the silicon wafer may have to do with it : My own microscopic experiment **Nr. 5** (see [Movie 5](#) and Fig. 5 on next page) indicates that probably a circular electric charged area on the surface of the silicon played an important role in the pattern formation. Devin Brown etched grooves in the silicon with an electron beam just beside the place where the water droplet evaporated. This probably caused an electric charge. A defect in the silicon wafer probably also played a role. Maybe this defect represents the center of an electric field and the center of the phyllotactic pattern where the large central water cluster was located. This large central Water Cluster has strongly influenced the structure of the pattern → see my explanation in **Chapter 6**. The whole pattern of smaller water clusters, which shows a lattice-like order, was clearly connected to, and influenced, by the large Central Water Cluster, maybe through charge flow to, or from, the center → [see also weblink: Overview of Water Cluster Hypothesis](#)

Similarity to the phyllotactic pattern of a Diatom (see also Appendix P.34) : The image below shows that the central area of the phyllotactic pattern of the **Diatom (Coccinodiscus)** see [weblinks: L1, L2, L3, L4](#) that looks similar to the central area of the water droplet pattern. The pattern of the Diatom also indicates that a large central cluster (a water cluster ?) was involved in the pattern formation ! The shown structure of the unicellular Diatom is the central area of the cellwall that is made of **SiO₂** ("hydrated" **silicon dioxide**). The silicon which the diatom used for its cellwall structure may be a connection to the silicon wafer case ! A **Diatom** is an unicellular algae that exists for \geq 200 million years. It may be the ancient plant species that first developed phyllotactic patterns (Phyllotaxis). **Please note the following important facts :**

Similarity to the phyllotactic pattern of a Diatom (see also Appendix P.34) : The image below shows that the central area of the phyllotactic pattern of the **Diatom (Coccinodiscus)** see [weblinks: L1, L2, L3, L4](#) that looks similar to the central area of the water droplet pattern. The pattern of the Diatom also indicates that a large central cluster (a water cluster ?) was involved in the pattern formation ! The shown structure of the unicellular Diatom is the central area of the cellwall that is made of **SiO₂** ("hydrated" **silicon dioxide**). The silicon which the diatom used for its cellwall structure may be a connection to the silicon wafer case ! A **Diatom** is an unicellular algae that exists for \geq 200 million years. It may be the ancient plant species that first developed phyllotactic patterns (Phyllotaxis). **Please note the following important facts :**

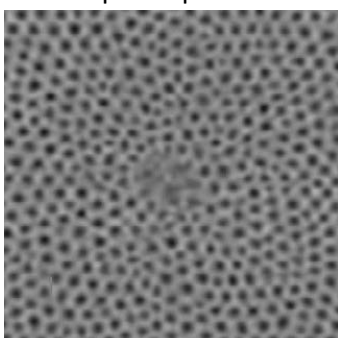


Fig. 2 : Center-area (50 μ m) of the Coccinodiscus Diatom

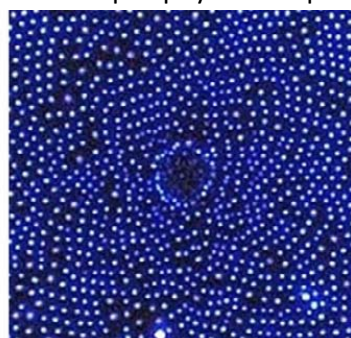


Fig. 3 : Center-area (220 μ m) of the evaporated water drop

- 1.) The porous cell wall of **diatoms** is called a **Frustule**, which is built of **hydrated Silica** made from **Silicic Acid**.
- 2.) **Hydrated Silica** is a form of silicon dioxide that contains water. When dehydrated it forms **Silica Gel**, a 3D-structure of **SiO₂** that **has nanometer-scale voids filled with Water**.
- 3.) The patterned silica structure in **diatoms** result from the activity of proteins like **Silaffins** and long chain **Polyamines**.
- 4.) Small quantities of **Silica** are absorbed from the soil by most plants, to be then excreted in the form of **Phytoliths**. **Phytoliths** are rigid microscopic structures which are made of **Silica** found in various plant tissues.

Microscopic experiments give some insight about the possible causes for the pattern formation

With these experiments I tried to find out what factors may be important to produce a phyllotactic pattern in an evaporating water droplet as shown in the image made by Devin K. Brown. I couldn't achieve a phyllotactic pattern, but at least some similar circular patterns with my experiments. And I can probably provide some first clues about some factors and conditions which may be required to produce a phyllotactic pattern as shown on Devin K. Brown's photo.

Description of the experiments : I used a Euromex Microscope with a 20x eyepiece and a smartphone with 4x zoom as digital camera. 4 different materials with mirror-like surfaces were used as support for the water-drops : **Gold, Silicon, Aluminium** and **Copper**. I could achieve **circular patterns** as shown in **Fig. 1** on the first three materials but not on copper. I used a fresh washed cotton cloth to clean the glass-container where I stored the distilled water. This contaminated the water with tiny amounts of **surfactant, peptides, polyamides** etc. as a **Raman spec (see below) of the residues** indicated, **Hydroxy groups & hydroxides (OH-)** were also indicated. Absolutely clean water didn't produce the circular patterns !

Conclusions: 1.) The visible clusters that form the circular patterns seem to be water-clusters which are surrounded by a thin layer (membrane) of **surfactant, peptides, polyamides** etc. so that stable micelle-/ liposom-like clusters formed. **2.)** These **micelle-, liposom- or cell-like** clusters are very stable. In some experiments they stayed constant in size and were absolutely stable, in other experiments they slowly shrank in size (evaporated) in a few minutes and left residues.

3.) The experiment shown in **Fig. 5** indicates that **a circular- or helical defect in the silicon may cause the circular pattern**

4.) Coulomb (electrostatic)-forces seem to play a role in the pattern formation. It seems the micelle-/ liposom-like clusters are electrically charged and repulsive forces act. Electron flow may increase the dynamic of pattern formation.

5.) An experiment with 1.5VDC (see Fig.3 below) showed a 10-20 times acceleration of the evaporation of the droplet !

6.) When the last water evaporates a circular-wave-pattern is visible in the center, that influences the pattern formation

7.) It seems the **electron beam of the lithography device** used by Devin Brown was partly responsible for the formation of the phyllotactic pattern, e.g by **electron diffraction aberration (electron flow)** to the etch-field limits (→ [page 101 here](#))

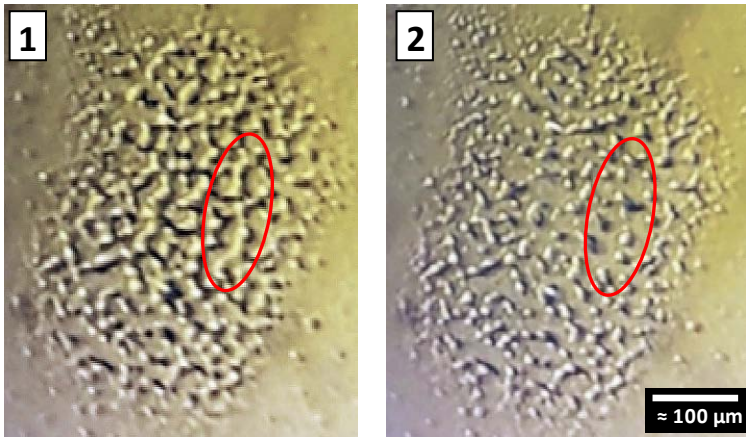


Fig. 1 : → **Movie 1** : shows the evaporation of a water drop on a gold surface. Image 1 shows the last „water-bridges“ between the micelle-, liposom- or cell-structures before they disappear and leave behind a stable circular pattern of these structures.

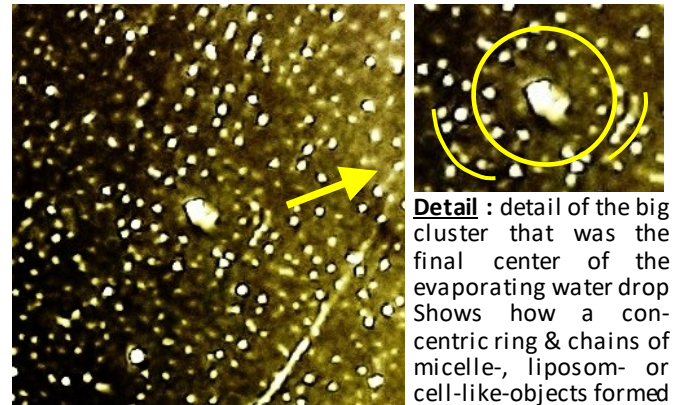


Fig. 2 : → **Movie 2** : Evaporation of a water droplet on a gold surface. The movie shows how the water drop finally shrinks (evaporates) around a larger cluster, that probably is a particle of the small amount of washing powder which I added to the distilled (clean) water.

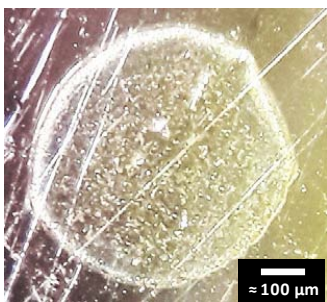


Fig. 3 : → **Movie 3** : This experiment shows the effect of electron-flow on the evaporation of a water drop. 1.5 VDC accelerate the evaporation by a factor of 10-20 !! Here I used distilled water without any contamination and added a very small amount of washing powder (‘‘Persil’’) ~ 0.1 vol%, which formed the shown circular pattern.



Fig. 4 : → **Movie 4** : Here a water drop is shown before it evaporated. Clusters in the water drop reflect the light of the light source. It is noticeable that the clusters keep approximately constant distances to each other. That indicates **Coulomb-forces** act

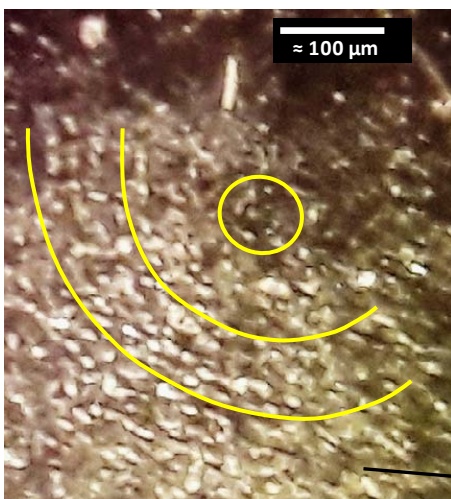
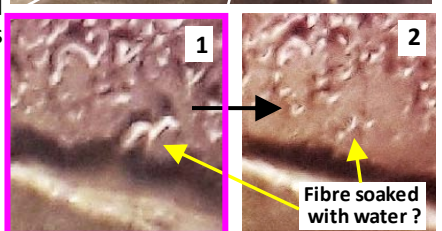
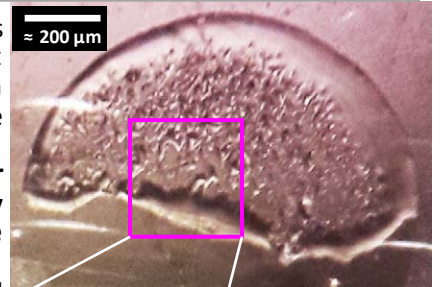
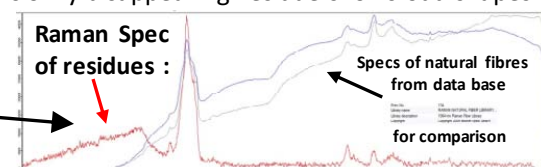


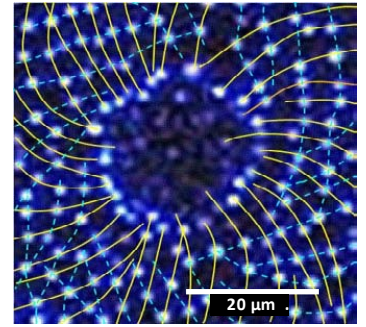
Fig. 5 (left) : → **Movie 5** : A water drop evaporates on a silicon surface. In the movie it is visible that **the small clusters in the drop already arrange in a pattern before the drop is evaporated !** The evaporated drop clearly shows a sector of a circular lattice ! **It seems that a circular- or helical defect in the silicon, that is partly located outside the drop, is causing the circular pattern !** (see yellow marks in Fig 5)

Fig. 6 (right) : shows the rest of an evaporated water drop on a silicon surface. The drop's slowly disappearing residue shows odd shapes !



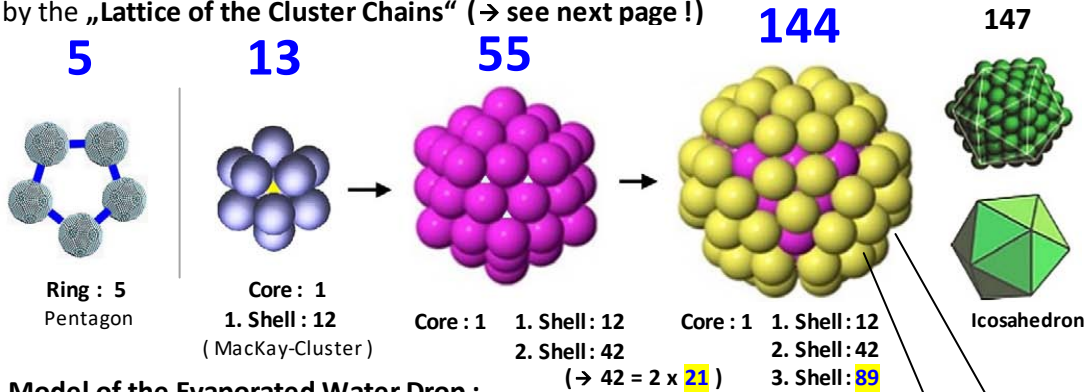
6 Fibonacci Numbers are defined by a large central Water-Cluster with Mackay-Cluster Geometry

There is a clear physical cause for phyllotactic Patterns, and for Fibonacci-Spiral patterns that appear in the apical meristem of plants, the site of organ formation. As the Image of the evaporated water drop shows (→ see right image & last two pages) a large central "Super Water Cluster Crystal" seems to cause the phyllotactic pattern. From each "Super Water Cluster" (→ white dots) of this "Cluster Crystal" a "chain of Super Water Clusters" is leading nearly radially outward on a slightly curved spiral-path (→ yellow lines). This set of "Super Water Cluster Chains" defines the first (1.) Fibonacci-Number! This number is precisely linked to the number of "Super Water Clusters" in the central "Super Water Cluster Crystal" which seems to be defined by icosahedral "Mackay"-Cluster geometry. A Mackay Cluster is a very stable Nanoparticle/Cluster due to its electron configuration. It is important to note that the first two Mackay clusters are defined by the Fibonacci-Number 13 & 55! And an extreme stable variation of the third Mackay-Cluster (147) has the Fibonacci-Number 144! The 2. Fibonacci-Number in the Fibonacci-pattern is defined by the „Lattice of the Cluster Chains“ (→ see next page!)



1. Fibonacci Number (→ yellow chains) 2. Fibonacci Number (→ blue chains)

Fig 2: Each cluster of the central "Super Water Cluster Crystal" is the start of a Water Cluster Chain

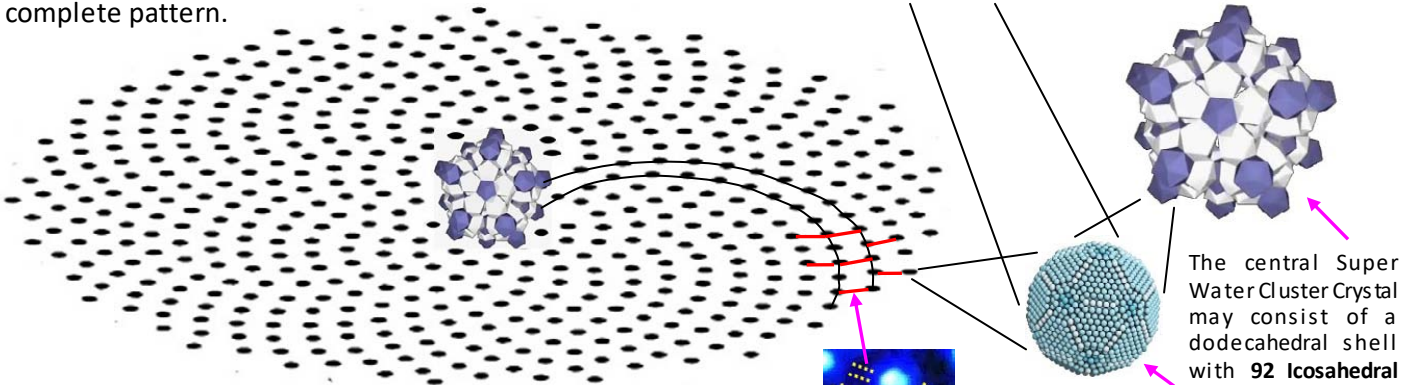


Model of the Evaporated Water Drop :

There is a "Super Water Cluster Crystal" in the center with either a dodecahedral shape or an icosahedral Mackay-Cluster. Each "Super Water Cluster" in this central "Cluster Crystal" is the starting point of a "Super Cluster Chain" which forms with other such chains the complete pattern.

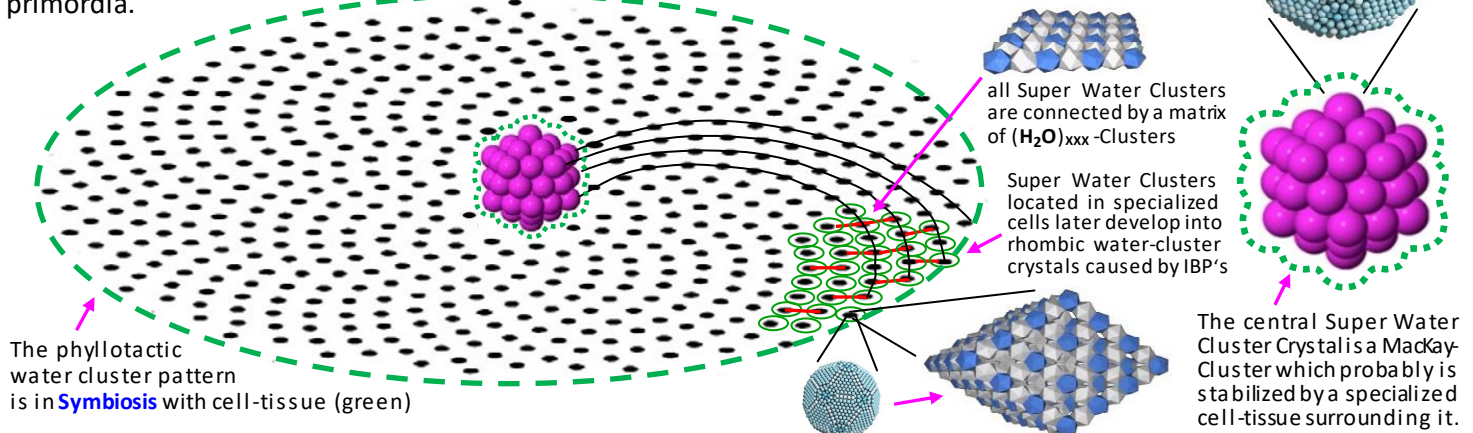
Fig 1: The image on the left shows the Cluster-Geometry of the central "Super Water Cluster Crystal" that probably defines the "1. Fibonacci-Spiral-Set" of a Fibonacci-Spiral-Pattern with the described „Super Water Cluster Chains“ which start at each of the "Super Water Clusters" in the Central Cluster Crystal.

(→ Here an example of an ultra-stable Mackay 144 Gold Cluster: $Au_{144}(SR)_{60}$) → see : [Weblink](#)
→ see also : [Magic numbers](#)



Model of the phyllotactic pattern source in the Sunflower meristem:

There is also a "Super Water Cluster Crystal" located in the center of the Sunflower meristem (capitulum). In all probability this cluster has an icosahedral Mackay-Cluster-geometry. And each "Super Water Cluster" in this central Cluster Crystal is the starting point of a "Super Water Cluster Chain" which forms the phyllotactic pattern, together with all other such Cluster Chains. But here the central cluster and the cluster-chains are probably stabilized by a specialized cell-tissue which uses special proteins (like IBP's) that help to stabilize the position and size of the central cluster and the super water cluster chains. From each super water cluster of the phyllotactic pattern later a rhombic Super Water Cluster Crystal (ice-crystal) evolves, with the help of IBP's, that defines the position of a floret primordia.



7 Fibonacci Spiral Patterns seem to be the result of a circular crystal-like lattice of Water Clusters

To generate a precise Fibonacci-Spiral Pattern the plant is using a crystal-lattice as reference ! This crystal-lattice in all probability is made of "Super Water Clusters" which in principle have an icosahedral geometry. These Super Water Clusters consist either of $(H_2O)_{100}$ or $(H_2O)_{280}$ icosahedral water Clusters, and they may reach diameters of up to $6\mu m$! This means cell-size ! Proof that such "Super Water Clusters" can form comes from an experimental study (see below)

The **Pentagon** and the **Icosahedron** are the only two geometrical objects where the **Golden Ratio**, the constant which defines Fibonacci-Numbers, is directly built into their geometrical structure ! Water molecules can form water clusters with icosahedral shape (large clusters) and water clusters with dodecahedral shape, made of pentagons (small clusters)

The following image describes in principle how a Fibonacci-Spiral Pattern can develop, based on a circular crystal lattice that either consists of icosahedral or pentagonal Water Clusters. The 1.Fibonacci-Number is defined by the number of Super Water Clusters in the Central Cluster. And the 2. Fibonacci-Number is defined by the "Water Cluster Lattice" which is surrounding the central cluster. In the image every pentagon or icosahedron represents a cluster chain

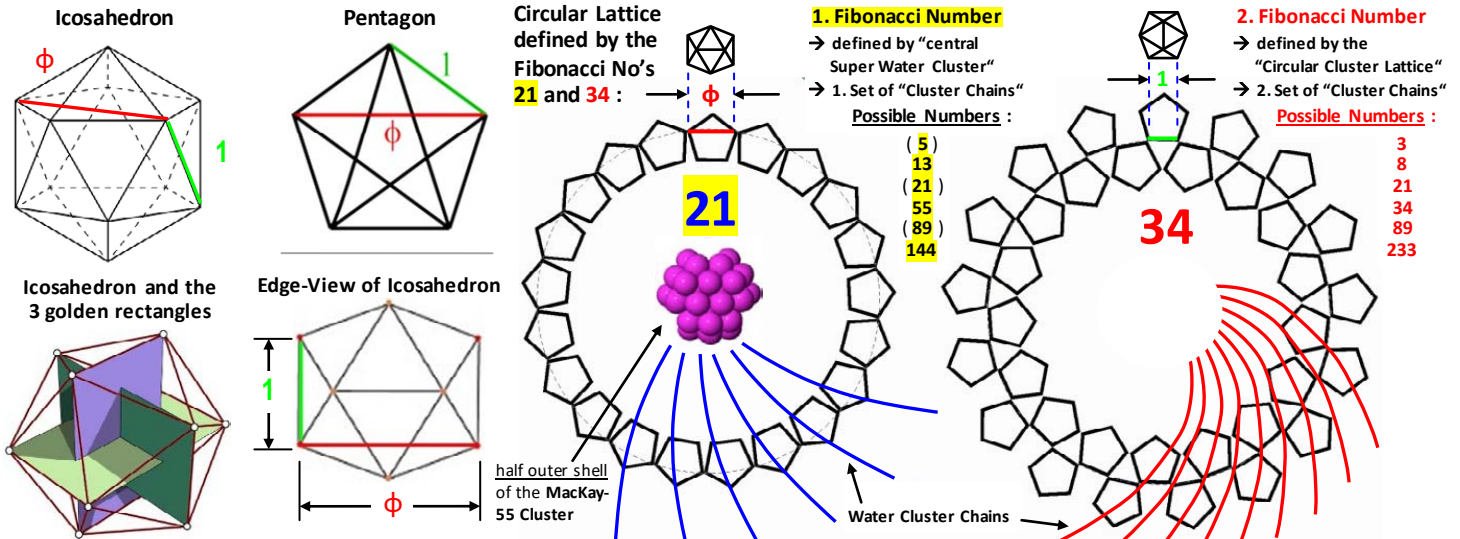
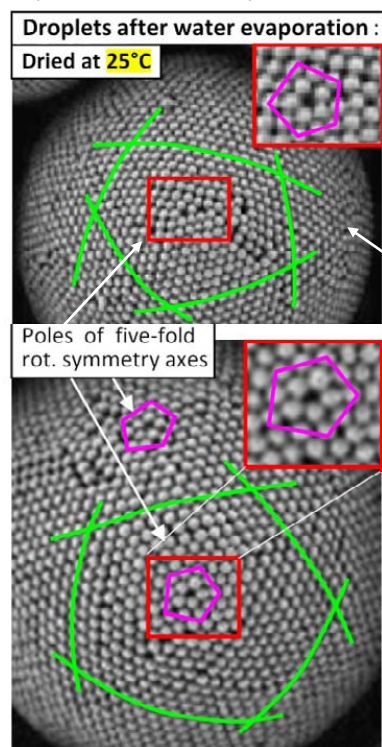


Fig 1: shows how the Golden Ratio (\rightarrow the ratio of constant Phi (ϕ) and 1) is built into the Geometry of the Pentagon and Icosahedron

Fig 2: A Fibonacci Spiral Pattern precisely defined by a circular crystal lattice that either consists of Icosahedral- or pentagonal Water-Clusters. The 1.Fibonacci-Number is defined by the number of Super Water Clusters in the central Cluster. The 2. Fibonacci-Number is defined by the "Cluster Lattice-(Geometry)" surrounding the central Cluster. The Fibonacci-Numbers 13,55,144 represent full Mackay-Clusters & 21,89 represent full or half outer shells

Experimental Study : \rightarrow PS-Clusters with a precise geometry which form during the evaporation of Water

In this study small spherical particles made out of Poly-Styrene (PS), with a diameter of $0.25\mu m$ (\rightarrow the little white spheres) were suspended in water. This mixture of water and PS-particles was then mixed with Oil to get an emulsion. Then Emulsion-droplets (water droplets + PS-particles) were collected & stored in 1.5 ml glass vials. These vials were then kept at different temperatures ($5^\circ C$, $25^\circ C$ & $85^\circ C$) for the controlled Water evaporation. At $5^\circ C$ PS-Clusters ($\phi 6\mu m$) with



precise defined shell structures formed during water evaporation (see Fig. 4). These Clusters have a Rhombicosidodecahedron-geometry, a mixture of an Icosahedron and a Dodecahedron. A $(H_2O)_{100}$ Water-Cluster has precisely the same geometry !! The authors of the study (\rightarrow summary of Study see in Chapter 11) say that especially capillary forces & entropy maximization are driving factors for the geometry. However this can't explain the formation of the quite complex five-fold rotational symmetry of the PS-particle balls (dried droplets) !! PS-Clusters dried at $25^\circ C$ show the birth of the five-fold symmetry axis which more likely is the result of molecular forces caused by e.g. $(H_2O)_{100}$ Water Clusters !

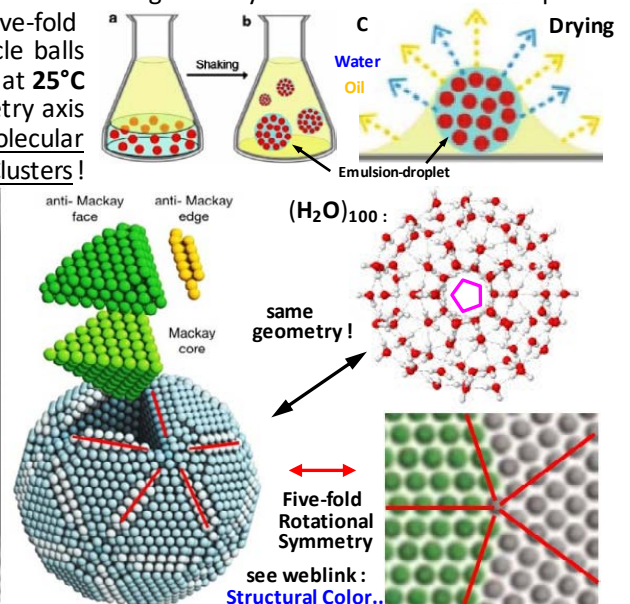
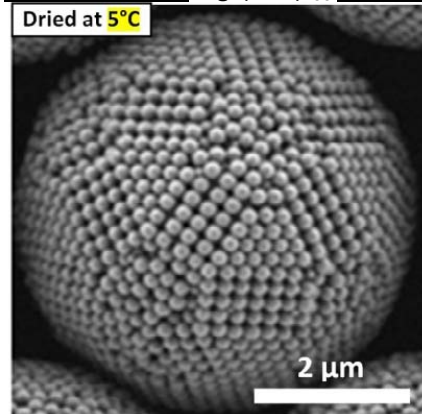


Fig 3: Emulsion droplets evaporated at $25^\circ C$ only show the birth of the five-fold symmetry axes on the surface

Fig 4: Emulsion droplets evaporated at $5^\circ C$ produce a precise geometry which is nearly identical to the $(H_2O)_{100}$ -Cluster geometry

Fig 5: Schematic of emulsion-droplet production and evaporation; dried PS-particle balls show internal icosahedral Mackay-Cluster geometry and five-fold symmetry

8 The asymptotic ratio of successive **Fibonacci numbers** leads to the **Golden Ratio constant φ (or Φ)**

The Fibonacci Sequences describe morphological patterns in a wide range of living organisms. This is the most remarkable organizing principles in nature, mathematically describing natural and manmade phenomena

If we want to understand where the Fibonacci Numbers in Phyllotaxis come from, we must have a look were else in nature, in the physical world, the **Golden Ratio Constant ($\Phi = \varphi$ or Φ)** appears. Because the Fibonacci Numbers and Phyllotaxis are defined by this constant ! In nature the pure constant **Phi** appears in crystals where it defines the crystal-lattice geometry. It appears especially in **Icosahedral**- and in **Dodecahedral Crystals**

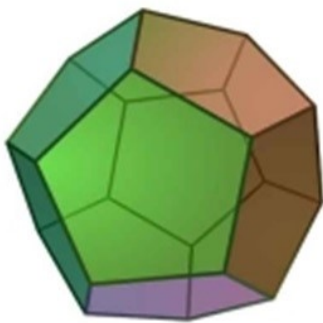
Note: The shape of crystals in the macro-scale mirrors structure & arrangement of molecules in the micro-scale

The Golden Ratio constant: $\varphi = x = \frac{1+\sqrt{5}}{2} = 1.618034\dots$

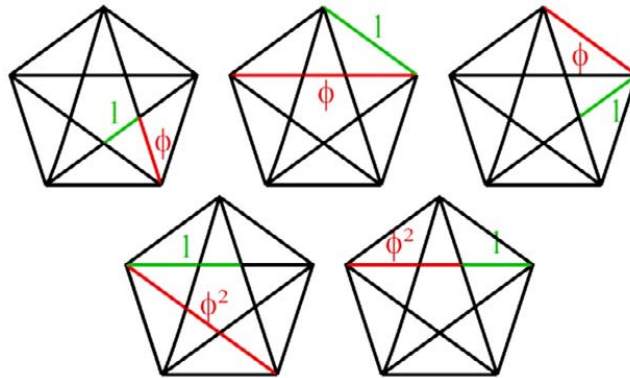


The Sunflower (Helianthus)

The **Pentagon** and its correlation with φ (ϕ) :
(edge-length = 1)



weblink : [Dodecahedron](#)

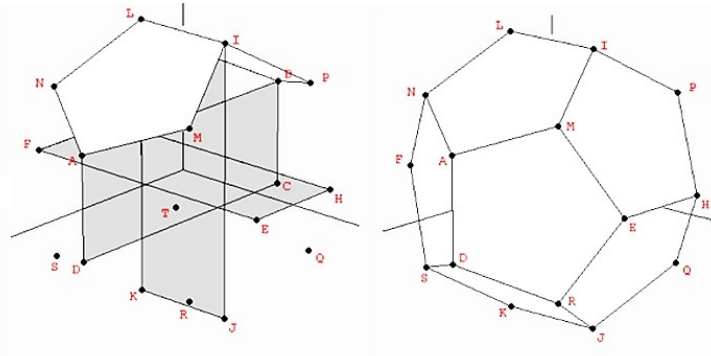
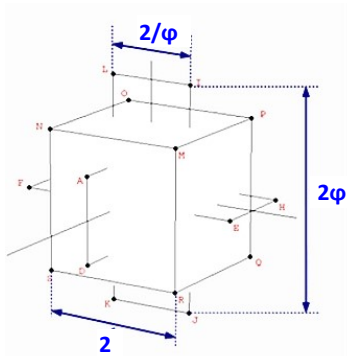


The **Fibonacci numbers** defined by φ :

1/1 = 1
2/1 = 2
3/2 = 1.5
5/3 = 1.667
8/5 = 1.6
13/8 = 1.625
21/13 = 1.615
34/21 = 1.619
55/34 = 1.618



The **Dodecahedron** in cartesian coordinates :



The vertices of the Dodecahedron expressed by constant φ and 1 :

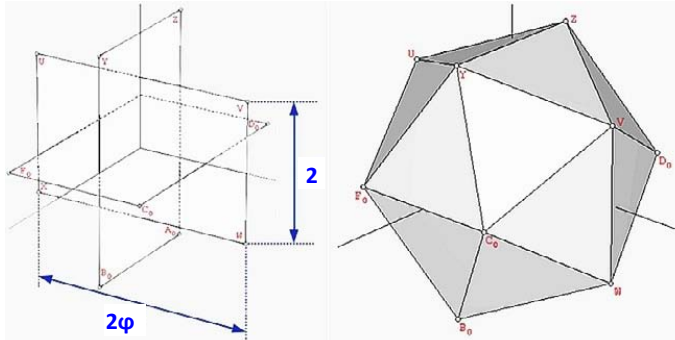
A (φ , 0, 1/φ)	M (1, 1, 1)
B (-φ, 0, 1/φ)	N (1, -1, 1)
C (-φ, 0, -1/φ)	O (-1, -1, 1)
D (φ, 0, -1/φ)	P (-1, 1, 1)
E (1/φ, φ, 0)	Q (-1, 1, -1)
F (1/φ, -φ, 0)	R (1, 1, -1)
G (-1/φ, -φ, 0)	S (1, -1, -1)
H (-1/φ, φ, 0)	T (-1, -1, -1)
I (0, 1/φ, φ)	
J (0, 1/φ, -φ)	
K (0, -1/φ, -φ)	
L (0, -1/φ, φ)	

The vertices of the dodecahedron obtained from the **cube** and **three orthogonal Golden Rectangles** with the side relationship $1 / \varphi^2$ (= $2/\varphi : 2\varphi$)

The **Icosahedron** in cartesian coordinates



weblink : [Icosahedron](#)



The vertices of the Icosahedron expressed by constant φ and 1 :

U (0, -φ, 1)	C _φ (φ, 1, 0)
V (0, φ, 1)	D _φ (-φ, 1, 0)
W (0, φ, -1)	E _φ (-φ, -1, 0)
X (0, -φ, -1)	F _φ (φ, -1, 0)
Y (1, 0, φ,)	
Z (-1, 0, φ,)	
A _φ (-1, 0, -φ,)	
B _φ (1, 0, -φ,)	

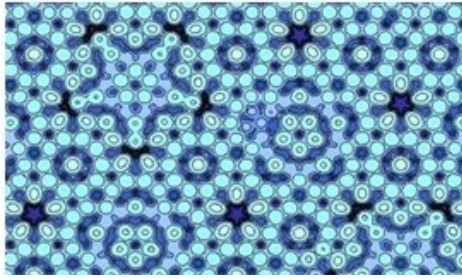
The vertices of the Icosahedron constructed with **three orthogonal Golden Rectangles** with the side relationship $1 / \varphi$ (= $2/2\varphi$)

→ see also weblink : [Phi-sacred-solids](#)

9 Icosahedral- and Dodecahedral Forms can be found in Crystals and they appear in many Organisms

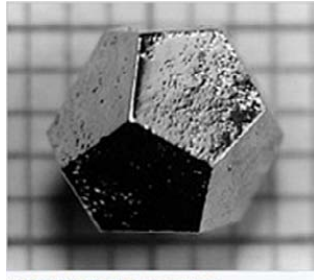
Polyhedral forms (e.g. Icosahedra) do not only appear in crystals, they also occur at different length scales in lifeforms, from marine organisms (like diatoms & radiolaria) to protein nanocontainers of viruses (e.g. with icosahedral symmetry)

Water Clusters seem to play a major role in the growth-process of diatoms, radiolaria, bacteria, viruses and of course in phyllotactic patterns in plants! The mentioned lifeforms and plants seem to use the structure of water clusters and water-cluster-lattices as reference for their own structure. They grow in **symbiosis** with the inorganic Water Clusters!



see: [Quasicrystals Structure and Dynamics](#)
→ [lecture: Quasicrystals Structure & Dynamics](#)

In German: "Strukturuntersuchungen von ikosaedrischen Quasikristallen": [Weblink PDF](#)



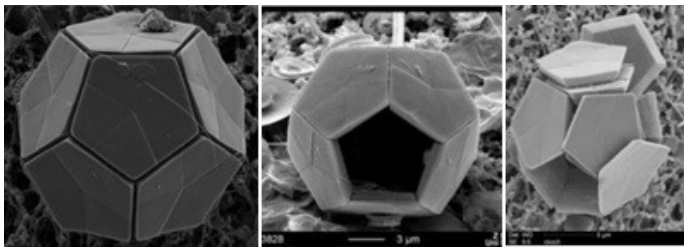
A Ho-Mg-Zn dodecahedral quasicrystal formed as a pentagonal dodecahedron, the dual of the icosahedron. The quasicrystal has faces that are true regular pentagons

A quasicrystal, or **Quasicrystal** is a structure that is ordered but not periodic. A quasicrystalline pattern can continuously fill all available space, but it lacks translational symmetry. While crystals, according to the classical crystallographic restriction theorem, can possess only two-, three-, four-, and six-fold rotational symmetries, the Bragg diffraction pattern of quasicrystals shows sharp peaks with other symmetry orders — for instance, **five-fold**. Roughly, an ordering is non-periodic if it lacks translational symmetry, which means that a shifted copy will never match exactly with its original.

In the higher-dimensional space we can describe a quasicrystalline structure as a **periodic one**. The actual quasicrystalline structure in the 3D-physical space can then be obtained by a appropriate projection/section techniques. Thus it is enough to define a single unit cell of the nD-structure. The contents of that nD-unit cell consists of "hyperatoms" (occupation domains, ..) in analogy to the atoms in a normal unit cell. This enables us to describe the whole quasicrystal structure with a finite set of parameters. If we described it in 3D-space only, we needed thousands of atoms to obtain a representative volume segment of the whole structure as well as all parameters that go with it (eg. thousands of positions). → [weblink](#)

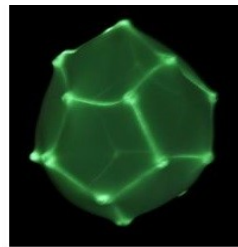
Diatoms are a major group of algae, specifically microalgae found in the oceans & waterways of the world. Living diatoms make up a significant portion of the Earth's biomass: they generate about 20 - 50 percent of the oxygen produced each year, take in over 6.7 billion metric tons of silicon each year from the waters in which they live, and contribute half of the organic material found in the oceans

Radiolaria are tiny protozoa (0.1 – 0.2mm) that produce intricate silica (mineral) skeletons. They are found as zooplankton and exist solitary and in colonies. The single-celled Radiolaria are complex, sophisticated organisms. The body is divided into a central capsule containing the endoplasm & nucleus and the extracapsulum which contains peripheral cytoplasm composed of a frothy bubble-like envelope of alveoli & a corona of ray-like axopodia and rhizopodia.

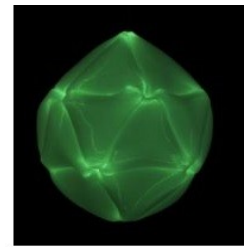


Braarudosphaera bigelowii – A perfect **Dodecahedron**

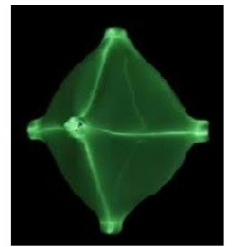
→ See [weblink: The geometry of Diatoms and Radiolaria](#)



Dodecahedral
(Pseudoglobulus footballi)



Icosahedral
(Metamorphosus lucidus)

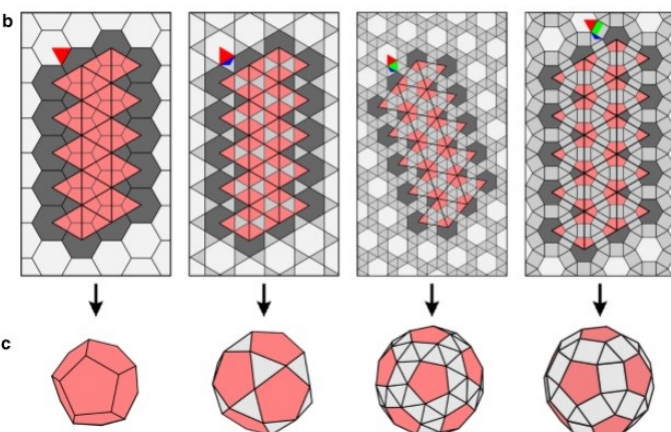


Octohedral
(Hexapodus inflatus)

Structural puzzles in virology solved with an overarching **Icosahedral** design principle

by Reidun Twarock & Antoni Luque - [Weblink to the study: Weblink 1](#); [PDF-document](#)

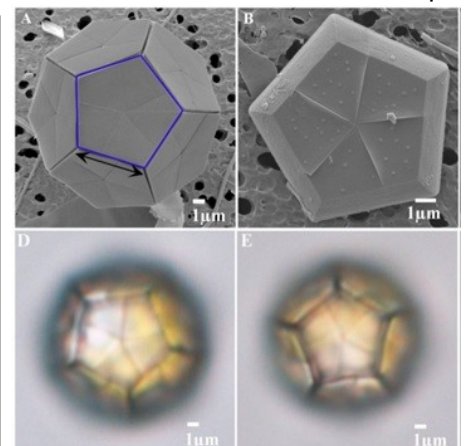
Extract from the study: Viruses have evolved protein containers with a wide spectrum of **icosahedral architectures**. The geometric constraints defining these container designs are still open problems in virology. We show that there is an overarching design principle for icosahedral, as well as octahedral, architectures that can be formulated in terms of the Archimedean lattices and their duals. **This design principle also applies to other Icosahedral Structures in nature**, and it offers alternative designs for man-made materials and nanocontainers in bio-nanotechnology.



b.) Shows the Construction of Archimedean solids via **replacement of the 12 hexagons by pentagons** in analogy to the **Caspar-Klug construction** (see also Fig. 1b).

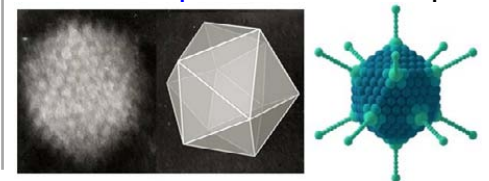
c.) The polyhedral shapes corresponding to the examples shown in b. They each correspond to the smallest polyhedron in an infinite series of polyhedra for the given lattice type.

Bacterium with Dodecahedral shape



[Weblink: https://imgur.com/gallery/wMKMv](https://imgur.com/gallery/wMKMv)

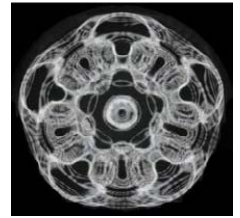
A **Virus** and a **Capsid** with **Icosahedral Shape**



10 Water Clusters

Water Clusters can have properties like a Liquid or a Solid, depending on cluster size and temperature.

The most stable and long-lived Water Clusters are the $(\text{H}_2\text{O})_{20}$; $(\text{H}_2\text{O})_{100}$ and $(\text{H}_2\text{O})_{280}$ Clusters. The onset of an ice-like structure occurs at a cluster-size of approximately $n = 275 \pm 25$ molecules. For cluster sizes $\geq n = 475 \pm 25$ the band of crystalline ice (3200 cm^{-1}) dominates the OH-stretching region. → Large Water Clusters can behave like solid ice. But the crystallization of water clusters strongly depends on the ambient temperature (→ **black-body**-(IR)-radiation). At higher temperatures $>4^\circ\text{C}$, pulsating water clusters can produce **standing-wave**-patterns with wave-lengths equal to around 2x their diameter, which may be very similar to the macro-scale standing wave patterns of Water ! →



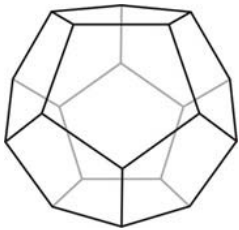
Water excited by Music
see more **Movies** in the **Appendix**

In chemistry a **Water-cluster** is a discrete hydrogen bonded assembly or cluster of molecules of **water**. These clusters have been found experimentally in various forms of water ; in **ice**, in crystal lattices and in bulk liquid water.

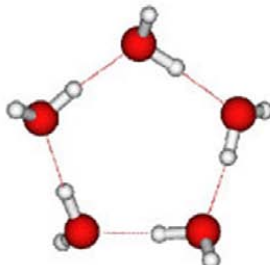
Water can form very larger clusters. **Li Shu et al.** reported images of large water clusters of up to **100 μm (0.1mm)** size ! Experimental data indicate that when water has its highest density at **4°C**, water clusters reach maximum sizes and stability (durability). Water Clusters may help to explain many anomalous water characteristics such as its highly unusual density temperature dependence, and they may be responsible in the stabilization of certain supramolecular structures. Support is growing behind the idea that Water Clusters play key roles in operations ranging from molecular binding to turning on and off basic cell processes. → see „**The Scientist**“: **Structured-water-is-changing-models**

For more information → see : [Cluster_Overview](#) ; [\(H2O\)100 Cluster](#) ; [Proof for \(H2O\)280 Cluster](#) ; [Icosahedral_Clusters](#)

Dodecahedron

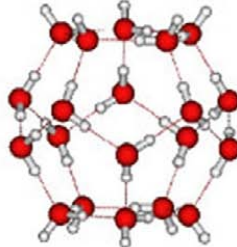


$(\text{H}_2\text{O})_5$



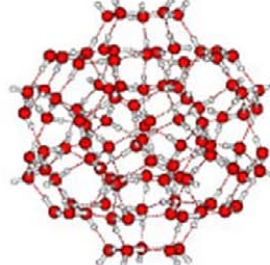
(a)

$(\text{H}_2\text{O})_{20}$



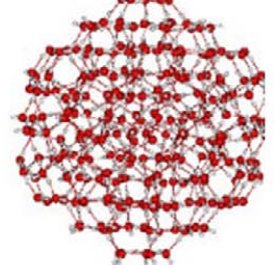
(b)

$(\text{H}_2\text{O})_{100}$



(c)

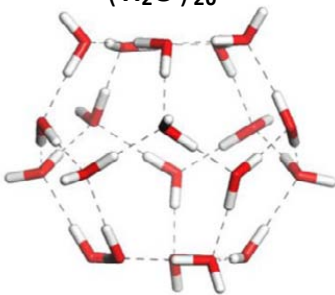
$(\text{H}_2\text{O})_{280}$



(d)

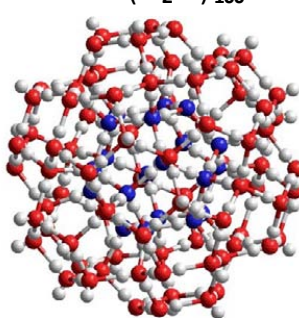
Pentamer (pentagonal) coordinated water network : (a) cyclic pentamer consisting out of 5 water molecules ; (b) **Dodecahedral water-cluster** $(\text{H}_2\text{O})_{20}$ consisting out of 20 water-molecules ; (c) **homological icosahedral water-cluster** $(\text{H}_2\text{O})_{100}$ → This cluster can break down in **5 dodecahedral clusters** and ; (d) The **icosahedral** $(\text{H}_2\text{O})_{280}$ cluster, can break down in **14 dodecahedral clusters**

$(\text{H}_2\text{O})_{20}$



Structure of the $(\text{H}_2\text{O})_{20}$ Dodecahedral water-cluster : The red sticks represent oxygen atoms, white sticks represent hydrogen atoms, and the black dashed lines represent hydrogen bonds

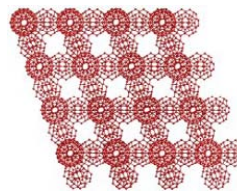
$(\text{H}_2\text{O})_{100}$



$(\text{H}_2\text{O})_{100}$ Icosahedral Water-Cluster ($\approx 2 \text{ nm}$ diameter)

The central dodecahedral $(\text{H}_2\text{O})_{20}$ cluster is shown in blue color.

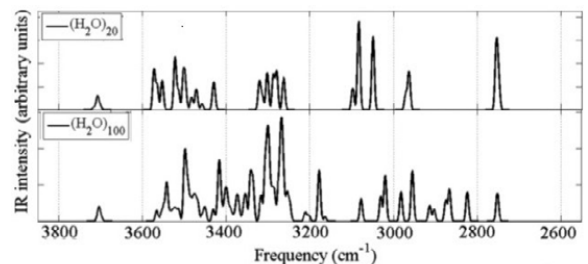
Matrix (lattice) of the $(\text{H}_2\text{O})_{100}$ water-cluster



Computed vibrational spectra for the $(\text{H}_2\text{O})_{20}$ & $(\text{H}_2\text{O})_{100}$ water-cluster : The absorption bands are in the frequency range of $2700\text{-}3700 \text{ cm}^{-1}$

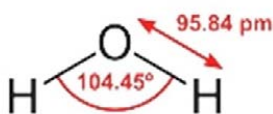
This corresponds to infrared radiation in the **wave-length range of approx. 4 to 6 μm**.

(→ see diagram below)



A few words to **water** and **water ice** :

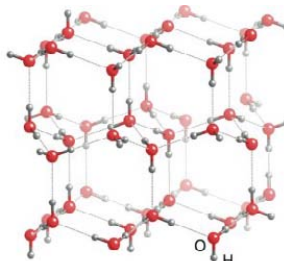
Water is described as the "solvent of life". It is the most abundant substance on Earth' surface



The shape and geometry of a Water-molecule

Note : the H-O-H gas phase bend angle of H_2O is **104.48°** which is close to the corner angle **108°** of a **Pentagon** ! **Pentamers** (Pentagons) & **Dodecahedra** are the perfect Geometry for H_2O

All the **Water-Ice** on Earth's surface is of a **hexagonal crystalline structure** denoted as **ice 1h**. The three-dimensional crystal structure of H_2O ice : **ice 1h** is composed of bases of H_2O ice molecules located on lattice points within the two-dimensional hexagonal space lattice. Ice 1h is remarkable in that the oxygen ions (O^{2-}) form an ordered lattice, while the protons (H^+) lack any kind of long-range order — in flat contradiction with the usual paradigm for solids. Like water, ice absorbs light at the red end of the spectrum preferentially as the result of an overtone of an oxygen-hydrogen (O-H) bond stretch.



Further information to **spectra of water-clusters** :

IR vibrational spectra of $(\text{H}_2\text{O})_{20}$ and $(\text{H}_2\text{O})_{100}$ clusters :

[Fingerprints_in_IR_OH_spectra_of_H2O_clusters](#)

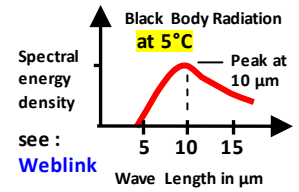
Spectra of $(\text{H}_2\text{O})_{20}$ cluster : [Spectra of \(H2O\)20 cluster](#)

→ [To the Structure and Stability of Water-Clusters](#)

Water clusters in plants : [Water clusters in plants.pdf](#)

11 Water-Clusters seem to cause the formation of PS-Particle-Clusters with icosahedral Geometry

An experimental study seems to provide evidence for the existence of "Super Water Clusters" with up to 6 μm diameter. At a temperature of 5°C Polystyrene (PS) Particle Clusters with a precise geometry develop out of evaporating water-droplets that contain PS-particles. The geometry of the final Clusters, which is nearly identical to the geometry of $(\text{H}_2\text{O})_{100}$ Clusters, indicates that in all probability Water Clusters are responsible for the formation of this crystal-like icosahedral structures! Low temperature = black-body (IR)-radiation with wave-lengths $>5 \mu\text{m}$ is also required for this process!



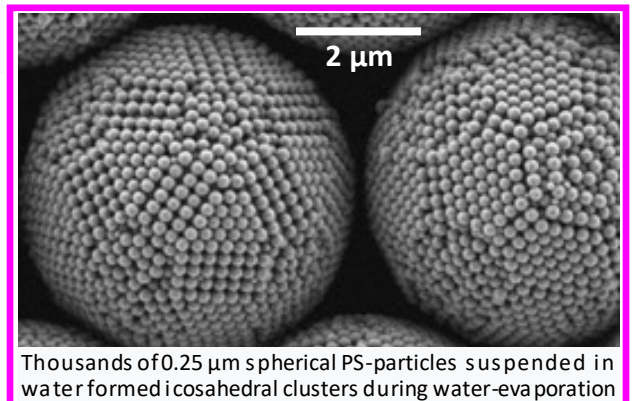
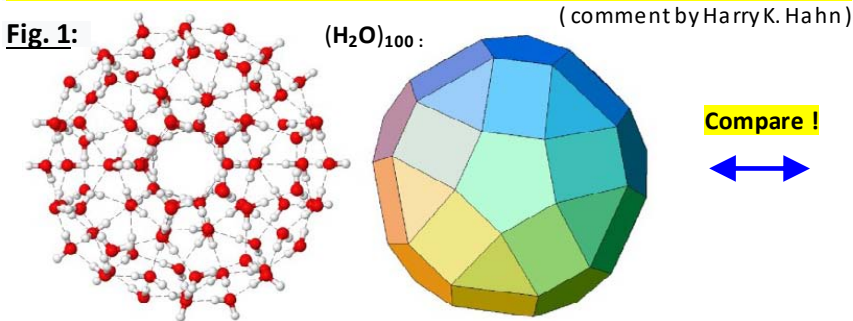
Study 3 : "Magic number colloidal clusters as minimum free energy structures"

- by Junwei Wang, Chrameh Fru Mbah & others - weblink to study : [Magic-number-colloidal-clusters](#)

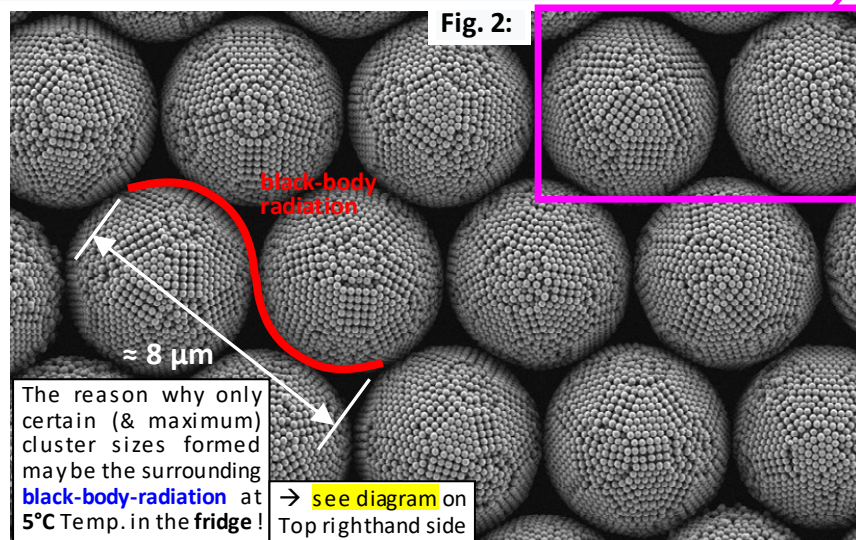
Abstract : Clusters in systems as diverse as metal atoms, virus proteins, noble gases, and nucleons have properties that depend sensitively on the number of constituent particles. Certain numbers are termed 'magic' because they grant the system with closed shells and exceptional stability. To this point, magic number clusters have been exclusively found with attractive interactions as present between atoms. Here we show that magic number clusters exist in a confined soft matter system with negligible interactions. Colloidal particles in an emulsion droplet spontaneously organize into a series of clusters with precisely defined shell structures. Crucially, free energy calculations demonstrate that colloidal clusters with magic numbers possess higher thermodynamic stability than those without magic numbers.....

Weblinks to similar Studies : 1.) [Colloidal Clusters](#)
2.) [Structural Color of icosahedral colloidal clusters](#)

The $(\text{H}_2\text{O})_{100}$ icosahedral Water Cluster has the same geometrical structure as the colloidal Clusters described in this study ! The colloidal clusters seem to be only a representation of the Water Clusters which form these Clusters!



Icosahedral Water Cluster $(\text{H}_2\text{O})_{100}$ and underlying geometrical structure !



Particle synthesis : The 0.25 μm spherical PS-Particles (\rightarrow the little white spheres) were made out of Styrene, acrylic acid, and ammonium peroxodisulfate. These small PS-colloidal (spherical) particles were synthesized in a surfactant (tensid)-free emulsion polymerization.

Colloidal cluster assembly : The 0.25 μm spherical PS-Particles, of 1wt%, were suspended in water and loaded into 1mL syringes. Then a special 0.1wt % surfactant (Tensid) was dissolved in perfluorinated carbon oil. The syringes were connected to microfluidics Syringe pumps by PE/2 tubings (0.38mm /1.09mm). The Syringe-pumps controlled the flow rate of the water- and the oil-phase (50 and 200 $\mu\text{L}/\text{h}$, respectively). Emulsion droplets were collected in 1.5mL glass vials and sealed with stretched parafilm at the opening. Small 0.4mm holes were punched into the parafilm to control the speed of evaporation from the vials. The vials were then kept at different temperatures, in the oven at 85°C, at room temperature at 25°C and in the fridge at 5°C for water evaporation.

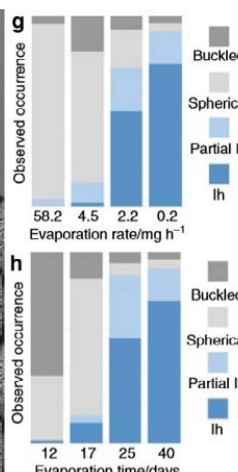
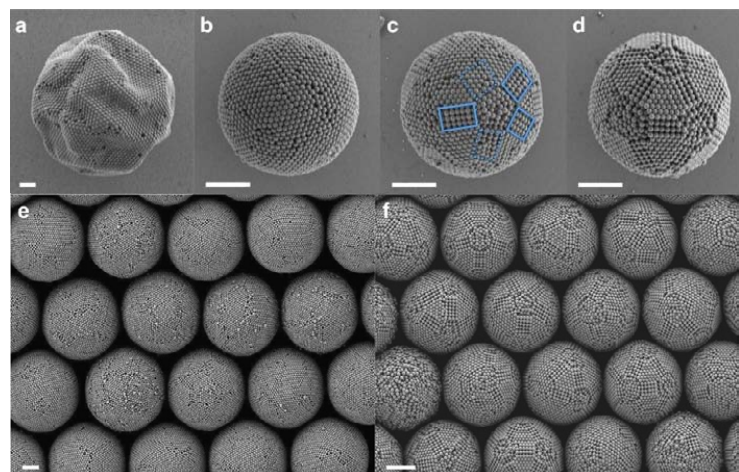


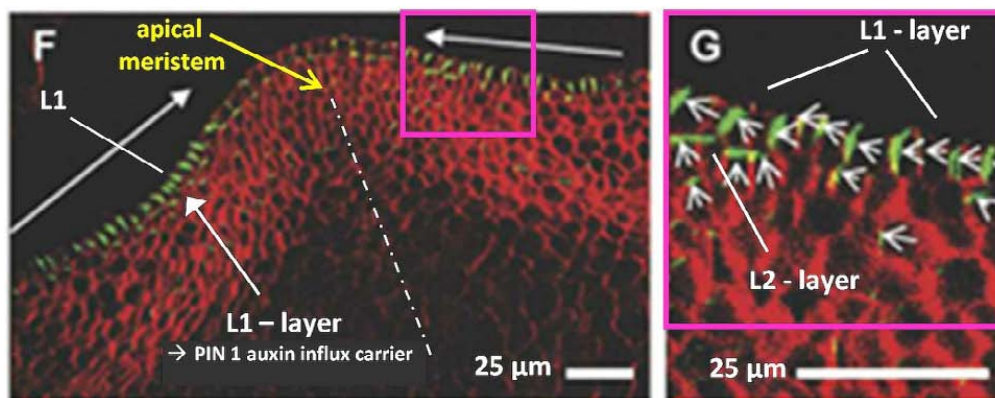
Fig. 3: Colloidal clusters from confined self-assembly in water-in-oil emulsion droplets. Four distinct cluster morphologies with increasing degree of ordering are observed: **a)** buckled clusters partially collapse upon evaporation into non-spherical shape; **b)** spherical clusters exhibit only local order; **c)** partial icosahedral clusters show one or more five-fold symmetry axes and incomplete faceting (dotted blue boxes); **d)** icosahedral clusters have well-defined facets, edges, and vertices and complete icosahedral symmetry. **e, f)** Low-magnification scanning electron microscopy (SEM) images highlight the uniformity in size and structure of the prepared clusters. Spherical and icosahedral clusters dominate in the limit of fast **(e)** and slow **(f)** evaporation, respectively. **g, h)** Show the statistical evaluation of the observed morphologies as a function of the evaporation rate **(g)** and as an evolution over time for the slowest evaporation rate **(h)** showing the progression from spherical to icosahedral (Ih). Scale bars = 2 μm

12 A physical mechanism (trigger) must be the fundamental cause of Phyllotaxis !

The following extracts from two studies indicate that plant hormones like Auxin, PIN1 etc. can't cause Phyllotaxis alone. The studies provide evidence that a yet unknown "physical mechanism" must be the fundamental cause (trigger) of Phyllotactic Patterns (Phyllotaxis) !

Study 4 : "Auxin influx carriers stabilize phyllotactic patterning"

Weblink: https://www.researchgate.net/publication/5505575_Auxin_influx_carriers_stabilize_phyllotactic_patterning



(F) Central section through a quad (apical) meristem with no recently initiated primordia, showing polarization of PIN1 toward the meristem summit in the L1 layer stretching to the periphery of the ZND. (G) Enlargement of the right-hand ZND of the meristem shown in F, showing polarization of PIN1 toward the meristem summit in the L1 and apical polarization in the L2. - White Bars, 25 μ m

Discussion : "The rapid generation of dynamic auxin gradients at the shoot apical meristem is essential for regular primordium initiation and spacing. Previous studies have focused on the role of the PIN1 auxin efflux carrier. Here, we show that in addition to PIN1, the AUX1 LAX family of auxin influx carriers is essential for stabilizing phyllotactic patterning.

This finding indicates the existence of a previously uncharacterized level of complexity in the regulation of auxin distribution in the shoot apical meristem.

The continuous generation of new primordia around the circumference of the meristem requires the rapid and dynamic formation of auxin peaks. Simulation models for auxin-mediated phyllotaxis propose that PIN1 orients toward a neighboring cell with a higher auxin concentration. AUX1 LAX could be part of the mechanism that orients PIN1 toward cells with highest auxin concentration.

The underlying molecular mechanism is, however, still unknown !

„One of the most striking features of plant architecture is the regular arrangement of leaves and flowers around the stem, known as phyllotaxis“.

It is believed that .."Peaks in concentration of the plant hormone auxin, generated by the polar localization of the PIN1 auxin efflux carrier, provide the instructive signal for primordium initiation" → This is only an assumption !

Study 5 : "A plausible model of phyllotaxis"

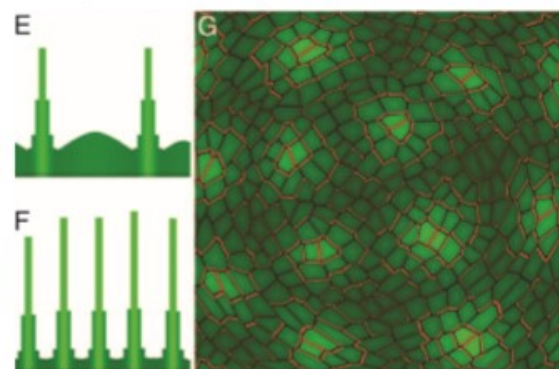
by Richard S. Smith*†, Soazig Guyomarc'h†‡, T. Mandel‡, D. Reinhardt‡, C. Kuhlemeier‡, & P. Prusinkiewicz* - Department of Computer Science, University of Calgary, Institute of Plant Sciences, CH-3013 Berne, Switzerland

Weblink: [A_plausible_model_of_phyllotaxis](#) ; alternativ: <https://www.pnas.org/content/103/5/1301>

Model of Phyllotactic Patterning. We initially hypothesized that phyllotaxis in Arabidopsis is determined directly by the transport-based patterning mechanism, operating on the growing surface of the apical meristem. **In simulations, however, we were not able to obtain**



Fig. 3. Pattern generation by the transport-based model. (A–D) Pattern emergence in a sequence of 50 cells with wraparound boundary conditions (the leftmost and the rightmost cell are considered neighbors). Taller bars (brighter green) indicate higher IAA concentration. Simulation steps 30, 60, 70, and 80 are shown. A small amount of noise present in the initial distribution is required to break symmetry.



(E and F) Pattern dependence on model parameters. Model parameters affect how many peaks a given number of cells will create. Higher values of the transport coefficient result in more peaks. If the transport coefficient is too low, no peaks will form at all. Transport coefficient: A–D, 4.0; E, 3.0; F, 10.0. (G) Pattern formed in a simulated cellular structure. PIN1 is depicted in red.

sustained spiral phyllotactic patterns by using that mechanism alone, although patterns of irregularly spaced primordia could easily be generated. This observation was upheld by many simulations, in which we used diverse parameter values and different formulas for polarizing PIN1. **"We thus conclude that additional factors play an important role in generating of phyllotactic patterns in Arabidopsis"**

Data Set 1: Phyllotactic Patterning Occurs in the Outer Layer of the Shoot Meristem (L1). The PIN1 protein is located primarily, although not exclusively, in the external L1 layer (figure 1 A and C in ref.10). **"This localization suggests that phyllotactic patterns may be formed essentially on the surface of the shoot apical meristem !"**

Our computer model suggests that **"phyllotaxis is not governed by a single mechanism, but represents a combined effect of several factors"**. This complexity may be needed in nature to generate phyllotactic patterns in the presence of noise

We were not able to recreate spiral phyllotactic patterns under these conditions and assumed a uniform production throughout the L1 in the peripheral zone instead, with an additional boost in the primordia.

Also, our model postulates localization of PIN1 toward the neighboring cells with the highest auxin concentration but **leaves open the question of what molecular mechanism may produce this localization.** The answers to these questions may lead to the integration of the model of phyllotaxis with a model of vasculature formation in the leaf and stem. Although both processes are mediated by auxin, the proposed mechanism of PIN1 polarization involved in phyllotaxis is almost opposite to the canalization mechanism proposed for veins. It is thus interesting

how these different mechanisms may be reconciled in the growing plant

13 Proof for a fundamental physical cause of Phyllotaxis that depends on Temperature / Radiation

Study 6 : - Extracts from a study produced by Dr. Iliya Iv. Vakarelov, University of Forestry, Bulgaria (1982-1994)

Title : “Changes in phyllotactic pattern structure (Fibonacci Sequences) in *Pinus mugo* due to changes in altitude“ from the book „Symmetry in Plants“ by Roger V. Jean and Denis Barabe, Universities of Quebec and Montreal, Canada (Part I. – Chapter 9 , pages 213 – 229), **weblinks**: [Weblink1](#) (Google Books), [Weblink2](#)

Research Site and methods :

Pinus Mugo grows in high mountainous parts at altitudes up to 2500m forming vast communities. The vertical profile of the research sites for *Pinus mugo* was situated along the northern slopes of the eastern part of the [Rila mountain](#), and **test specimens were collected from the following altitudes : 1900, 2200 and 2500 m**. Test specimens were also collected from the city of Sofia (**at 550 m**) where *Pinus mugo* is grown as decorative plant.

The research was carried out over a period of 12 years (except of altitude 550m here research was carried out only around 6 years). The initiation of leaf primordia in the bud (meristem) occurs at the end of the growing period. The apical meristem of *Pinus mugo* starts this process around the beginning of mid of August and ends in autumn when the air temperature goes below a certain point.



Fig 1: *Pinus mugo*

The interesting results of the study :

(3) With the increase of altitude from 1900m to 2500m the phyllotactic pattern structure of “Pinus mugo” twigs changes considerably, the number of patterns (different Fibonacci Sequences) grows from 3 to 12, and the relative frequency of the main sequence decreases from 88 % to 38 %.

At the upper boundary of *Pinus mugo* natural distribution – at about 2500m, the variation of phyllotactic twig pattern structure (entropy) becomes cyclic, with six year duration of the cycles.

(5) The changes in temperature during the period of phyllotactic pattern formation of *Pinus mugo* twigs determine about 48 % of the changes in pattern structure, the latter lagging behind with one or two years.

It is obvious that when the altitude increases, the number of phyllotactic patterns (Fibonacci-Sequences) of the vegetative organs of *Pinus mugo* also increases above a given altitude. → see Table below !

Sequence No.	FIBONACCI-Sequences present in given altitude	Altitude in (m)								Total	
		550		1900		2200		2500			
		Frequency	Relative Frequency	Frequency	Relative Frequency	Frequency	Relative Frequency	Frequency	Relative Frequency	Frequency	Relative Frequency
F1	<1,2,3,5,8,13,...>	231	0.902	431	0.885	619	F1 0.812	246	F1 0.381	1527	0.710
F3	2<1,2,3,5,8,13,...>	16	0.063	34	0.070	35	F3 0.046	111	F3 0.172	196	0.092
F2	<1,3,4,7,11,18,...>	3	0.012	22	0.045	49	F2 0.064	86	F2 0.133	160	0.074
F4	3<1,2,3,5,13,...>	6	0.023	-	-	29	F4 0.038	98	F4 0.152	133	0.062
F8	<2,5,7,12,19,31,...>	-	-	-	-	10	0.013	50	0.077	60	0.028
F11	<3,7,10,17,27,44,...>	-	-	-	-	5	0.007	18	0.028	23	0.011
F6	<1,4,5,9,14,23,...>	-	-	-	-	1	0.001	8	0.012	9	0.004
F9	2<1,3,4,7,11,18,...>	-	-	-	-	4	0.005	7	0.011	11	0.005
(?) F6	<1,7,8,15,23,38,...>	-	-	-	-	2	0.003	7	0.011	9	0.004
F5	4<1,2,3,5,8,13,...>	-	-	-	-	8	0.011	9	0.013	17	0.008
(?) F13	<1,6,7,13,20,33,...>	-	-	-	-	-	-	3	0.005	3	0.001
F10	<2,7,9,16,25,41,...>	-	-	-	-	-	-	3	0.005	3	0.001

Note : The number of Fibonacci-Sequences is increasing with altitude

Table 1 : Data on the frequency and relative frequency of the different phyllotactic patterns for *Pinus mugo* twigs at different altitudes. Specimen formed during the period 1982-1994 have been tested for all sites except for the one at 550 m where the period covers the years 1989 – 1993.

13.1 Different Temperatures at different altitudes caused changes in Phyllotactic-pattern-variation

Different temperatures at the research sites at different altitudes (550 – 2500 m), during the period of phyllotactic pattern formation, caused the changes in variability of the found phyllotactic patterns.

The number of found patterns (different **Fibonacci Sequences**) increased with altitude.

But because „temperature at different altitudes“ is a complex subject, **we need to understand „temperature at different altitudes“ more precisely** in order to understand the causes of phyllotactic pattern variability !

Some fundamental facts about „Temperature“ :

The temperature (thermal energy) of a solid body (e.g. a plant) is associated primarily with the vibrations of it's molecules. Heat transfer to the plant happens through thermal conduction or thermal radiation. **Here especially heat transfer through thermal radiation to the plant must be examined more closely !** This is the transfer of energy by means of electromagnetic waves (photons). Especially **Infrared-Radiation** is important for the heat transfer to the plant

Infrared radiation lies energetically in the area of the rotation niveaus of small molecules and in the area of the oscillation niveaus of molecule bindings. That means the absorption of infrared light (infrared radiation) leads to an **vibration excitation of the molecule bindings** and of the matter in the plant in general, or in other words to an increase of the heat energy (temperature) of the plant. The energetic **Near-Infrared-Radiation (IR-A/B)**, with approximately **0.7 to 3 µm** wavelength can excite **overtone or harmonic vibrations** in matter (in the plant molecules /plant structure)

13.2 Radiation is different at different altitudes

The temperature (thermal energy) of the plant increases or decreases by absorbing (see **Spectroscopy**) or by emitting radiation, or through thermal conduction.

Especially **Near-Infrared-Radiation** with wave-lengths of **0.7 to 3 µm** is absorbed by the water molecules of the plant and is responsible for the temperature of the plant

The **distribution of Infrared-Radiation in the atmosphere is different in different altitudes**, as the diagram on the right clearly shows. The sun's **IR-A/B-radiation with 1 to 3 µm wave-length** is absorbed by H₂O, CO₂ and other atmospheric gas, more and more **on it's way from 10 km altitude to sealevel**. But also IRC and Far-IR radiation with **3-50 µm** gets absorbed more & more

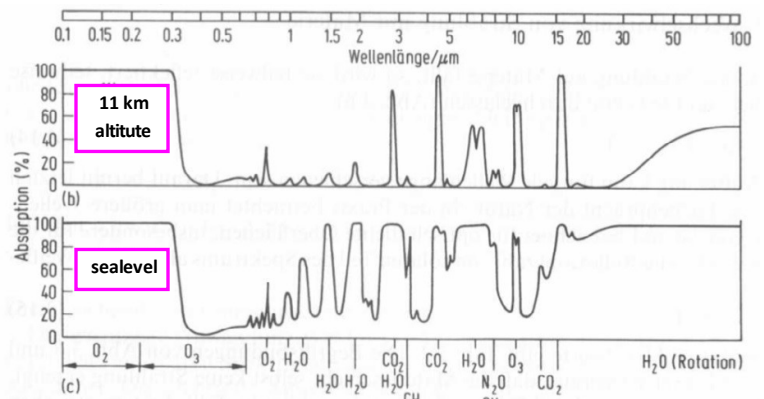
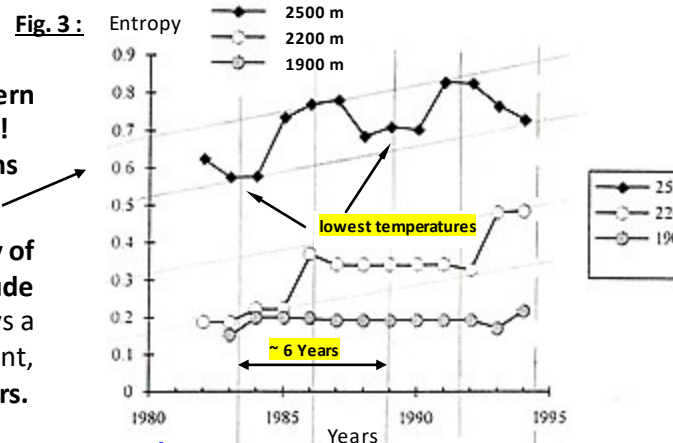


Fig. 2: Distribution of radiation in the atmosphere, at 11 km altitude and at sealevel. It is obvious that at higher altitude the variation of radiation with different wave lengths is higher than at sea level

Another important result of Dr. Vakarelov's study :

Additional Dr. Vakarelov's study showed that the **phyllotactic pattern variability (Fibonacci Sequence-variability)** changed over the years ! The study also showed that **the variability of the phyllotactic patterns in high altitude changed cyclic, with six year duration of the cycles.**

Figure 3 : The diagram on the righthand side shows the variability of entropy (variability of **Fibonacci Sequences**) with respect to altitude for „Pinus Mugo“ twigs. It is obvious that at 2500 m the curve shows a clear **cyclic process**, while at 2200 m the cyclic process is less significant, and at 1900 m nonexistent. **The cyclic process has a period of ~6 Years.**



13.3 Phyllotactic-pattern-variability seems to vary with the sunspot-cycle

Figure 4 : The next diagram on the right shows how **sunspot-numbers, cosmic ray flux, X-ray's and proton flux** changes with the 11 to 12 year sunspot-cycle. A weak correlation between **phyllotactic-pattern-variability** and cosmic ray flux is noticeable.

How does the radiation in the atmosphere change with the sunspot-cycle ? :

Solar X-ray radiation and **Ultraviolet radiation** (especially extreme UV (EUV) with **10 to 124 nm** wavelength varies markedly over the sunspot-cycle (**UV-B at 300 nm** (by up to 400% !). This radiation has a big impact on Earth's upper atmosphere. Increased X-ray & UV-radiation leads to **heating of the Ionosphere**. The ionisation of the Ionosphere also affects the propagation of **radio-waves**. Especially the **HF-radio spectrum** (3-30 MHz), but also the MF- & VHF-radio-spectrum is effected (MF=300kHz-3MHz & VHF=30-100 MHz). 30 MHz corresponds to 10 m wave-length.

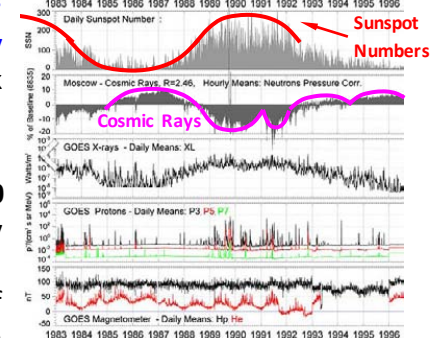


Fig. 4: see: **Sun-Climate-Connections**

13.4 Two more quantitative studies to **phyllotactic-pattern-variations** in Pine-Cones & Sunflowers

The results of the two quantitative studies do not refer to research sites at different altitudes. But the results of **Study 7** are interesting in reference to **Dr. Vakarelov's study**. And the results of the quantitative **Study 8** to **Sunflower-seedheads** : → shows interesting **Fibonacci-Pattern-Variations in the Sunflower-seedhead**.

Study 7 : „Aberrant phyllotactic patterns in cones of some conifers : a quantitative study“

by Veronika Fierz , **Weblink** : “**Aberrant phyllotactic patterns in cones of some conifers**“

Pinus nigra

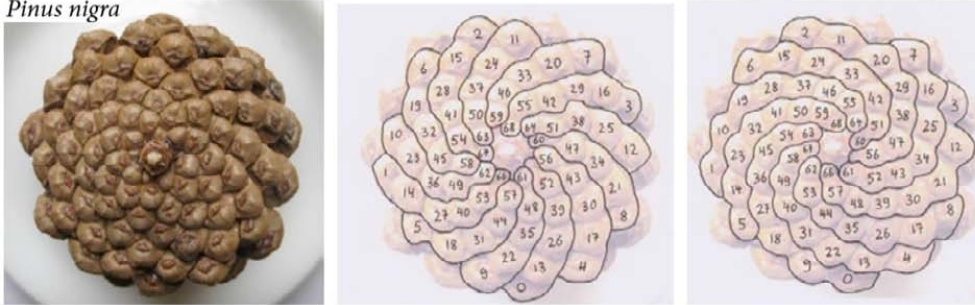


Fig. 2 – a cone with the very rare spiral pattern 9:13 (Fibonacci-sequence 4, 9, 13, 22, 35, 57, ..)

Fibonacci-type sequence	Spiral pattern m:n	Number N of Pinus nigra cones	FIBONACCI-Sequences	Frequency	Relative Frequency
1, 2, 3, 5, 8, 13, ...	F1 8:13 normal	5838 (97%)	F1 {1,2,3,5,8,13,...}	231	0.902
2, 4, 6, 10, 16, ...	F3 10:16	69	F3 2{1,2,3,5,8,13,...}	16	0.063
1, 3, 4, 7, 11, ...	F2 7:11	20	F2 {1,3,4,7,11,18,...}	3	0.012
3, 6, 9, 15, ...	F4 9:15	9	F4 3{1,2,3,5,13,...}	6	0.023
1, 4, 5, 9, 14, ...	F6 9:14	3	F8 {2,5,7,12,19,31,...}	-	-
2, 5, 7, 12, ...	F8 7:12	3			
4, 8, 12, 20, ...	F5 8:12	5			
1, 5, 6, 11, 17, ...	F7 6:11	1			
4, 9, 13, 22, ...	F14 9:13	2			
3, 7, 10, 17, ...	F11 7:10	1			

Compare !

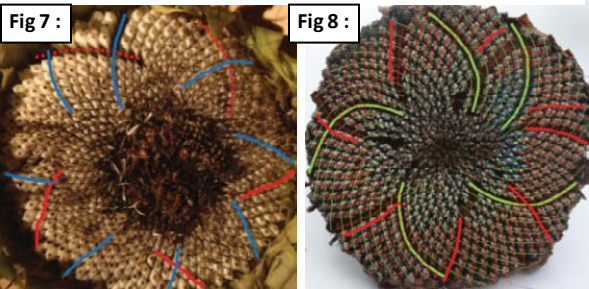


Vakarelov's study 6 : The ~270 *Pinus Mugo* examined by Vakarelov at 550m altitude show **similar phyllotactic-pattern-variability !**

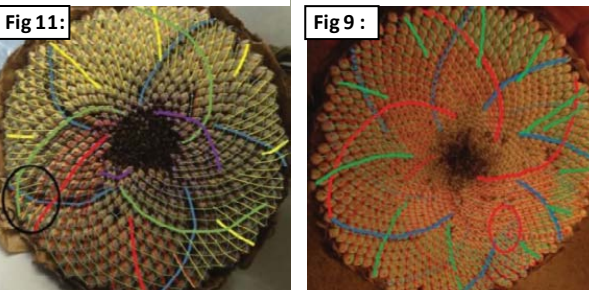
Methods & Results : In search for aberrant (unusual) patterns in „European black pine“, **6000 cones from one single tree have been examined**, almost its whole cone production of about two years. This tree was planted more than 60 years ago in a garden in Küsnacht near Zürich, Switzerland **at 560 m altitude**. Apart from the usual pattern 8:13, **nine different types of unusual patterns have been found**. The bijugy pattern 10:16 (69 cones), the first accessory pattern 7:11 (20 cones) and the trijugy pattern 9:15 (9 cones) were the most frequent. The patterns 8:12, 9:14 and 7:12 followed with 3–5 cones, and **the rarest patterns were : (F14) 9:13 (2 cones), (F7) 6:11 (one cone) and (F11) 7:10 (one cone)**.

Study 8 : „Novel Fibonacci and non-Fibonacci structure in the Sunflower“ – by J. Swinton, E. Ochu & Others

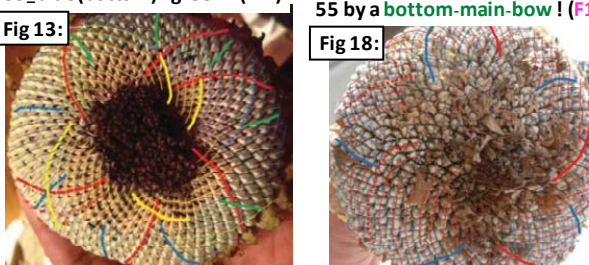
Sample 171: parastichy-pair : **Sample 113**: parastichy-pair : 76_blue , 47_red - (F2-Lucas) 73_red , 45_yellow - (F7)



Sample 667: 50 blue, 31 green additional : inner 19 (purple), outer 81 (yellow/red) - (F8)
Sample 669: 69 blue, 43 red additional : a competing outer 112 parastichy (green) - (F27)



Sample 165: 55 red, 34 yellow +blue(top) -additional : outer 89_blue(bottom)+green - (F1)
Sample 161: 50_blue, 48_red **Two nearly identical numbers ! 48 & 50 are close connected to 55 by a bottom-main-bow ! (F1)**



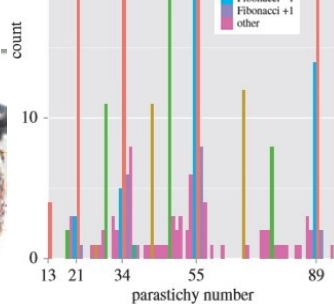
Weblink: [Novel Fibonacci and non-Fibonacci structure in the sunflower](#)

Fibonacci-structures in the spirals of Sunflower seedheads were evaluated. We collected data on **657 sunflowers**. In our most reliable data subset, we evaluated 768 clockwise or anticlockwise parastichy numbers of which 565 were Fibonacci numbers, and a further 67 had Fibonacci structure of a predefined type. **We also found more complex Fibonacci structures not previously reported in sunflowers**.

Important Results of this study :

Different parastichy-(Fibonacci)-numbers visible in one seedhead are always smaller at the center, and larger at the outer rim of the seedhead (see sample images : **Fig 9,11,13**), and **there are up to 4 different parastichy-numbers visible per seed-head** (from the same Fibonacci-Sequence). Beside the standard **F1-Fibonacci-Numbers** : 21,34,55,89 normally visible in Sunflowers, there are also parastichy-numbers of other **Fibonacci-Sequences like F2 (Lucas), F7, F8, F27** visible in a small number of samples.

The parastichy-number count (spiral-pattern) normally is more orderly in one direction than in the other. The unusual parastichy-pair **48, 50** (Fig. 18) is a special case !



Naming of different Fibonacci-Sequences My Study - Study 5

F2	F3
F3	F2
F6	F4
F7	F5
F8	-
F27	F8

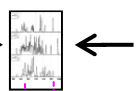
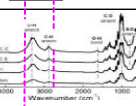
pair type	count	ID (parastichy pair)
Fibonacci structure	272	
high Fibonacci	2	(F5 or F8)
Fibonacci ±1	41	
Fibonacci ±2	29	
Fibonacci ±3	7	
approximately Fibonacci	5	63(83,49), 151(79,47), 220(84,54), 296(49,32), 569(55,38)
similar counts	4	36(21,20), 43(29,20), 161(50,48), 369(19,18)
competing parastichies	3	165(59,55), 464(80,68), 667(50,31)
rotationally asymmetric	1	461(73,55)
anomalous	2	502(77,56), 702(62,31)

Classification by type of parastichy-pair

14 Electromagnetic-Radiation from specific wave-length-ranges can change Phyllotactic Patterns

As described in **Chapter 13** the number of different phyllotactic patterns (**Fibonacci Sequences**) visible in the twig-patterns of "*Pinus mugo*" threes, increases with increasing altitude. The main reason for this increase of phyllotactic-pattern variation, at higher altitudes, are different environmental conditions. Especially changes in temperature, or more precise, changes in the „radiation-mix“ (or radiation composition) seem to be responsible for the increase of phyllotactic-pattern variation, at higher altitudes. **At higher altitudes there are more wave-length ranges present, that can affect (change) the phyllotactic (Fibonacci) pattern formation** In the following we have a closer look at the electromagnetic Spectrum at sealevel and at a higher altitude to identify the wave-length ranges which may be responsible for the increase in phyllotactic pattern formation.

Wave-length-range	Property of Radiation	Effect on the plant
200 nm to 2000 nm and (> 120 mm)	Has a penetration depth > 1mm in water . - See diagram 5 The radiation-range from Ultraviolet to the Near Infrared radiation contains $\approx 90\%$ of the Sun's radiation energy	This radiation from the sun can reach the Apical Meristem , and so it can change and affect phyllotactic pattern formation
280 nm to 450 nm	Ultraviolet radiation and strong Blue Light (>30 Wm ²) This is the most energetic radiation from the Sun It has a damaging effect on plant cells (Chloroplasts)	Causes strong Chloroplast Movements (see following studies : Study 10 ; Study-II) -> can disturb Water Cluster formation
380-480 & 620-688 nm	main Absorptions bands of Chlorophyll a/b (visible light)	-> radiation absorbed by Chlorophyll
700 nm to 2000 nm (0.7 to 2 μm)	red light and higher energy Infrared-Radiation (IR-A/B) can excite overtone and harmonic vibrations in matter --> many absorption lines of Water in this radiation range	This radiation is absorbed by different molecules in the plant cells. It seems to trigger floral bud induction -> see Study 9
$\approx 6 - 20 \mu\text{m}$ (peak at $10 \mu\text{m}$)	Black-body Radiation of a body at 20°C (293 K) temperature	--> radiation that matter at 20°C emits

Diagram 3 : The small diagram on the right (top) shows **Water-Cluster absorption spectra** →  ← The diagram (bottom) shows the **Cellulose absorption spectra**. → In high altitude there is **more infrared radiation** available in the spectral range of **4.5 to 8 μm** which can cause increased excitation in this spectral range → 

Water Cluster formation can be affected by the following radiation :
The high energetic wave-length-range **280 to 450 nm** causes strong Chloroplast motion in cells that can disturb Water Cluster formation.
The energetic **Infrared** wave-length-range **700 to 2000 nm** can excite strong vibrations in molecules (H₂O) in the Apical-Meristem
And the **4500 - 8000 nm** range can excite large **Water-Clusters**

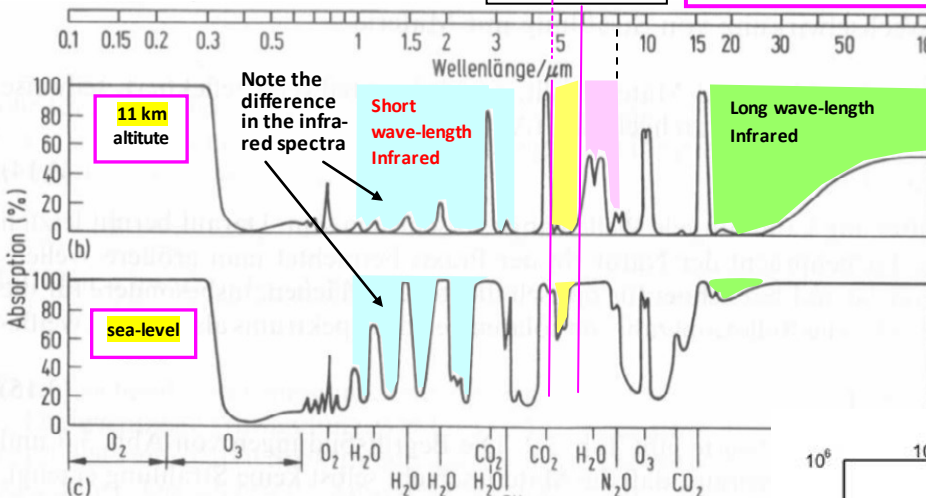


Diagram 1 : Distribution of radiation in the atmosphere at 11 km altitude and at Sea-level. The colored areas indicate wave-length-ranges where there is a considerable difference in Absorption through atmospheric gases between the sea level and high altitude (11 km). The larger the colored area the more radiation of this wave-length-range is available in the given altitude.

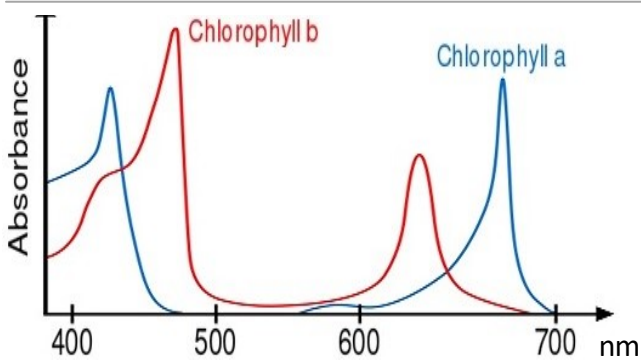


Diagram 4 : Absorption Spectrum of Chlorophyll a & b

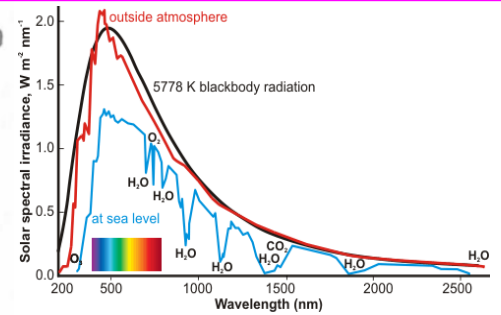


Diagram 2 : Solar spectral irradiance (radiation) outside of atmosphere and at sea-level (in W/m²)

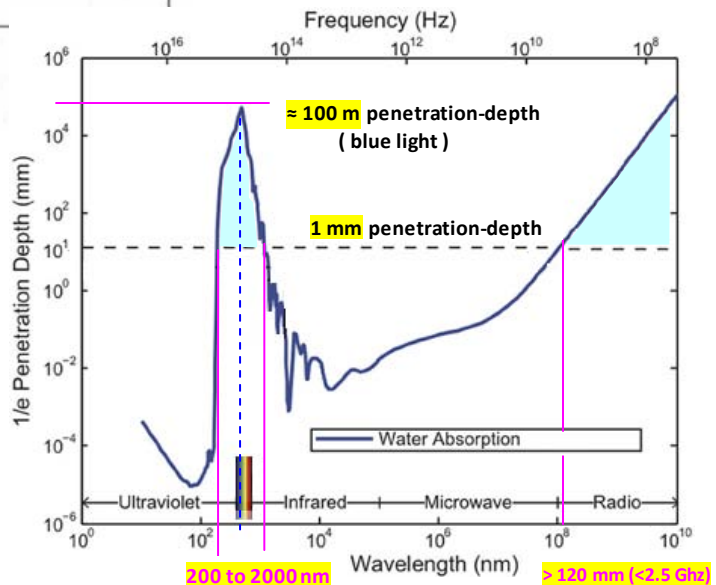


Diagram 5 : Penetration-depth of electromagnetic radiation in Water in Millimeter, from the Ultraviolet- to the Radio-wavelength-Range. Blue Light has the maximum penetration with $\approx 100\text{m}$ water-depth. The blue marked areas indicate a water penetration-depth > 1mm.

15 Phyllotactic-pattern (bud induction) caused by far-red & infrared light : 750 nm to ≈ 2000 nm

This study No 9 shows that **far-red and infrared radiation with wave-lengths > 750 nm must be the trigger for phyllotactic-pattern formation & bud-induction**, in short-day-strawberry plants (*Fragaria ananassa*) examined in this study. Radiation with wave-lengths < 750 nm didn't reach the apical meristem in this test setup, because it was filtered (eliminated) by heavy leaf-cover above the apical meristem. **But the true source of the IR-radiation > 780 nm isn't clear because triphosphor-fluorescent-lamps don't produce this radiation !!** The source of the IR-radiation probably were additional strong infrared lamps or maybe a heater in the growth chamber, which caused strong IR-radiation in the range of 780 - 2000 nm which could penetrate the leaf cover

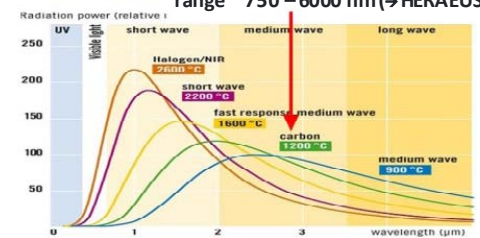
Study 9 : „Red Light Affects Flowering under long days in a Short-day Strawberry Cultivar“

by Fumiomi Takeda & D. Michael Glenn – USDA-ARS, Appalachian Fruit Research Station, WV 25430

Abstract. July-plugged transplants of short-day cv. Strawberry Festival (*Fragaria × ananassa*) flowered in October and November although they were grown under long photoperiods and warm temperatures (greater than 21 °C) in July and August. These unexpected results were attributed to a high plant density (320 transplants/m²) that provided continuous and heavy leaf cover, which eliminated red light (less than 700 nm) from reaching the crowns. This hypothesis was tested by illuminating crowns of transplants growing in 50-cell packs for 16 h·d⁻¹ with red light-emitting diode lamps (maximum wavelength at 639 nm and 80% of output between 617 and 655 nm). Red light treatment caused a significant reduction in fall flowering. It is proposed that a high ratio of far-red light to visible light reaching the crown will play a role in floral bud induction, possibly as early as mid-August. Transplants of some short-day cultivars started as plug plants in early July have the capacity to flower and fruit in the fall and the next spring, enabling growers in the mid-Atlantic coast region to obtain two harvests within 1 year from a single planting. [Weblinks to study : Weblink 1 , Weblink 2](#)



Fig 4 : Maybe something like a Carbon Infrared Emitter (CIR) was also used in the growth chamber : The main emission of this lamp lies within the main absorption bands of water : Wave-length range ~ 750 – 6000 nm (→ HERAEUS)



Summary of the experiment and important results of this study :

Short-day strawberry cultivars have been induced to flower in the fall (autumn) without exposing the plants to the normally required cold temperatures or short-day conditions, needed for bud induction.

July-plugged plants grown in a greenhouse at high plant density, under long days, and at temperatures >21 °C during day and night flowered in the fall (autumn). Early in August 4 trays of "short-day" strawberry plants (320 transplants/m²) were placed in an EGC M-36 growth chamber.

On two trays the crowns (SAM) of the plants were illuminated with red-LED's (80% of LED output was in the 617 – 655nm range).

On the control plants (the other two trays), the crowns (the SAM) were not illuminated with the red LED's.

Spectroradiometric measurements [on the control plants](#), in mid-August (in the growth chamber), showed no transmission of red light and shorter wave-length light through the leaves to the crowns, but only far-red & near-infrared light was reaching the crowns (SAM) - see Fig.3

The crowns (SAM) of the plants were under a dense (heavy) leaf cover (leaf canopy). **The light reaching the crowns (SAM) of the plants was depleted of wavelengths less than 700 nm because of the heavy leaf cover (canopy) above the crowns. Only far-red and infrared light >700 nm reached the crowns (SAM) in the control plants !. → See Fig. 3**

The final results showed that **red light from the LED-lamps** directed at the crown **actually delayed the flower bud induction**. Flower bud emergence was observed in only 17% of plants, which were illuminated with the red LED, compared with 38% of the control plants which were **not** illuminated with red LED'S. By late November 95% of the **not** illuminated control plants had open flowers, compared with only 54% of those illuminated with the red LED'S !

The high ratio of infrared light to visible light, which reached the crowns (Shoot Apical Meristem) played a significant role in floral bud induction ! Light is absorbed by photo-receptors, which promote the expression of genes that change the fate of the shoot apical meristem (SAM) from vegetative growth to reproductive development.

In this experiment selective filtering by the heavy leaf cover, resulted in the illumination of the apical meristem with only light with wave-lengths > 700 nm . This shift in spectral composition of the received light was biologically significant, regarding the floral bud induction and the reproductive development of the flowers. It is possible that **transition to flowering in the SAM, can be achieved by a high share of far-red and infrared light >750 nm**, and only a small share or none visible light < 750 nm present → see spectra „crown level“ in Fig. 3

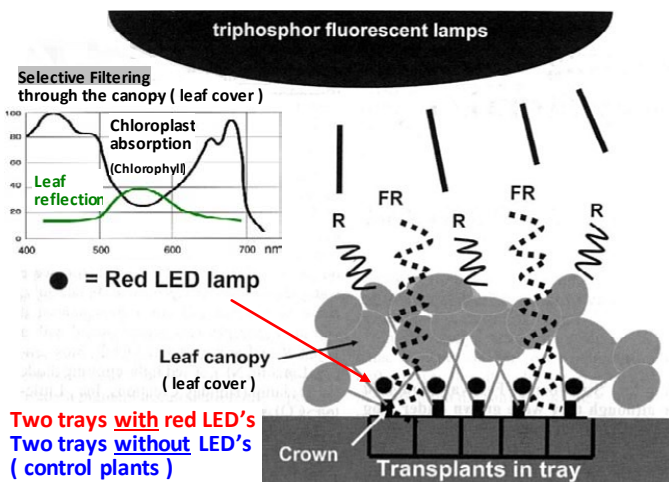


Fig 1 : red light-emitting diode (LED) treatment in the growth chamber. Triphosphor fluorescent lamps and probably additional infrared emitters were placed above the leaf cover. **Only far-red and infrared light passed through the leaf cover.** Chloroplast absorption and leaf reflection acted as a selective filter

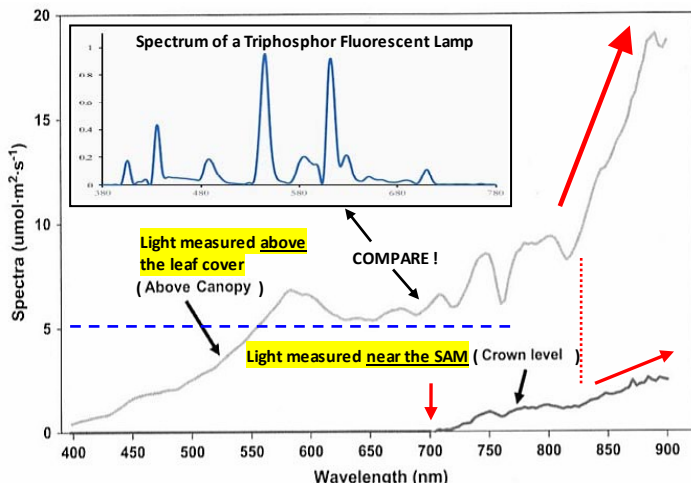


Fig. 3 : Intercepted light measured above the leaf canopy (leaf cover) and transmitted light measured near the crowns (near the SAM) . Light reaching the SAM was depleted in wave-lengths less than 700nm because of the absorption and reflection by the heavy (dense) leaf cover (canopy) –see Fig. 1

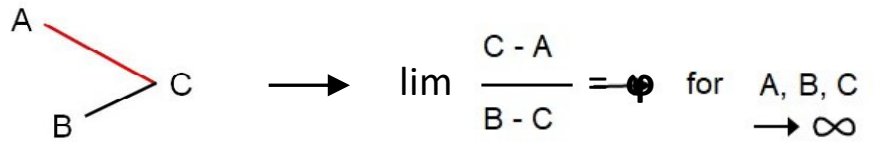
16 From the Fibonacci-Sequences shown by *Pinus mugo* at 2500m an infinite Fibonacci-Table was developed :

There are clear spatial interdependencies noticeable between the different Fibonacci-Sequences, which are connected by the golden ratio ϕ . There is a complex network visible between the numbers of all Sequences. This table of Fibonacci-Number Sequences can be extended towards infinity and all natural numbers are contained in the lower half only once!

For 3 numbers A, B and C in the below shown arrangement, which belong to the same 3 (or 2) different Fibonacci-Sequences, the following rule is true :

The ratio of the difference (C-A) indicated by a "red line", to the difference (B-C) indicated by a "black line" is approaching the golden ratio ϕ for the further progressing Fibonacci-Number Sequences towards infinity (downwards in the table).

„Main Bow-Structures“ are also linked by the „golden ratio“ ϕ !



FIBONACCI – Number Sequences No. 1 to 14 (F1 - F14) → see extended table in the Appendix !

Row No.	F1 Fibonacci-Base-Sequence	F2 Lucas-Sequence	F3 Fibonacci-Sequence (x 2)	F4 Fibonacci-Sequence (x 3)	F5 Fibonacci-Sequence (x 4)	F6	F7	F8	F9 Lucas-Sequence (x 2)	F10	F11	F12	F13 Lucas-Sequence (x 3)	F14
1	1	1	1	1	1	1	1	1	1	1	1	1	1	1
2	2	3	2	2	2	2	2	2	2	2	2	2	2	2
3	3	4	3	3	3	3	3	3	3	3	3	3	3	3
4	4	5	4	4	4	4	4	4	4	4	4	4	4	4
5	5	6	5	5	5	5	5	5	5	5	5	5	5	5
6	6	7	6	6	6	6	6	6	6	6	6	6	6	6
7	7	8	7	7	7	7	7	7	7	7	7	7	7	7
8	8	9	8	8	8	8	8	8	8	8	8	8	8	8
9	9	10	9	9	9	9	9	9	9	9	9	9	9	9
10	10	11	10	10	10	10	10	10	10	10	10	10	10	10
11	11	12	11	11	11	11	11	11	11	11	11	11	11	11
12	12	13	12	12	12	12	12	12	12	12	12	12	12	12
13	13	14	13	13	13	13	13	13	13	13	13	13	13	13
14	14	15	14	14	14	14	14	14	14	14	14	14	14	14
15	15	16	15	15	15	15	15	15	15	15	15	15	15	15
16	16	17	16	16	16	16	16	16	16	16	16	16	16	16
17	17	18	17	17	17	17	17	17	17	17	17	17	17	17
18	18	19	18	18	18	18	18	18	18	18	18	18	18	18
19	19	20	19	19	19	19	19	19	19	19	19	19	19	19
20	20	21	20	20	20	20	20	20	20	20	20	20	20	20
21	21	22	21	21	21	21	21	21	21	21	21	21	21	21
22	22	23	22	22	22	22	22	22	22	22	22	22	22	22
23	23	24	23	23	23	23	23	23	23	23	23	23	23	23
24	24	25	24	24	24	24	24	24	24	24	24	24	24	24
25	25	26	25	25	25	25	25	25	25	25	25	25	25	25
26	26	27	26	26	26	26	26	26	26	26	26	26	26	26
27	27	28	27	27	27	27	27	27	27	27	27	27	27	27
28	28	29	28	28	28	28	28	28	28	28	28	28	28	28
29	29	30	29	29	29	29	29	29	29	29	29	29	29	29
30	30	31	30	30	30	30	30	30	30	30	30	30	30	30
31	31	32	31	31	31	31	31	31	31	31	31	31	31	31
32	32	33	32	32	32	32	32	32	32	32	32	32	32	32
33	33	34	33	33	33	33	33	33	33	33	33	33	33	33
34	34	35	34	34	34	34	34	34	34	34	34	34	34	34
35	35	36	35	35	35	35	35	35	35	35	35	35	35	35
36	36	37	36	36	36	36	36	36	36	36	36	36	36	36
37	37	38	37	37	37	37	37	37	37	37	37	37	37	37
38	38	39	38	38	38	38	38	38	38	38	38	38	38	38
39	39	40	39	39	39	39	39	39	39	39	39	39	39	39
40	40	41	40	40	40	40	40	40	40	40	40	40	40	40
41	41	42	41	41	41	41	41	41	41	41	41	41	41	41
42	42	43	42	42	42	42	42	42	42	42	42	42	42	42
43	43	44	43	43	43	43	43	43	43	43	43	43	43	43
44	44	45	44	44	44	44	44	44	44	44	44	44	44	44
45	45	46	45	45	45	45	45	45	45	45	45	45	45	45
46	46	47	46	46	46	46	46	46	46	46	46	46	46	46
47	47	48	47	47	47	47	47	47	47	47	47	47	47	47
48	48	49	48	48	48	48	48	48	48	48	48	48	48	48
49	49	50	49	49	49	49	49	49	49	49	49	49	49	49
50	50	51	50	50	50	50	50	50	50	50	50	50	50	50
51	51	52	51	51	51	51	51	51	51	51	51	51	51	51
52	52	53	52	52	52	52	52	52	52	52	52	52	52	52
53	53	54	53	53	53	53	53	53	53	53	53	53	53	53
54	54	55	54	54	54	54	54	54	54	54	54	54	54	54
55	55	56	55	55	55	55	55	55	55	55	55	55	55	55
56	56	57	56	56	56	56	56	56	56	56	56	56	56	56
57	57	58	57	57	57	57	57	57	57	57	57	57	57	57
58	58	59	58	58	58	58	58	58	58	58	58	58	58	58
59	59	60	59	59	59	59	59	59	59	59	59	59	59	59
60	60		60											

Note : Below this line all natural numbers are contained in the Fibonacci Sequences just once!

Fibonacci-Sequence (top main bows)

Lucas-Sequence (bottom main bows)

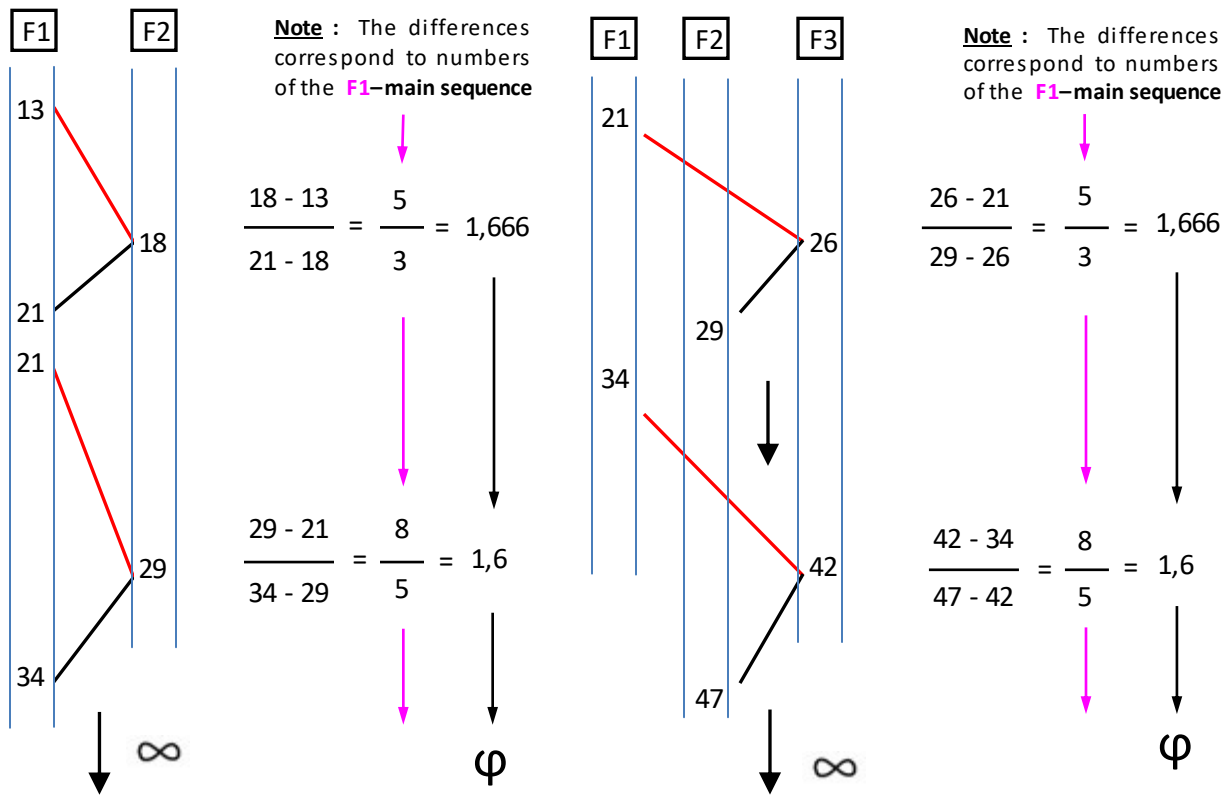


17 A general rule exists which connects numbers of different Fibonacci-Sequences by the golden ratio ϕ

→ The following two examples explain the rule which was described in general on the previous page :

The examples show how the quotient of the differences between the numbers of designated Fibonacci-Sequences (indicated by red- and black-lines in the table), is approaching the golden ratio for the number sequences progressing towards infinity.

For the examples we look at the Fibonacci Sequences **F1**, **F2** and **F3** (→ F2 is the Lucas-Sequence, F3 = F1 x 2)



17.1 Interesting properties of the Fibonacci-F1 Sequence (and other Fibonacci-Sequences) :

- The numbers of the **Fibonacci F1** – Number Sequence seem to contain all prime numbers as prime factors !
- This is not the case for all other Fibonacci-Sequences where certain prime factors are missing ! (see **Appendix**)
- And all prime factors appear periodic in defined “number-distances” in the sequence (see left side of table)
- This is the case for all Fibonacci-Sequences ! (→ These mentioned properties must be analysed in more detail !)

Table 2 : Periodicity of the prime factors of the **Fibonacci F1** - Number Sequence :

some prime factors shown in table form													in prime factors factorized Fibonacci-Numbers		sum of digits	Fibonacci-Sequence F1			
41	37	31	29	23	19	17	13	11	7	5	3	2	repeating products	new products		F	F'	F''	Nr.
															1			1	
															1			2	
															2	1		3	
															3	1		4	
															5	2	1	5	
															8	3	1	6	
															4	5	2	7	
									7		3				3	8	3	8	
						17					2				7	13	5	9	
								11	5						10	21	8	10	
										3 ²	2 ⁴				17	34	34	11	
															9	55	21	12	
															8	89	55	13	
															17	144	89	14	
															9	233	144	15	
															8	377	233	16	
															17	610	377	17	
															7	987	610	18	
															24	1597	987	19	
															8	2584	1597	20	
															17	4181	2584	21	
															7	6765	4181	22	
															22			23	
															19			24	
															14			25	
															24			26	
															19			27	
															14			28	
															24			29	
															19			30	
															14			31	
															24			32	
															19			33	
															14			34	
															24			35	
															19			36	
															14			37	
															24			38	
															19			39	
															14			40	
															24			41	
															19			42	
															14			43	
															24			44	
															19			45	
															14			46	
															24			47	
															19			48	
															14			49	
															24			50	
															19			51	
															14			52	
															24			53	
															19			54	
															14			55	
															24			56	
															19			57	
															14			58	
															24			59	
															19			60	
															14			61	
															24			62	
															19			63	
															14			64	
															24			65	
															19			66	
															14			67	
															24			68	
															19			69	
															14			70	
															24			71	
															19			72	
															14			73	
															24			74	
															19			75	
															14			76	
															24			77	
															19			78	
															14			79	
															24			80	
															19			81	
															14			82	
															24			83	
															19			84	
															14			85	
															24			86	
															19			87	
															14			88	
															24			89	
															19			90	
															14			91	
															24			92	
															19			93	
															14			94	
															24			95	
															19			96	
															14			97	
															24			98	
															19			99	
															14			100	

→ See some selected Fibonacci-Sequences in more detail in the **Appendix** !

17.2 Constant φ (Φ) defines all Fibonacci-Sequences and the square roots of all natural numbers

The asymptotic ratio of successive Fibonacci numbers leads to the Golden Ratio constant φ (or Φ)

The Fibonacci Sequences describe morphological patterns in a wide range of living organisms. It is one of the most remarkable organizing principles mathematically describing natural and manmade phenomena.

The constant φ is the positive solution of the following quadratic equation :

$$x + 1 = x^2$$

$$\rightarrow \varphi = \frac{1 + \sqrt{5}}{2} = 1.618034\dots$$

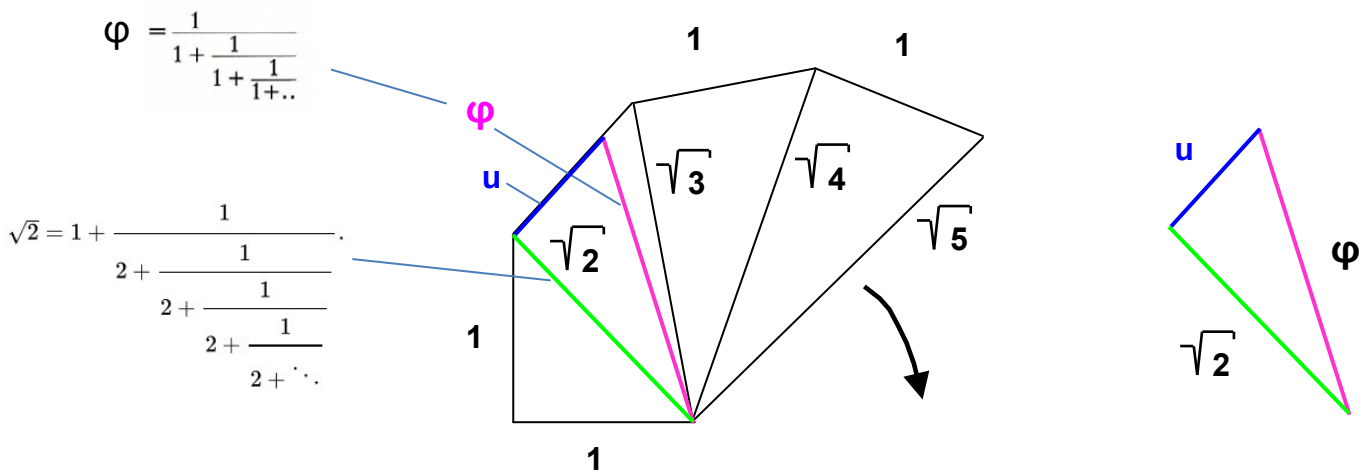


Because the value of constant φ is close to the **square root of 2** and the **square root of 3**, I draw φ into the start section of the **Square Root Spiral** :

17.3 To the discovery of an important algebraic equation regarding Constant φ (Phi)

→ This discovery indicates that constant φ and the base unit **1** form the base of mathematics and geometry.
And the distribution and structure of matter (energy) in space, is fundamentally based on constant Phi and 1

The start of the **Square Root Spiral** is shown with the constant φ drawn in :



Now we see what we can do with this arrangement of right triangles, and with the help of the **Pythagorean theorem**.

From the right triangle φ , square root of 2 & **u** follows :

$$\varphi^2 = (\sqrt{2})^2 + u^2 \quad ; \quad \text{application of the Pythagorean theorem}$$

$$\rightarrow u = \sqrt{\varphi^2 - 2} = 0,786151377\dots \quad ; \quad \text{we can calculate this value of } u \text{ with the calculator}$$

I did research with Google, and I found a study where the constant **u** was expressed with an algebraic term !

With the help of this algebraic term it was possible to find interesting new properties of constant φ !

→ see next page !

17.4 The algebraic calculation of the square roots of all natural numbers only with constant φ & 1

From Equation (4.10) from the study shown on the righthand side I have found the algebraic term which describes the calculated value of u :

$$\frac{\sqrt{2\sqrt{5} - 2}}{2} = 0,786151377... = u$$

From this algebraic term it follows :

$$\sqrt{\varphi^2 - 2} = \frac{\sqrt{2\sqrt{5} - 2}}{2} ;$$

now we can equate the two algebraic terms which represent the same constant !

$$\rightarrow 4\varphi^2 - 8 = 2\sqrt{5} - 2 ; \text{ we square both sides and transform}$$

$$\varphi^2 = \frac{\sqrt{5} + 3}{2} ; \quad (1) \quad \text{we solve for } \varphi^2$$

Compare !



$$\varphi = \frac{\sqrt{5} + 1}{2}$$

$$\sqrt{5} = 2\varphi^2 - 3 ; \quad (2) \quad \text{we solve for } \sqrt{5}$$

Now we go back to the square root spiral and use the following right triangle :

$$(\sqrt{6})^2 = (\sqrt{5})^2 + 1^2 ; \quad \text{application of the Pythagorean theorem}$$

$$6 = (2\varphi^2 - 3)^2 + 1 ; \quad \text{we replace } \sqrt{5} \text{ by equation (2) and transform}$$

$$\rightarrow 3 = \frac{\varphi^4 + 1}{\varphi^2} \quad (3) \quad \rightarrow \quad \sqrt{3} = \sqrt{\frac{\varphi^4 + 1}{\varphi^2}} \quad (4) ; \quad \text{square root 3 expressed by } \varphi \text{ and 1 !}$$

Now we use the following right triangle :

$$(\sqrt{3})^2 = (\sqrt{2})^2 + 1^2 ; \quad \text{application of the Pythagorean theorem \& inserting equation (3)}$$

$$\rightarrow 2 = \frac{\varphi^4 + 1}{\varphi^2} - 1 \quad \rightarrow \quad 2 = \frac{\varphi^4 - \varphi^2 + 1}{\varphi^2} \quad (5) \quad \text{and} \quad \sqrt{2} = \sqrt{\frac{\varphi^4 - \varphi^2 + 1}{\varphi^2}} \quad (6)$$

Now we insert equation (3) in equation (2) :

$$\rightarrow \sqrt{5} = 2\varphi^2 - \frac{\varphi^4 + 1}{\varphi^2} \quad \rightarrow \quad \sqrt{5} = \frac{\varphi^4 - 1}{\varphi^2} ; \quad (7) ; \quad \text{square root 5 expressed by } \varphi \text{ and 1}$$

PHASE SPACES IN SPECIAL RELATIVITY : TOWARDS ELIMINATING GRAVITATIONAL SINGULARITIES

from PETER DANENHOWER \rightarrow see weblink : <https://arxiv.org/pdf/0706.2043.pdf>

Abstract : This paper shows one way to construct phase spaces in special relativity by expanding Minkowski Space. These spaces appear to indicate that we can dispense with gravitational singularities. The key mathematical ideas in the present approach are to include a complex phase factor, such as, $e^{i\phi}$ in the Lorentz transformation and to use both the proper time and the proper mass as parameters. To develop the most general case, a complex parameter $\sigma = s + im$, is introduced, where s is the proper time, and m is the proper mass, and σ and $\sigma/|\sigma|$ are used to parameterize the position of a particle (or reference frame) in space-time-matter phase space. A new reference variable, $u = m/r$, is needed (in addition to velocity), and assumed to be bounded by 0 and $c^2/G = 1$, in geometrized units. Several results are derived: The equation $E = mc^2$ apparently needs to be modified to $E^2 = (s^2 c^{10})/G^2 + m^2 c^4$, but a simpler (invariant) parameter is the "energy to length" ratio, which is c^4/G for any spherical region of space-time-matter. The generalized "momentum vector" becomes completely "masslike" for $u \approx 0.7861...$, which we think indicates the existence of a maximal gravity field. Thus, gravitational singularities do not occur.

Instead, as $u \rightarrow 1$ matter is apparently simply crushed into free space. In the last section of this paper we attempt some further generalizations of the phase space ideas developed in this paper.

Now we use the following right triangle :

$$(\sqrt{6})^2 = (\sqrt{5})^2 + 1^2 \quad ; \quad \text{application of the Pythagorean theorem \& inserting equation (7)}$$

$$\rightarrow 6 = \left(\frac{\varphi^4 - 1}{\varphi^2} \right)^2 + 1 \quad \rightarrow \quad 6 = \frac{\varphi^8 - \varphi^4 + 1}{\varphi^4} \quad (8) \quad \text{and} \quad \sqrt{6} = \sqrt{\frac{\varphi^8 - \varphi^4 + 1}{\varphi^4}} \quad (9)$$

We can now continue and use the following right triangles of the square root spiral :

$$(\sqrt{7})^2 = (\sqrt{6})^2 + 1^2 \quad ; \quad \text{application of the Pythagorean theorem \& inserting equation (8)}$$

$$\rightarrow 7 = \frac{\varphi^8 + 1}{\varphi^4} \quad (10) \quad \rightarrow \quad \sqrt{7} = \sqrt{\frac{\varphi^8 + 1}{\varphi^4}} \quad (11)$$

In the same way we can now calculate all square roots of all natural numbers with the next right triangles :

$$\rightarrow 8 = \frac{\varphi^8 + \varphi^4 + 1}{\varphi^4} \quad (12) \quad \text{and} \quad \sqrt{8} = \sqrt{\frac{\varphi^8 + \varphi^4 + 1}{\varphi^4}} \quad (13)$$

$$\rightarrow 10 = \frac{\varphi^8 + 3\varphi^4 + 1}{\varphi^4} \quad (14) \quad \text{and} \quad \sqrt{10} = \sqrt{\frac{\varphi^8 + 3\varphi^4 + 1}{\varphi^4}} \quad (15)$$

$$\rightarrow 11 = \frac{\varphi^8 + 4\varphi^4 + 1}{\varphi^4} \quad (16) \quad \text{and} \quad \sqrt{11} = \sqrt{\frac{\varphi^8 + 4\varphi^4 + 1}{\varphi^4}} \quad (17)$$

$$\rightarrow 12 = \frac{\varphi^8 + 5\varphi^4 + 1}{\varphi^4} \quad (18) \quad \text{and} \quad \sqrt{12} = \sqrt{\frac{\varphi^8 + 5\varphi^4 + 1}{\varphi^4}} \quad (19)$$

From the above shown formulas (equations) I have realized **a general rule** for all natural numbers > 10 :

Note : \rightarrow The expression $(3+n)$ in the rule can be replaced by **products and / or sums** of the equations (3) to (13)

$$\rightarrow (10 + n) = \frac{\varphi^8 + (3+n)\varphi^4 + 1}{\varphi^4} \quad (20) \quad \text{and} \quad \sqrt{(10 + n)} = \sqrt{\frac{\varphi^8 + (3+n)\varphi^4 + 1}{\varphi^4}} \quad (30)$$

For $n \rightarrow \infty$

With this general formula we can express all natural numbers ≥ 10 and their square roots only with φ and 1 !

This statement is also valid for all rationals (fractions) and their square roots. This is a quite interesting discovery !!

Constant Phi (φ) which defines the structure of the Dodecahedron and Icosahedron (together with base unit 1) is a very important (space structure) constant for the real / physical world ! Please also read my following study :

\rightarrow [The Black Hole in M87 \(EHT2017\) may provide evidence for a Poincare Dodecahedral Space Universe](#)

Weblink 1 to the study : <http://vixra.org/abs/1907.0348> ; alternative : Weblink 2 : [Weblink to archive.org](#)

17.5 Constant Pi (π) can also be expressed by only using constant φ and 1 !

Viete's formula from 1593 :

$$\pi = \frac{2}{\sqrt{2}} \frac{2}{\sqrt{2+\sqrt{2}}} \frac{2}{\sqrt{2+\sqrt{2+\sqrt{2}}}} \dots$$

→ It is also possible to derive from Viète's formula a related formula for π that still involves nested square roots of two, but uses only one multiplication :

$$\pi = \lim_{k \rightarrow \infty} 2^k \underbrace{\sqrt{2 - \sqrt{2 + \sqrt{2 + \sqrt{2 + \sqrt{2 + \dots + \sqrt{2}}}}}}}_{k \text{ square roots}}$$

If we replace the number 2 in the above shown formulas by the found equation (5) where number 2 can be expressed by constant φ and 1, then we can express the constant Pi (π) also by only using the constant φ and 1 !

Replace Number 2 in the above shown formulas with this term.

$$\rightarrow 2 = \frac{\varphi^4 + 1}{\varphi^2} - 1 \quad \rightarrow \quad \boxed{2 = \frac{\varphi^4 - \varphi^2 + 1}{\varphi^2}} \quad (5) \quad \text{and} \quad \sqrt{2} = \sqrt{\frac{\varphi^4 - \varphi^2 + 1}{\varphi^2}} \quad (6)$$

It becomes clear that the irrationality of Pi (π) is also only based on the constant φ and 1, in the same way as the irrationality of all irrational square roots, is only based on constant φ & 1 ! Numbers don't exist! Only φ & 1 exist!

Constant Pi (π) can now be expressed in this way, by only using constant φ and 1 :

$$\pi = \lim_{k \rightarrow \infty} \left[\frac{\varphi^4 - \varphi^2 + 1}{\varphi^2} \right]^k \underbrace{\sqrt{\frac{\varphi^4 - \varphi^2 + 1}{\varphi^2} - \sqrt{\frac{\varphi^4 - \varphi^2 + 1}{\varphi^2} + \sqrt{\frac{\varphi^4 - \varphi^2 + 1}{\varphi^2} + \dots + \sqrt{\frac{\varphi^4 - \varphi^2 + 1}{\varphi^2}}}}}_{k \text{ square roots}}$$

It becomes clear that the irrationality of Pi (π) is only based on constant φ and 1, in the same way as the irrationality of all irrational square roots, is only based on constant φ & 1 !

Natural Numbers, their square roots and irrational and transcendental constants like Pi (π) can be expressed (calculated) by only using constant φ and 1 ! This is also valid for all rationals (fractions) and their square roots.

Numbers and number-systems don't seem to exist ! They are manmade and therefore can be eliminated.

This is an interesting discovery because it allows to define most (maybe all) geometrical objects only with φ & 1 ! The result of this discovery may lead to a new base of number theory. Not numbers like 1, 2, 3,..... and constants like Pi (π) etc. are the base of Number Theory ! Only the constant φ and the base unit 1 (which shouldn't be considered as a number) form the base of mathematics and geometry. This will certainly also have an impact on Physics !

Constant φ and the base unit 1 must be considered as the fundamental „space structure constants“ of the real physical world !

In the physical world the geometries of all possible crystal-lattice-structures are fundamentally based on Phi and 1.

There probably isn't something like a base unit if we consider a „wave model“ as the base of physics and if we see the universe as one oscillating unit. In the universe everything is connected with everything. see : [Quantum Entanglement](#)

→ Please also read my 12 Conjectures on the next page (Chapter 17.6)

Chapter 17.6 :

Referring to my discovery regarding constant φ (Phi), I want to define the following 12 Conjectures :

Here the 12 conjectures : (\rightarrow you can call them **Harry K. Hahn's conjectures**)

1.) All Natural Numbers and their square roots can be expressed (calculated) by only using the mathematical constant Phi (golden mean = 1.618..) and number 1. This statement is also valid for all rationals (fractions) and their square roots

2.) All existing irrational numbers seem to be constructions out of Phi and 1.

For example the irrational transcendental constant Pi (3.1415926....) can also be expressed by only using Phi and 1 !

3.) Phi and 1 are the base units of Mathematics ! Numbers and number-systems don't exist ! They are manmade and therefore can be eliminated. In principle Mathematical Science can be carried out by only using Phi and 1, as base units.

4.) All geometrical objects, including the Platonic Solids can be described by only using constant Phi and 1.

Because all natural numbers, their square roots, rationals (fractions) and probably all irrational and all transcendental numbers too, can be expressed by only using Phi and 1.

5.) Point 4.) leads me to the conclusion that in the physical world the geometries of all possible crystal-lattice-structures are fundamentally based on Phi and 1. The more fundamental the lattice the simpler it can be expressed by Phi and 1.

6.) Point 4.) 5.) & 7.) leads me to the conclusion that on the molecular level (and probably on the atomic level too), as well as on the macroscopic (cosmic) level the distribution and structure of matter (=energy) in space, is fundamentally based on constant Phi and 1. \rightarrow **Phi represents a fundamental physical „Space Structure Constant“**

Together with Point 7.) this indicates that the curvature of spacetime at the molecular level (crystals) and at the atomic level, as well as on the macroscopic level is defined only by the "Space Structure Constant Phi" and the base unit 1.

\rightarrow This idea will help to unify General Relativity with Quantum Mechanics ! If the gravitational singularity in M87 indeed has a dodecahedral structure then gravitation, which is the geometric property of spacetime, can be described in Quantum Mechanics and at the cosmic level by the same constant duo : Phi and base unit 1 !

7.) The structure of the M87 black hole (\rightarrow **EHT2017**) indicates a dodecahedral structure. The distribution of matter in gravitational singularities therefore seems to be defined essentially by constant Phi and base unit 1 ! The largescale distribution of matter in the universe seems to be predominantly based on an order-5 Poincare-Dodecahedral-Space. \rightarrow [weblink to my study](#) (or alternatively here : <http://vixra.org/abs/1907.0348>)

Title : "EHT2017 may provide evidence for a Poincare Dodecahedral Space Universe"

8.) The natural numbers can be assigned to a defined infinite set of Fibonacci-Number Sequences.

9.) This infinite set of Fibonacci-Number Sequences, and the numbers contained in these sequences, are connected to each other by a complex precisely defined spatial network based on constant Phi. (\rightarrow **see table in Appendix C**). For the progressing Fibonacci-Sequences towards infinity, the connections between the numbers approach constant Phi.

\rightarrow **see Chapter 16 and 17 and Appendix C**

10.) Constant Phi (golden mean = 1.618..) must be a fundamental constant of the final equation(s) of the universal mathematical and physical theory. (\rightarrow It may be the only irrational constant that appears in the(se) equation(s))

11.) The number-5-oscillation (\rightarrow the numbers divisible by 5) in the two number sequences $6n+5$ (Sequence 1) and $6n+1$ (Sequence 2), with $n=(0,1,2,3,...)$, defines the distribution of the prime numbers and non-prime-numbers. The number-5-oscillation defines the starting point and the wave length of defined non-prime-number-oscillations in these Sequences 1+2 (SQ1 & SQ2). (Note : the combination of the two sequences SQ1 & SQ2 is considered here)

\rightarrow weblink to my study : <https://arxiv.org/abs/0801.4049> (or alternatively here : <http://vixra.org/abs/1907.0355>)

For a quick overview please see **pages 15 to 18** in this study : [weblink to the study](#) : **"EHT2017 may provide evidence..."**

12.) The importance of the number-5-oscillation for the distribution of primes and non-primes is a further indication for the conjecture that the largescale structure of the universe seems to be predominantly (mainly) based on an order-5 Poincare-Dodecahedral-Space structure. \rightarrow The space structure of the universe seems to be based essentially on the **5.Platonic Solid : the Dodecahedron** (\rightarrow consisting of 12 regular pentagonal faces, three faces meeting at each vertex)

The time will show if my Conjectures are correct !

18 References :

- Symmetry in Plants** - by Roger V. Jean & Denis Barabe (1998) – University Quebec, CA - ISBN No. : 981-02-2621-7
Weblink (Google Books) : https://books.google.de/books/about/Symmetry_In_Plants.html?id=2fbsCgAAQBAJ&redir_esc=y
- Transductions for the Expression of Structural Pattern Analysis in Sunflower** - by Luis F. Hernandez & P.B. Gree
https://www.researchgate.net/publication/11139668_Transductions_for_the_Expression_of_Structural_Pattern_Analysis_in_Sunflower
- Ice-Binding Proteins in Plants** - by Melissa Bredow & Virginia K. Walker - Queen's University, Kingston, ON, Canada
Study 1 : <https://www.frontiersin.org/artides/10.3389/fpls.2017.02153/full>
- Study 2** : **Poly-pentagonal ice-like water networks emerge solely in an activity-improved variant of ice-binding protein**
by Sheikh Mahatabuddin, Daichi Fukami, Tatsuya Arai and others - Hokkaido University, Sapporo, Japan
PDF : <https://www.pnas.org/content/pnas/115/21/5456.full.pdf> - **Weblink 2** : <https://www.pnas.org/content/115/21/5456>
- Ice-binding proteins and the 'domain of unknown function'** - by T. D. R. Vance, M. Bayer-Giraldi, P.L. Davies & others
https://epic.awi.de/id/eprint/49204/1/Vance_et_al-2019-The_FEBS_Journal.pdf
- From ice-binding proteins to bio-inspired antifreeze materials** - by I. K. Voets
<https://pubs.rsc.org/en/content/articlehtml/2017/sm/c6sm02867e>
- Microscopic-Image of an evaporated (dried) Water-Droplet** - credit: Devin K. Brown, from IEN at Georgia Tech
See this News article : <https://www.discovermagazine.com/environment/the-microscopic-beauty-of-a-water-splatter>
- Overview of the Microscopic Experiments to the evaporated water drop** : **Overview of Water Cluster Hypothesis**
- Microscopic Experiments to the evaporated Water Drop** : → [Movie 1](#), [Movie 2](#), [Movie 3](#), [Movie 4](#), [Movie 5](#), [Movie 6](#)
- Interfacial Water** : **Explanation of the complex air-water surface system** - **weblink** : [Interfacial water](#)
- Free energy and surface tension of arbitrarily large Mackay icosahedral clusters** - by R.B. McClurg & R.C. Flagan
→ see : I-Introduction; II-A; I-Summary & III-Discussion ; <http://www.wag.caltech.edu/publications/sup/pdf/318.pdf>
- Shells of Atoms** → see **Chapter 2 : Mackay-Icosahedra – Classification of shells** - by T.P. Martin
<https://carma.newcastle.edu.au/resources/jon/Preprints/Papers/Published-InPress/Ising/Papers/shells.pdf>
- Cluster als Bausteine funktioneller Nanomaterialien** (→ in German) - by Susanne Pietsch / Universität Konstanz
Weblink : https://www.researchgate.net/publication/283068433_Cluster_als_Bausteine_funktioneller_Nanomaterialien
- Structural puzzles in virology solved with an overarching icosahedral design principle** - by Reidun Twarock & Antoni Luque - **Weblink 1** : <https://www.nature.com/articles/s41467-019-12367-3> **Weblink 2 (PDF)** : [PDF-document](#)
- Structured Water is changing models** - News article from the "The Scientist" - magazine
<https://www.the-scientist.com/research/structured-water-is-changing-models-49389>
- Fingerprints in IR OH vibrational spectra of (H₂O)₂₀ und (H₂O)₁₀₀ Clusters from different H-bond conformations**
By Yuan Liu & Lars Ojamäe - **Weblink** : [Fingerprints_in_IR_OH_spectra_of_H2O_clusters](#)
- Structure and Stability of Water Clusters (H₂O)₈₋₂₀** - by Shruti Maheswary and Nitin Patel
[https://www.semanticscholar.org/paper/Structure-and-Stability-of-Water-Clusters-\(H-2-O-\)/](https://www.semanticscholar.org/paper/Structure-and-Stability-of-Water-Clusters-(H-2-O-)/)
- Solid water clusters in the size range of tens–thousands of H₂O** - by V. Buch, S. Bauerecker, J. P. Devlin and others
<http://www.pci.tu-bs.de/agbauerecker/Ebert/BuchBauereckerDevlinBuckKazimirskiIRCP2004.pdf>
- Water structured in the golden ratio** → Spectra of (H₂O)₂₀ Water Cluster
https://www.i-sis.org.uk/Water_Structured_in_the_Golden_Ratio.php
- Water clusters in plants** - by Kristina Zubow, Anatolij Viktorovich Zubow & Viktor Anatolijevich Zubow
https://www.scirp.org/pdf/JBPC20100100001_39788190.pdf
- Study 3** : **"Magic number colloidal clusters as minimum free energy structures"** - by Junwei Wang, Chameh Fru Mbah & others - **Weblink** : <https://www.fau.eu/2018/12/13/news/research/magic-number-colloidal-clusters/>
- Structural Color of Colloidal Clusters as a Tool to investigate Structure and Dynamics** - by Junwei Wang, U.Sultan, and others - **Weblink** : <https://www.researchgate.net/figure/Structural-color-of-icosahedral-colloidal-clusters>
- Entropy-driven formation of large icosahedral colloidal clusters** - by Bart de Nijs, S. Dussi, F. Smallenburg,..
<https://www.nature.com/articles/nmat4072?proof=true&in%EF%BB%BF>

Study 4 : “Auxin influx carriers stabilize phyllotactic patterning” - by K. Bainbridge, S. Guyomarc’h, E. Bayer etc.
https://www.researchgate.net/publication/5505575_Auxin_influx_carriers_stabilize_phyllotactic_patterning

Study 5 : “A plausible model of phyllotaxis” (PIN 1 polarizing simulations) – by R.S.Smith ; S. Guyomarch & others
https://www.researchgate.net/publication/7341401_A_plausible_model_of_phyllotaxis ; **alternative** : [Weblink 2](#)

Study 6 : “Changes in phyllotactic pattern structure in Pinus mugo due to changes in altitude”
Study to Fibonacci pattern variation in Pinus Mugo by Dr. Iliya Iv. Vakarelov, University of Forestry, Bulgaria (1982-1994)
From the book „**Symmetry in Plants**“ by Roger V. Jean and Denis Barabe, Universities of Quebec and Montreal, Canada
(Part I. Chapter 9 , pages 213-229) , ISBN : 981-02-2621-7 , **Weblinks** : [Weblink1](#)(Google Books); [Weblink2](#)

Study 7 : „Aberrant phyllotactic patterns in cones of some conifers : a quantitative study“ - by Veronika Fierz
Weblink : [Aberrant phyllotactic patterns in cones of some conifers](#) (researchgate.net)

Study 8 : „Novel Fibonacci and non-Fibonacci structure in the Sunflower“ - by J. Swinton, E. Ochu & Others
https://www.researchgate.net/publication/303354855_Novel_Fibonacci_and_non-Fibonacci_structure_in_the_sunflower; [Weblink2](#)

Study 9 : “Red Light Affects Flowering under long days in a Short-day Strawberry Cultivar”
by Fumiomi Takeda & D. Michael Glenn – USDA-ARS, Appalachian Fruit Research Station (USA), Kearneysville, WV 25430 – publication: HortScience 43(7):2245-2247.2008 - **Weblinks to study** : [Weblink1](#), [Weblink2](#)

Study 10 : “Chloroplast Photorelocation Movement” - by N. Suetsugu and M. Wada
https://www.researchgate.net/publication/226792663_Chloroplast_Photorelocation_Movement/link/56e8d3d608ae166360e533fc/download

To the importance of constant Phi for the physical world : → see Chapter 17.2 to 17.6

Phase Spaces in Special Relativity : Towards eliminating Gravitational Singularities
by Peter Danenhower , [Weblink](#) : <https://arxiv.org/pdf/0706.2043.pdf>

The Black Hole in M87 (EHT2017) may provide evidence for a Poincare Dodecahedral Space Universe - by Harry K. Hahn
<https://archive.org/details/TheBlackHoleInM87EHT2017MayProvideEvidenceForAPoincareDodecahedralSpaceUniverse/page/n1>
alternative [Weblink](#) : <http://vixra.org/abs/1907.0348>

The golden ratio Phi (ϕ) in Platonic Solids : <http://www.sacred-geometry.es/?q=en/content/phi-sacred-solids>

The Ordered Distribution of Natural Numbers on the Square Root Spiral - by Harry K. Hahn
<http://front.math.ucdavis.edu/0712.2184> **PDF** : <http://arxiv.org/pdf/0712.2184>

Appendix : Movie - Weblinks :

Movie_1 (short_3min) : Amazing Resonance Experiment with Chladni-plates - see also : **Movie-1 (long_8min + tone)**
<https://www.youtube.com/watch?v=wwJAgUBF4w> & <https://www.youtube.com/watch?v=1yaqUI4b974>

Movie_2 : Cymatic Music (in Water) - <https://www.youtube.com/watch?v=sThS9OfnM1s>

Movie_3 : Amazing Resonance Experiment with Metal and Water (Cymatics) → see from 3:35 Min
https://www.youtube.com/watch?v=_0FWp3GxI9g

Movie_4 : Sound monolith resonance patterns - Water - <https://www.youtube.com/watch?v=F95Oowfg4pA>

Movie_5 : The beauty of twelve piano notes made visible on CymaScope in Water
<https://www.youtube.com/watch?v=9aI397N6Tzs>

Movie_6 : Cymatics / Cimatica - Experiment 16 (432 Hz) - experiment with sound water & light - **Start at 1:45 min**
https://www.youtube.com/watch?v=iD6XUSyFN_A

Movie_7 : Sound Frequencies in Water: A=440 Hz & A=432Hz Using Sine, Square & Sawtooth Waves
<https://www.youtube.com/watch?v=UyXxGK-hwh4>

Movie_8 : Cymatik 2 - Vibrationen auf dem Wasser
<https://www.youtube.com/watch?v=Zfv6IMF5eIlg>

Movie_9 : Sound Resonance of Water Droplet
<https://www.youtube.com/watch?v=NGeGPt0qJtk>

Movie_11 : Cornstarch and vibrations
<https://www.youtube.com/watch?v=UU7iuJ98fRQ>

Appendix A.) :

Standing-Wave-Patterns and Acoustic-Resonance in Water

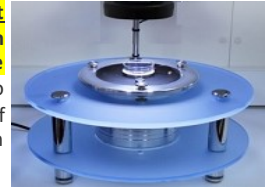
The following movies show water which was excited with defined frequencies by using a tone-generator, or a loud-speaker, or a special scientific instrument which is called a **CymaScope**. Please have a look at these YouTube-movies !

In the **apical meristem** of plants the water probably gets excited by a large pulsating central water cluster (crystal) which may produce similar patterns in the **micro-scale** as the following shown **macro-scale patterns**.

There is a similarity between some of the standing-wave patterns in the movies and phyllotactic patterns in plants ! If we consider that plant cells in the **apical meristem** consist to 80 % of water, then it is easy to imagine that phyllotactic patterns in plants may have a similar physical cause !

CymaScope :

The CymaScope is a scientific instrument that makes sound visible. Great detail could be obtained by imprinting sonic vibrations on the surface of ultra pure water. The surface tension of water has high flexibility and fast response to imposed vibrations, even with transients as short-lived as a few milliseconds. Water is able to translate many sinusoidal periodicities, of a given sound sample, into physical sinusoidal structures on the water's surface. **Current limits to imprinting sound on water** occur in the higher harmonics and are due mainly to there being **insufficient energy available in this area of the audio spectrum** to cause excursions of the surface tension membrane



Movie_2 : Cymatic Music



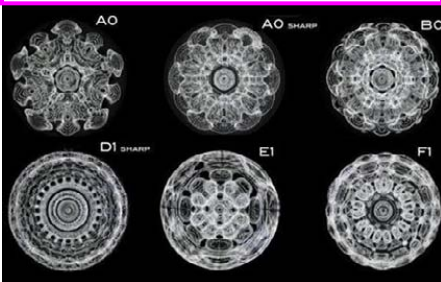
Movie_3 : Amazing Resonance Experiment
→ see section starting at 3:35 min



Movie_4 : Sound monolith resonance pattern – water (excited by sound)



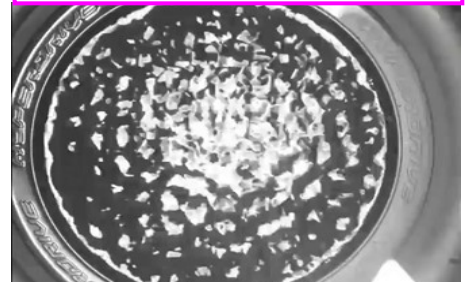
Movie_5 : The beauty of twelve piano notes made visible on the CymaScope



Movie_6 : Cymatics Experiment 16 (432 Hz)
→ see section starting at 1:45 min



Movie_7 : Water excited with A=440 Hz & A=432Hz Sine, Square & Sawtooth Waves



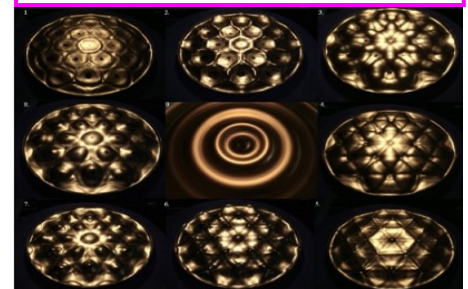
Movie_8 : Vibrationen aufdem Wasser



Movie_9 : Sound Resonance of Droplet



Study : Standing waves at 14 Hz , in different fluids : methanol, ethanol etc.



Cymatics_wikipedia weblink : Cymatics is a subset of modal vibrational phenomena



Movie_11 : Cornstarch and vibrations



Movie_12 : Non-Newtonian Fluid on a Speaker Cone (→ Corn starch, a shear thickening non-newtonian fluid was used)

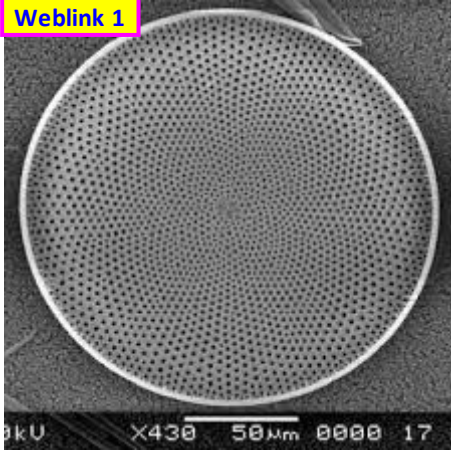


Appendix B.) : Phyllotactic-Patterns (Phyllotaxis) visible in *Coscinodiscus* - Diatoms :

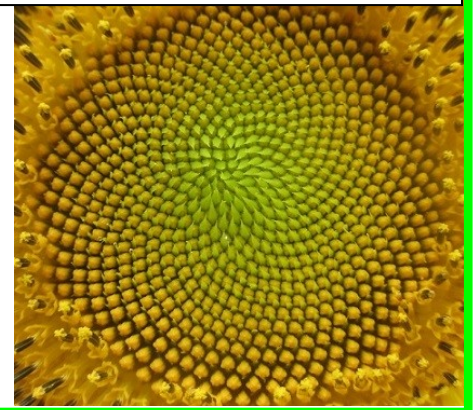
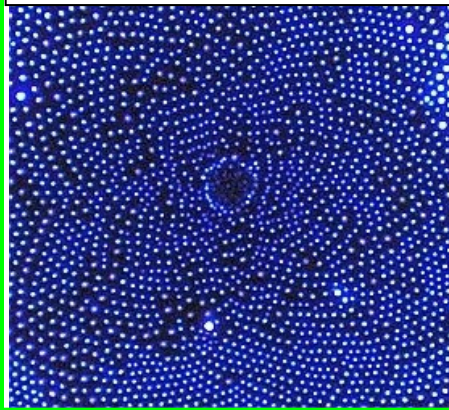
The following images show microscopic photographs of the small micro-algae *Coscinodiscus* which is a *Diatom*. *Diatoms* are a class of unicellular microalgae, found in the oceans, waterways and soils of the world. They exist for ≥ 200 million years in the world's oceans. Individual cells (diatoms) range in size from 2 to 200 micrometers. The shown phyllotactic patterns represent the cellwall of the *Coscinodiscus* *Diatom* which is made of *Silica* : SiO_2 (or more precise *hydrated silicon dioxide*). → The Images which all show **phyllotactic patterns** are from different *Coscinodiscus* Species.

Diatoms may be the plant ancestor that first developed phyllotactic patterns (**Phyllotaxis**) ! Therefore a microscopic live-observation of the dynamic formation of the phyllotactic patterns in Diatoms may solve the **Phyllotaxis** Mystery ! Because only few *Coscinodiscus* *Diatoms* show real phyllotactic patterns, far-red- or **IR-radiation** may be required for the formation of a perfect phyllotactic pattern, and **diatoms** may have to be close to the water-surface in this process !

Weblink 1



For comparison : 1.) central area of evaporated water drop ; 2.) Sunflower capitulum

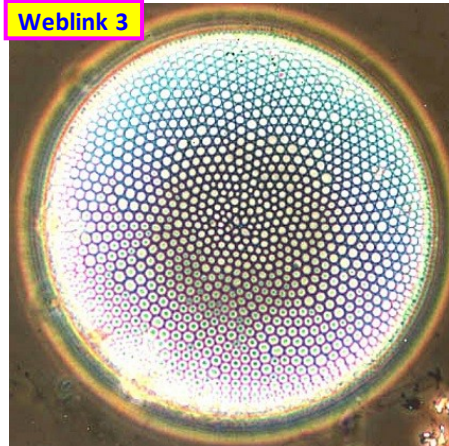


Weblink 2

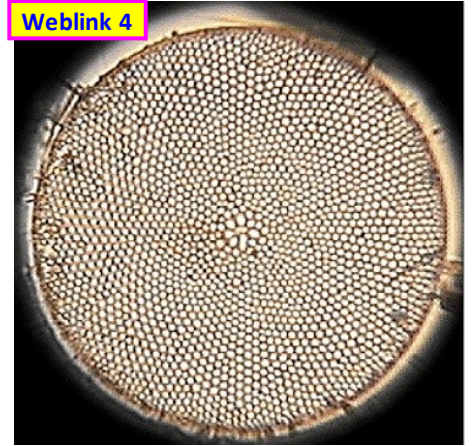


Figure a: epilithic diatom flora of the Cali River basin, Colombia
- a. *Coscinodiscus kurzii*; Scales: 30 μm .

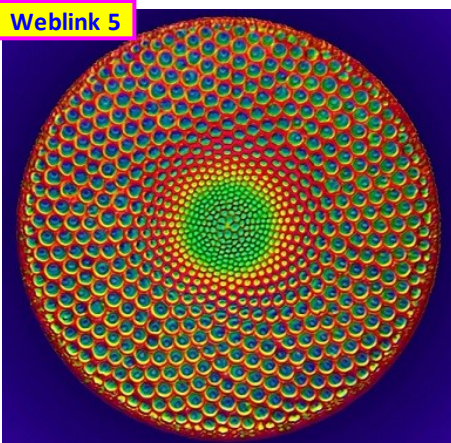
Weblink 3



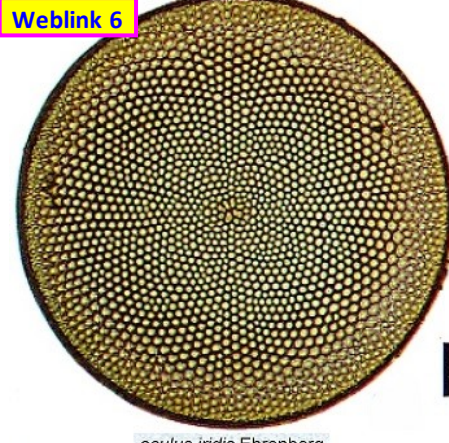
Weblink 4



Weblink 5

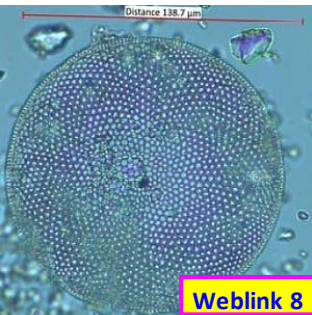


Weblink 6

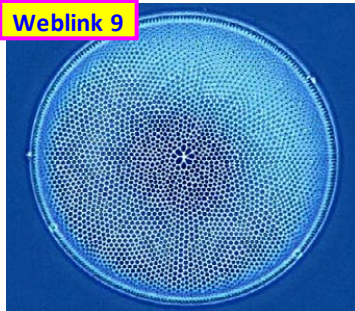


oculus iridis Ehrenberg

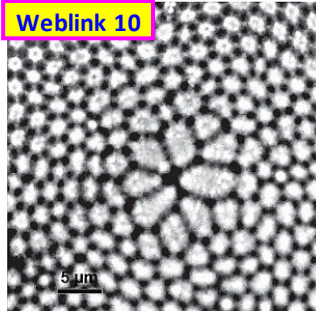
Weblink 7



Weblink 9



Weblink 10



Weblink 11

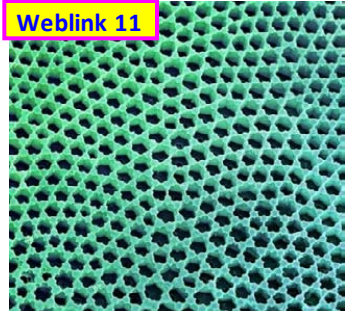


Table 3 : Periodicity of some of the prime factors of the numbers of the **Fibonacci F2 (Lucas)** - Number Sequence :

some prime factors shown in table form												in prime factors factorized Fibonacci-Numbers		Fibonacci-Sequence F2 (Lucas-Sequence)					
41	37	31	29	23	19	17	13	11	7	5	3	2	repeating products	new products	sum of digits	L	L'	L''	No.
															1	1			1
															3	3			2
												2^2		2x2	4	4	1		3
															7	7	3		4
											3^2	2		2x3x3	4	11	4	1	5
															9	18	7	3	6
															11	29	11	4	7
															11	47	18	7	8
					19							2^2		2x2x19	13	76	29	11	9
41											3			3x41	6	123	47	18	10
															19	199	76	29	11
				23					7			2		2x7x23	7	322	123	47	12
											3			3x281	8	521	199	76	13
												2^2		2x2x11x31	15	843	322	123	14
		31						11			3^2	2		2x3x3x3	14	1364	521	199	15
															11	2207	843	322	16
															16	3571	1364	521	17
															27	5778	2207	843	18
															25	9349	3571	1364	19
															16	15127	5778	2207	20
			29									2^2		2x2x29x211	23	24476	9349	3571	21
											3			3x43x307	21	39603	15127	5778	22
														139x461	26	64079	24476	9349	23
												2		2x47x1103	20	103682	39603	15127	24
														11x101x151	28	167761	64079	24476	25
											3			3x90481	21	271443	103682	39603	26
												2^2		2x2x19x5779	22	439204	167761	64079	27
														7x7x14503	25	710647	271443	103682	28
														59x19489	29	1149851	439204	167761	29
41											3^2	2		3x41x2x3x2521	36	1860498	710647	271443	30
															20	3010349	1149851	439204	31
															38	4870847	1860498	710647	32
												2^2		2x2x199x9901	40	7881196	3010349	1149851	33
											3			3x67x63443	24	12752043	4870847	1860498	34
			29											11x29x71x911	28	20633239	7881196	3010349	35
				23								2		2x7x23x103681	34	33385282	12752043	4870847	36
															26	54018521	20633239	7881196	37
											3			3x29134601	33	87403803	33385282	12752043	38
												2^2		2x2x79x521x859	23	141422324	54018521	20633239	39
														47x1601x3041	38	228826127	87403803	33385282	40
															34	370248451	141422324	54018521	41
											3^2	2		3x281x2x3x83x1427	54	599074578	228826127	87403803	42
															43	969323029	370248451	141422324	43
															52	1568397607	599074578	228826127	44
		31										2^2		2x2x11x31x19x181x541	41	2537720636	969323029	370248451	45
											3			3x4969x275449	30	4106118243	1568397607	599074578	46
															62	6643838879	2537720636	969323029	47
												2		2x769x2207x3167	47	10749957122	4106118243	1568397607	48
			29											29x599786069	46	17393796001	6643838879	2537720636	49
41											3			3x41x401x570601	39	28143753123	10749957122	4106118243	50

Note : all prime numbers are marked in yellow and all numbers not divisible by 2, 3 or 5 are marked in orange

Table 4 : Periodicity of some of the prime factors of the numbers of the **Fibonacci F6 - Number Sequence :**

Periodicity of the prime factors 2 - 41 shown in table form												in prime factors factorized Fibonacci-(F6)-Numbers	Fibonacci-F6 Sequence				
41	37	31	29	23	19	17	13	11	7	5	3	2	sum of digits	F6	F6'	F6''	Nr.
???														2x2			
												2 ²					2
													3x3				3
									7			2	2x7				4
																	5
										5	3	2 ²	2x2x3x5				6
																	7
												2					8
													2x127				9
													3x137				10
									7	5			5x7x19				11
												2 ²	2x2x269				12
																	13
													3x3x313				14
												2	2x43x53				15
													5x5x5x59				16
																	17
												2 ²	2x2x3x1609				18
									7				7x4463				19
																	20
										5		2	2x5x8179				21
											3		3x31x1423				22
												2 ²					23
													2x2x37x2341				24
																	25
										5	3 ²		3x3x5x6719				26
									7			2	2x7x79x1327				27
													23x223x463				28
													19x202231				29
												2 ²	2x2x3x379x1367				30
										5			5x227x8863				31
												2					32
													2x641x20543				33
													3x1637x8677				34
									7				7x181x54419				35
										5		2 ²	2x2x5x5578081				36
																	37
												2	3x3x32452457				38
													2x1109x213067				39
													67x2083x5479				40
													5x5x49489493				41
												2 ²	2x2x3x53x3147629				42
													7x7x37x1786613				43
													71x3613x20431				44
												2	2x167x3607x7039				45
										5	3		3x5x914744813				46
													19x83x14078201				47
												2 ²	2x2x337x2664083				48
													129631x448379				49
													3x3x2671x3912239				50
										7	5	2	2x5x7x2173859021				51
													23x31x345324607				52
																	53
																	54
																	55

Note : all prime numbers are marked in yellow and all numbers not divisible by 2, 3 or 5 are marked in orange

